Towards two-dimensional organo-metallic molecular architecture via interface chemistry

Ana Cristina Gomez Herrero

Communauté
UNIVERSITÉ Grenoble Alpes

THÈSE

Pour obtenir le grade de

DOCTEUR DE LA COMMUNAUTE UNIVERSITE GRENOBLE ALPES

Spécialité : Physique de la Matière Condensée et du Rayonnement

Arrêté ministériel : 25 mai 2016

Présentée par

Ana Cristina GOMEZ HERRERO

Thèse dirigée par **Johann CORAUX**, Chargé de recherche, Communauté Université Grenoble Alpes.

préparée au sein du **Laboratoire Institut Néel (CNRS)**
dans **l'École Doctorale Physique.**

Vers une architecture moléculaire organométallique bidimensionnelle par chimie d'interface

Towards two-dimensional organo-metallic molecular architecture via interface chemistry

Thèse soutenue publiquement le **6 décembre 2019**, devant le jury composé de :

Mme. Marie-Claire SAINT-LAGER
Président du jury, DIRECTRICE DE RECHERCHE, CNRS- Délégation Alpes.
M. Sylvain CLAIR
Rapporteur du jury, Chargé de Recherche (HDR), CNRS- Délégation Provence et Corse.
M. Jean-Christophe LACROIX
Rapporteur du jury, Professeur Université Paris 7.
Mme. Amandine BELLEC
Examinatrice, Chargée de Recherche (HDR), CNRS- Délégation Île-de-France Villejuif.
Mme. Véronique LANGLAIS
Examinatrice, Chargée de Recherche, CNRS- Délégation Occitanie Ouest.
M. Thierry MELIN
Examinateur, Directeur de Recherche, CNRS- Délégation Hauts-de-France

Résumé

Contrairement aux matériaux bidimensionnels inorganiques (e.g. graphene, dichalcogénures de métaux de transition), les matériaux bidimensionnels organiques sont synthétique, et présentent une structure plus complexe héritée de leur briques de construction. Une gamme plus riche de propriétés est attendue pour cette raison, et leur production devrait être á bas coût.

Dans ce manuscrit de thèse nous présentons nos résultats obtenus selon deux stratégies visant la formation de telles couches organiques bi-dimensionnelles, ou au moins ultraminces. Ces deux stratégies exploitent une chimie interfaciale. La première stratégie s'appuie sur des outils de science des surfaces (microscopie à effet tunnel, spectroscopies de photoélectronique et de seuil d'absorption par rayons X, théorie de la fonctionnelle de la densité) et se concentre sur une molécule dérivée du triphénylène et ses modifications sur la surface (111) bien définie du cuivre. Si nous ne sommes pas parvenus á élaborer un matériaux bidimensionnel étendu, nous avons découvert que les molécules sont catalytiquement oxydées et dans le même temps changent de structure, d'organisation sur la surface, et d'interaction avec le substrat. Les molécules totalement oxydées se révèlent être d'excellents accepteurs électroniques, meilleurs que la plupart des molécules connues. La seconde stratégie est basée sur une synthèse en solution et des caractérisations plus versatiles (spectroscopies UV-visible et Raman, microscopies optique et électroniques). Elle exploite la chimie dynamique des liaisons imines, avec comme monomère un composé arène(ruthenium), conduisant á la formation d'une nanocouche organométallique polymérique, qui peut être manipulée facilement pour être par exemple reportee sur

Abstract

Compared to inorganic two-dimensional materials (e.g. graphene, transition metal dichalcogenides), organic two-dimensional materials are all synthetic materials, that additionally have a more complex structure inherited from their building blocks. A richer set of properties is for this reason expected from them, and their production should be inexpensive.

In this thesis manuscript we present our work on two strategies toward the formation of such organic two-dimensional, or at least ultrathin organic sheet materials. These strategies rely on interfacial chemistry, on one hand at the vacuum/solid interface, and on the other hand at liquid/liquid interface. The first strategy is based on surface science tools (scanning tunneling microscopy, X-ray photoelectron and absorption near-edge spectroscopies, density functional theory) and addressed triphenylene derivative molecules experiencing chemical modifications on the well-defined (111) surface of copper. Although we did not yet manage to prepare an extended two-dimensional material in this system, we discovered that the molecules get catalytically oxidized and concomitantly change in shape, surface organization, and interaction with the substrate. We establish that the fully-oxidized molecules are stronger electron acceptor than most known molecules. The second strategy is based on in-solution synthesis and more versatile characterization (UV-visible and Raman spectroscopies, optical and electron microscopies). It exploits dynamic imine bond chemistry starting from ruthenium(arene) monomers, to form polymeric organometallic nanosheets that are conveniently manipulated and can, for instance, be suspended across membranes.

Acknowledgements

I would like to start this section thanking the members of the jury, for their great involvement in my defense. The discussion had great interest both for the construction of future projects from this manuscript and from a personal point of view.

I am really grateful to ESISNA group at Material Science Institute of Madrid because thanks to them I discovered an amazing research field by which I felt attracted from the first time I visited their laboratory during the Master's degree. Many thanks to Prof. José Ángel Martín-Gago and Dr. Paqui López, to gave me the opportunity to work with them. As part of this team, I can not forget Carlos and Irene teaching me how to make pure science during my Master's internship and to do not despair when the microscope went into a "poltergeist mode". Fortunately, we never lost the contact, since they were involved in my collaborations during my thesis. And at this point, I need to thank also José Ignacio (or Nacho for friends) and Carlos (yes, again), for all the discussions, analysis and moral support, especially in the panic moments of the last period of the thesis. Thanks also to, Nerea, Pablo, Jon, Koen, Mario,... for making me feel part of your group.

As soon as I arrived in Grenoble three years ago, the adventure started. With it, the first person I met... Johann, my thesis director. Your patience, understanding, rigorously and organisation have been the base of this project. Lots of things I have learnt from you, not only pure physics which I was a bit scared of, but also the ability to value and trust what I can do. Because you trusted me from the very first moment and you gave me the opportunity to build together this "explorative" project from almost zero. Thanks for the freedom you gave me always to decide what to do step by step. Another important character from this thesis, is Fred, the project's father. A close person, always available and reactive, you have been an essential pillar of this. Because I have never doubted in asking you whatever I needed or I did not understand, that was an invaluable tranquillity.

Valérie et Philippe (ou Philippe et Valérie), pour vous je vais essayer quelques mots en Français. En tant que capitaines du labo, vous avez vu mon évolution en beaucoup d'aspects, surtout dans cette langue... impossible de prononcer correctement pour une espagnole invétérée. Sans aucun doute, cette thèse aurait pas été possible sans vous, parce vous avez été là TOUJOURS, sans horaires et avec pleine

dévouement des professionnels. Je voudrais faire une mention spéciale à Valérie. Merci pour notre jour à jour, et nos conversations de n'importe quoi. Merci pour ton compréhension infinie et tes conseils de "maman", que beaucop des fois m'ont bien soutenu.

Also, as an essential part of my live in Néel, I would like to thank the Hybrid team. Diverse in topics and charged of humanity and amazing people, I felt more than welcome from the first day. I am very grateful to Laetitia, Nedjma, Julien and Vincent, always available for guide me with the new "manips" or techniques I needed to learn, or for any question I had (from science, to lab organization, and in worst cases, for French administration). Without being officially my supervisors, all of you have contributed to the development of my project, but more importantly, to my learning and evolution during these three years. As a large group, plenty of PhD students, post-doc and visitors compose the totality of this team, making it rich in cultures and funny lunches and coffee breaks. Alexander, Sudipta, Dipankar, Riadh, Gom, Pauline, Simone, Thanasis, Van-Dung, Guilliam, Priyank (or Pryank??), Brice, Kazy, Abhishek, Maria Teresa and Enzo. Thanks for the discussions about everything (except science during the lunch time because it was forbidden), the jokes (special mention to quantum fluctuations topic), the complicity with some of you, the excursions, the "soirées" and "crémaillères". I would like to thank Roberto and Estelle, my comrades, all their support and friendship. I was very lucky to start and end my thesis with you. Un merci spécial à ma sœur Estelle, compagne de tout pendant ces trois années. Une belle découverte en tant que personne et merveilleux professeure de français, ça c'est grâce à toi. Que la distance ne sépare pas ce que la thèse a unie!

Fortunately, I also had the opportunity to work with plenty of people out of my team: Valérie REITA, David JEGOUSO, Corinne FELIX, Martien DEN-HERTOG, I feel infinite gratitude for the time you have invested on me and on this project. Many thanks also to the people of the financial management and administrative departments I was in contact with: Florence Pois, Otmane and Angelique, and also to Patrick and Julien, from the informatic service, for had solved my big headaches with the computer. For other people I just see every day in the corridors and they always had a smile for me, or I shared seminars, office, meetings, coffee breaks: Arnaud, Pierre MALLET, Pierre GIROUX, Benjamin CANALS, Shridevi, Alexis, José, Isabelle, Maria, Michael, Everton, Corentin, Marco, Juliette, Hugo,.. Thank you kindly, for this nice daily routine we have constructed.

As part of my life in Grenoble, my other family. Nanochurros people, unstoppable: Kimon, Tona, Roberto, Thanasis and Antonio, we have built good memories either in the beach or in the snow, with Chartreusse (and then, the Pastis) as brooch

of our great moments. Y cómo dejarme atrás a Alvarito, autético como poca gente he conocido y sincero. Fuiste un gran apoyo en los primeros momentos, que a veces fueron tan duros. Espero que nuestro periodo de "coloc" no fuera muy traumático. Nos debemos una juerga en Torre!! Y aquí una lista de personas con las que he tenido la grandísima suerte de coincidir y compartir momentos inolvidables durante estos tres años: Tomás, Raquel, Marie Lau, Vanni y Marila, Jaio, Maddi, Javi, Isa, Kike, Xenia, Ana y Mark, Eugenia y Nico, Robert y Sandy, Ricardo e Inés. Gracias con mayusculas, por haberme acogido sin reparos y sin dudarlo como una más. Vosotros habeis conseguido que me sintiera como en casa estando lejos de ella. Y hablando de personas importantes para mí, no podía faltar Jorge. La persona que aparece cuando más lo necesitas para tenderte la mano y guiarte como un hermano mayor. Una de las mejores personas que conozco y una amistad, sin duda, para toda la vida. Siempre será tuya la frase de "Antes todo esto era campo!".

También querría agradecer, y mucho, a aquellas personas que desde mi más tierna juventud me han visto evolucionar y que he tenido la suerte de mantener a mi lado a pesar de la distacia. Mi Moni y Mari Sierra, que siga pareciendo que no pasa el tiempo cada vez nos encontramos. Diana, contigo descubrí lo que significa la palabra amistad que hemos mantenido contra viento y marea. Una persona leal y fuerte donde las haya y de gran corazón. Gracias por todo tu tiempo. Mi querido grupo de la Universidad, variado y singular como las piezas de un puzzle que al final acaban encajando para espero, que no se separe jamás. Kike, Sandra, Elena, Iris, Victor, MK y, de reciente adquisición, Clemens. Gracias a todos por vuestra complicidad y por sentiros siempre cerca, en especial a mis niñas, porque la distancia, paradójicamente nos unió más. Os quiero.

Y un especial gracias para Dani (o MK para los amigos), mi compañero de aventuras y en especial de esta que se llama Grenoble. Porque sin duda Grenoble no hubiera sido, ni sería, lo mismo sin tí aquí a mi lado. Porque me comprendes y me apoyas en cualquier decisión que he tomado y porque, sobretodo, me haces ser mejor persona.

Y por último, pero no por ello menos importante, gracias a mi familia. A mis padres que con tanta pena como orgullo me vieron partir para comenzar esta nueva etapa de mi vida. Este logro, ha sido gracias a vosotros, por haberme enseñado el sentido del sacrifio y esfuerzo desde vuestro amor más infinito. A mis tíos y primos, que siempre me recuerdan donde están mis orígenes y llevan ligada la palabra morriña (término imposible de explicar aquí a quien no conoce el español), y a mis abuelos, que de la nada construistéis tanto. Os quiero. Y por último, a mi pequeño Flequi, cuya partida pareció que puso punto final a esta hermosa etapa.

Contents

1 Introduction and motivation

The first isolation of graphene in 2004 has spurred considerable interest on ultrathin two-dimensional materials, involving various scientific communities. As a result of their low-dimensionality, interesting properties are usually different from their three-dimensional counterparts. A variety of candidates have emerged (transition metal dichalcogenides, and boron nitride among many others) and new candidates based on the combination of organic molecules have come up in recent years. The organic molecules are cheap, generally stable and easy to handle. The wide experience of organic chemists allows the design and synthesis of 'à la carte' organic molecules with specific chemical groups that can guide the subsequent synthesis of larger-scale materials, molecular block by molecular block, or that can act as electron donors or acceptors in composite materials combining several molecules or a molecule and a metallic electrode for instance. The latter examples are highly relevant in the raising field of molecular electronics in view of passive (electron/charge transport channels) or active (charge separation, switches, amplifiers) elements. A focused introduction of both types of materials and of related synthesis strategies, from early examples to most recent advances, is given in chapter 2. This chapter also intends to give an overview, without entering much into details, of the great number of applications in which these new classes of materials can be employed.

With these premises, the study of two-dimensional organometallic architectures has been addressed in this thesis via interface reactions *i.e.* at the vacuum/solid interface (on-surface chemistry), and at the liquid/liquid interface. In a first part of the work (chapter 4), the interaction and chemical transformation of organic molecules with a metallic substrate has been investigated in details. For this purpose we have made use of different surface science techniques and experimental protocols. This work relies on the use of ultra-high vacuum (UHV) equipments and techniques, including scanning tunneling microscopy (STM), X-ray photoelectron spectroscopy (XPS), and near edge X-ray absorption fine structure (NEXAFS) that gave us complementary information about the interactions of the molecules with neighbour molecules and the substrate, about their chemical modifications, and about their organization on the surface. We also make use of density functional theory calculations (DFT) to rationalize our observations and obtain further microscopic insights into the structural, chemical, and electronic properties. A brief description of the working principles is given in chapter 3. In a second part of

the work (chapter 5), we have explored the synthesis of polymer nano-sheets at a liquid/liquid interface. To confirm the formation of new bonds and integrity of the polymer in the form of an ultrathin film (nanosheet) several techniques including Raman and ultra violet-visible spectroscopies (SEM, TEM), and scanning and transmission electron microscopies have been employed. The basic working principles of these techniques is described in chapter 3.

The study of the chemical structure, morphology and interaction of hexahydroltriphenylene (HHTP) molecules deposited is the topic of chapter 4. Widely employed in the synthesis of two-dimensional covalent and organo-metallic materials, as regards on-surface chemistry studies, HHTP molecules have been exclusively deposited on Ag(111) and Au(111). Our work is a systematic analysis of HHTP molecules on Cu(111) at room temperature and after annealing at 530 K. An stepwise oxidation of the molecules (*i.e.* a loss of hydrogen atoms of the hydroxyl groups) is witnessed in high resolution spectroscopy data. The catalytic effect of the substrate became evident when the molecules were partially dehydrogenated already at room temperature on the substrate, upon mere deposition. Changes in their chemical reactivity were detected directly with leading to different self-assembly networks observed before and after the thermal treatment. According to DFT calculations, the degree of oxidation of the HHTP molecules has strong consequences on their chemical structure, since the molecules adopt a bowl shape when they are partially dehydrogenated, and a dome shape when they reach their maximum oxidation state. Directly related to these structural changes, the interaction of the molecules, with the substrate and with other molecules, changes. When molecules adopt the bowl shape, their interaction with Cu is through C atoms of the central ring, whereas for the dome shape the O atoms are closest to the surface, forming strong bonds with it. We find that this different orientation towards de substrate alters substantially the charge transfer produced from the surface to the molecules, whose value increases from 1.2 electrons (for bowl shape and partially dehydrogenated molecules) to 1.9 electrons per molecule (for dome shape and fully dehydrogenated molecules). This strong electron-acceptor character of the HHTP molecules is quite interesting from the molecular electronics point of view. In a sense, the oxidation that accompanies the departure of hydrogen atoms is here compensated by the presence of the substrate, which can be seen as a charge reservoir that compensates the oxidation of the molecule, and stabilizing the molecule in the form of a system with four aromatic rings and six outer oxygen atoms bearing significant partial charges, a situation that has not been observed thus far in solution to our knowledge.

Indications of the premises of the formation of organo-metallic structures are found in the dehydrogenated system, close to defects in the molecular lattice. These defects are composed by three molecules pointed in the same direction presumably

enclosing a small cluster of copper atoms. DFT calculations revealed the enhancement of molecular bonding associated with the inclusion of Cu clusters in the centre of the hollow site defined by the three molecules. All these observations are crucial for further investigations based on the combination of these molecules with other organic ligands or metallic centres with the aim of forming long-range ordered systems.

Finally, in chapter 5 the synthesis of polymeric nanosheets grown at liquid/liquid interface is reported. A new synthesis scheme based on dynamic imine chemistry is presented, which is based on a Shiff-base condensation reaction between diamine and (arene)ruthenium-trialdehyde monomers. The formation of an ultrathin ($<$ 20 nm), self-supported nanosheet on see-through membranes across 500 nm, is observed by SEM and TEM analysis. Then, the formation of new bonds (C=N) between monomers is demonstrated by the localized analysis on the same spots that were investigated with SEM/TEM, by Raman spectroscopy. Our new synthesis strategy produces a polymer that includes metallic centers but does not rely on these metallic centers to propagate the polymerization reaction. This is at variance with the majority of the polymerization schemes for organometallic systems. We expect that the polymerization reaction results in the extension of the π-conjugation over the whole system, yielding a polymeric nanosheet that could serve as a flexible electronic conductor, or thermoelectric material, where also the presence of high-atomic-number metallic centres is crucial.

2 State of the art

Contents

'Nano' is a universal prefix used today in science and technology. One nanometre (nm) is equal to one-billionth of a meter (10^{-9} m). For comparison, a single human hair is about 80,000 nm in diameter, a blood cell is approximately 7,000 nm wide and a water molecule is almost 0.3 nm along. The study of the phenomena and manipulation of materials at nanometre scale (i.e, control over atoms, molecules or macromolecules) from the size of atoms to typically 100 nm, is the basis of what is known nowadays as nanoscience. Often, the smaller the size the most prominent the modification of the properties compared to those of the bulk material. These changes are based on the increased relative surface area, which results in a corresponding enhance of chemical reactivity, and the dominance of quantum effects, which can significantly change the material's optical, magnetic and electrical properties. For instance, depending on their size, gold particles can appear red, blue or gold in colour, and historically, gold and silver nanoparticles have been used as coloured pigments in glass and ceramics since the 10^{th} century.
Directly linked to nanoscience is the nanotechnology. Conceived to exploit the material's properties developed by nanoscience, its goal is to fabricate structures, devices and systems with novel functions due to their size. The conceptual basis of nanotechnology were set by the physicist Richard Feynman in 1959 in his famous lecture 'There's plenty room at the bottom'.[1] He explored the possibility of manipulating and controlling things on a small scale, for instance to write the entire 24 volumes of the Encyclopedia Brittanica on the head of a pin, and foreseeing the increasing ability to examine and control matter at the nanoscale.

Making and manipulating matter on the sub-100 nm length scale is a great challenge for both scientists and engineers. A key point for nanomaterial's synthesis is the control over the morphology, the composition and the size, which altogether define the physical properties of the resulting material. Hence the tremendous importance of materials science in the development of this discipline, which we will address more extensively in Section 2.4.1. Then, to fully exploit the integration of new nanostructures with device elements and organized them at different scales, a hierarchical assembly is required (i.e. final architecture or spacing between elements). In this case, the chemists' ability for, not only the control but also the understanding of the most basic interactions that governs matter (e.g. dispersive forces and steric repulsion), are of paramount relevance in this aspect. The nanoscale (1-100 nm) spans an extraordinary extended domain comprising various kinds of characteristic length scales, that they have historically explored by designing new forms of matter assembled with atoms and molecular groups (e.g. polymers, colloids, large molecules, all built starting from tiny organic subunits). Therefore, based on this expertise, great contributions to nanoscience can be provided by chemistry:

– As an efficient supplier of *à la carte* nanostructures, that can be directly

used or combined to build more complex materials. The control over the size or functionalization of building blocks, will determine the future material's properties.

– As data source on how to produce new materials whose properties depend on their size, in a reproducible, economical way and in quantities. This contribution is of great of interest on boththe development of new materials and their large-scale production.

The multidisciplinary character of nanoscience and nanotechnology is evident in the broad field of applications that they address, from electronics, to photonics, metrology, biotechnologies and nanomedecine to name a few. Nanomaterials are considered as one of the first outcome of nanoscience and can be defined as those which have structural components with at least one dimension less than 100 nm. Materials that are extended in two-dimensions and have one dimension in the nanoscale are layers, such as thin films or surface coating. This includes materials that are nanoscale in two-dimensions such as nanowires and nanotubes, and finally, materials with the three dimensions in the nanoscale, namely particles, like precipitates, colloids and quantum dots.[2]

There are two main classes of processes that are used to obtain nanomaterials: 'top-down' and 'bottom-up'.

Top-down fabrication consists in transforming materials into nanomaterials by etching or milling processes. For instance, lithography has been developed and refined by the semiconductor industry over the past 30 years. Likewise, exfoliation of bulk layered materials is considered also a top-down approach for two-dimensional (2D) materials synthesis, which offers high quality monolayer or few-layered samples, easily transferable to a variety of substrates. In general, these techniques are well-suited to design devices with sometimes complex structure, but they are energetically costly and a higher source of waste than bottom-up processes.[3]

In contrast, the bottom-up building of structures involves atom-by-atom or molecule -by-molecule assembly. Related growth techniques can be classified into three categories: chemical synthesis (which produces raw materials such as molecules or particles), positional assembly (in which single atoms or molecules can be placed one-by-one), or self-assembly (which implies the spontaneous organization of molecules into structurally well-defined and rather stable arrangement through non-covalent interactions). Specially, from an economical and environmental point of view, self-assembly processes have become of highly relevance as a promising method for

large-scale fabrication of functional nanostructures, with less waste and energy consumption than top-down processes.[3] More details about self-assembly approaches will be given in the following section.

2.1 Molecular self-assembly

Nature is a master in designing compatible chemical building blocks that can be organized into more complex structures. One well-known example is the silky assembly. A silk worm can spin thousand monomeric silk fibroins, with nanometre size, into silk materials over two kilometres in length. Since the structure determines the functionality, it is of paramount relevance to control the positioning of the monomers in the self-assembled structures. Another example is given by the proteins involved in the capture of light to activate the photosynthetic reactions. The efficiency of these proteins depends on a very specific spatial distribution of the pigments (chlorophyll molecules), which impede the exciton recombination and allows the development of redox reactions at specific moment and place after the photon absorption.[4]

Organic molecules are probably the most extensively used nano-objects for molecular self-assemblies. Their specific functionalization will allow the control over their mutual interactions and their interaction with the environment, and is the key to the desired specific self-organization. In this sense, a chemical complementarity and structural compatibility between nano-objects are indispensable. Independent of the organization, new features can be added to the final structure by the presence of specific chemical functions on the building blocks. Specific functions can accordingly be implemented, for applications in optoelectronics, photovoltaics, or sensing.

Various kinds of interactions play a role in the self-organization of nano-objects.[3] London forces are one example of attractive Van der Waals interactions. They are generated by fluctuations of the molecular electron density, giving rise to an instantaneous electrical dipole that generates another dipole inside a polarizable neighbour molecule. The interaction is thus an attractive induced diplole-induced dipole interaction. Similar phenomena occur when the molecules feature permanent dipoles. The dipolar interactions may be partly screened by the substrate, or induce dipoles in the substrate itself. Contrary to van der Waals interactions, at short distances the electron-electron interaction (between the electron clouds of each molecule) is repulsive. The balance of this so-called steric hinderance with the effect of attractive van der Waals interactions leads to a variety of self-assembled molecular lattices.

An additional kind of intermolecular interaction, which plays a key role in molecular self-assemblies, is the hydrogen bond. It is considered as a dipole-dipole interaction, related to the permanent polarization of chemical link involving the H atom, which is less electronegative than atoms it is often bond to, e.g. C, N, or O. Due to its complexity, a broad definition is required, as the one proposed by Thomas Steiner: "An X–H···A interaction is called a hydrogen bond if 1) it constitutes a local bond, and 2) X–H acts as a proton donor to A".[5] The hydrogen bond includes several contributions that are different in their nature, such as; electrostatic, polarization, charge transfer, dispersion and exchange repulsion. The relative weight of these contributions, implies that the hydrogen bond can be as weak as a Van der Waals interaction or on the contrary as strong as a covalent bond. The calculated energies for hydrogen bonding range from 0.2 to 40 kcal mol^{-1}. The most important parameters that additionally influence the strength of the bond are of geometrical nature, namely the distance between the atoms and the relative angles formed between the bonds. Again, these two parameters evolve differently with respect to the relative weight of the different contributions (e.g. electrostatic, polarisation). For instance, of all components the electrostatic contribution reduces the slowest with increasing the distance. Thus, for a donor–acceptor combination, the electrostatic contribution will dominate at long distances. Usually, the electrostatic term is the largest one. However, in the weakest kind of hydrogen bonds, the dispersion term may contribute as much as the electrostatic one. More detailed discussions about the hydrogen bond can be found is review papers.[5,6]

The non-covalent character of interactions in supramolecular assemblies, put limits on their chemical and thermal stability, and often hinders post-synthetic modifications. Reticular synthesis is another route to the bottom-up fabrication of ordered organic lattices. The most relevant products derived from this strategy are the covalent and metal organic frameworks, which will be discussed in the following section.

2.2 Reticular synthesis

Reticular synthesis consists of the conception of an extended network by a pre-identification and design of well-defined and rigid molecular building blocks, that will maintain their structural integrity during the construction process.[7,8] The network comprises reticulation nodes (also named vertex), usually in the form of molecular units having more than two branches forming bonds. Also, they include linkers, usually molecular units or atomic centres forming with two branches, which generate bonds (or linkages) with the reticulation nodes. This approach is different from the retro-synthesis of organic compounds, since the integrity and rigidity of the building components is kept. The vast variety of organic molecules with specific

functionalities and shapes, is often considered as a tool-box to design networks with desired geometry and properties. The synthetic conditions are obviously critical to control the degree of order (crystallinity). As it will be discussed in Section 2.4 by balancing the thermodynamics and the kinetics of the synthesis, crystalline two and three-dimensional frameworks can be obtained.[9,10]

Due to the increased interest shown in the past years for mastering the synthetic reactions in a controlled manner, a vast variety of new materials emerged, and hence, a flurry of new definitions arose. In this regard, two-dimensional (2D) polymers term has been re-defined in the time based on synthetic conditions or crystallinity degree, for instance.[11,12] In this thesis, Sakamoto *et al.* definition is followed and a 2D polymer is considered as a topologically planar, separable covalent monolayer sheet with internal periodicity.[13] Extensive definitions of metal and covalent organic frameworks will be given below, attending to the bonding nature without restriction of dimensionality. Thus, two-dimensional covalent and metal organic frameworks are considered as 2D polymers as well.

Metal organic frameworks (MOFs) are defined as extended crystalline and porous structures built by organic ligands and metallic centres and they are synthesised following the reticulation strategy. Here, the linkage consists in coordination complexes with molecular linkers or molecular reticulation nodes arranged around the metal centres. Although the coordination bond is usually more labile than the 'pure' covalent one, it is considered a strong interaction since the energy range values found are from 10 to 30 kcal mol^{-1}.[14] This moderate strength allows continuous association/dissociation processes of linkages, which gives the growing network the possibility to dynamically re-arrange, healing defects such as low-coordinated metal centres or polygonal pores creating costly crystal defects in the network. A well-chosen set of synthetic conditions (e.g. temperature, reactant concentrations) sometimes exists that allows to approach a close-to-thermodynamical equilibrium growth, leading to large MOF crystal with very few defects, and low energy. A single-layer and a few-layer two-dimensional metal organic networks synthesised by Sakamoto *et al.* presented domain sizes of > 10 μm on one side with hexagonal in-plane periodicity.[15] The optical properties shown by the single-layer material allow the confirmation of the successful complexation reaction between the organic ligands and the metal centres, yielding the formation of low-defected material.

The use of transition metal gives easy access to directional bonds with specific orientations, since their electronic structures give rise to specific geometries and coordination numbers.[14] First attempts to build metal organic frameworks with specific geometric pores, were achieved by Striklen et al. in 1983, when they synthesised the first square ring network by combining metal-complexes (metal = Cr,

W) with di-phosphine bridging ligands (Figure 2.1).[16]

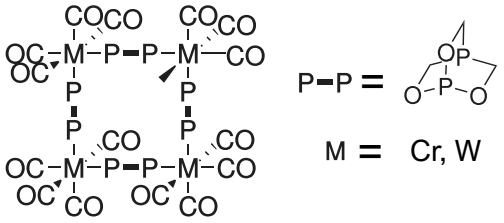

Figure 2.1: Complexation of a linear ligand with two bridgehead phosphorus atoms with a metal precursor leading to the formation of the first example of square coordination complex. Reproduced and adapted from reference 16.

After this discovery, plenty of new organometallic-based structures appeared following the rational design of precursors which will occupy specific positions (reticulation nodes or linkers) of the target polygon structure.[17–19] Baxter *et al.* shown the synthesis of a 3×3 closed inorganic superstructure with specific location of 6 ligands and 9 metal ions. This work opened the doors for a whole family of polynuclear inorganic (square- or rectangular-) grids with interesting prospects for the development of electronic devices for information storage.[20] The same approach was employed for the construction of three-dimensional structures or cages. An interesting review is done by Yoshizawa *et al.*, where they highlighted the developments in the application of artificial, self-assembled molecular hosts as functional molecular flasks. These systems can facilitate unusual chemical reactivity or isolate molecules and promoting new physical properties.[21] Enzymes are natural molecular flasks, which provide molecular-sized and -shaped pockets capable of binding substrates and catalyzing unique reactions.

The huge progress in the preparation, characterization and study developed on the MOFs in the past decades has been driven mainly by the broad scope of technological applications in which these materials can be employed. Their exceptional porosity, mainly stemming form the use of long organic linkers that yield void spaces, makes them suitable for gas storage, separation and catalysis.[22] Comparing with permanent-porous inorganic materials, like zeolites, the advantages of metal-organic counterparts are their flexibility in design and functionalization. One of the major advances in this regard was achieved by Li *et al.* when the formation of a robust three-dimensional cubic framework built by $Zn_4O(CO_2)_6$ octahedral clusters each linked by six chelating 1,4-benzenedicarboxylate BDC_2^- units was achieved.[23] The calculated pore volume values for this structure were from 0.54 to 0.61 cm^{-3} cm^3 (for different gas sorbates), which were comparable to and even higher than those

found for zeolites, that typically range from 0.18 to 0.47 cm^{-3} cm^3.

Covalent organic frameworks (COFs) are the other class of systems that can be produced by reticular synthesis. They are defined as crystalline extended organic structures in which the building blocks are linked by strong covalent bonds. Unlike in the coordination bonds, not all chemical reactions yielding covalent bonds allow dynamic exchange processes, that we discussed in the case of MOFs. To benefit from the added-value of the dynamic exchange process, specific reactions need to be selected. Generally, these reactions can be classified in terms of the linkages they form (Figure 2.2), and they are generally condensation reactions (that release water molecules upon the formation of the new covalent bond). Most commonly linkages employed in COFs synthesis are:

- B–O bond formation via boronate condensation.[9,24]
- C=N bond formation via imine condensation.[25]
- C=N_{Ar} bond formation.[26]
- C=C bond formation via Knoevenagel condensation.[27]
- C–N bond formation, via imide or amide condensation.[28]
- B=N bond formation via borazine condensation.[29]
- N=N bond formation.[30]

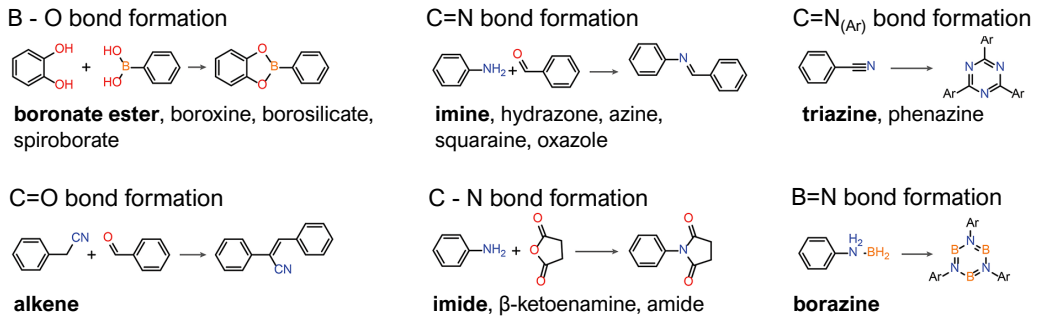

Figure 2.2: Typical linkages that have been used for the synthesis of the COFs. Taken from reference 8.

Covalent-organic networks were discovered by Côté *et al.* and they can be constituted by either one or two kinds of single molecules. The first synthesised COF is shown in Figure 2.3 and is obtained by the boronate condensation between benzene

diboronic acid molecules.[9] Here, the benzene structure is considered the linker, whereas the diboronic acid groups will lead to the linkages that will form the reticulation nodes of the structure, in this case by boroxine -O–B–O bonds. The molecules react to form a two-dimensional planar network with constant pore size of 15 Å.

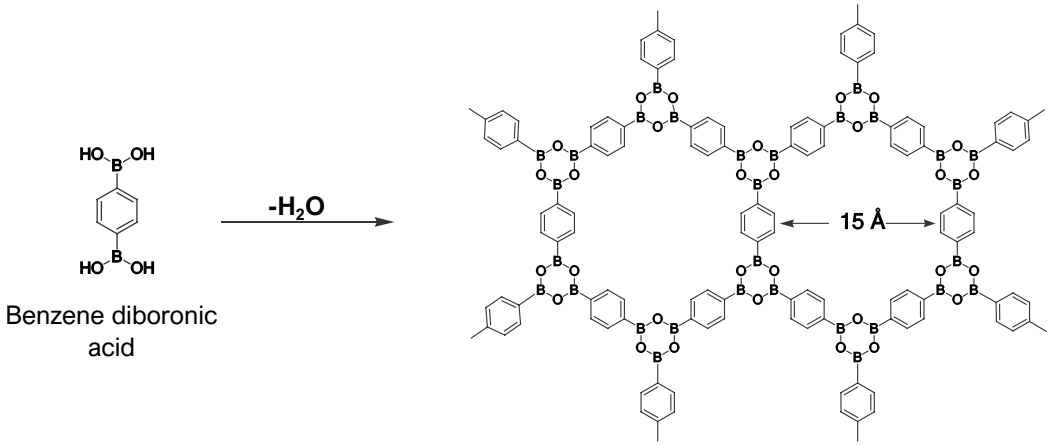

Figure 2.3: Synthesis reaction of first COF, based on the dehydration of benzene diboronic acid. Adapted from reference 9.

Another example of a COF synthesised by the condensation of two different organic molecules is exposed in the same work, following the a similar synthetic route.[9] In that case, benzene diboronic acid was mixed with hexahydroxy-triphenylene molecules leading to a bigger two-dimensional planar network with a porous size of 27 Å. For both systems, two-dimensional layered crystal structures were obtained, with distinct stacking modes. A staggered AB arrangement (analogous to the Bernal structure of graphite) of the reticulated molecular planes was obtained for the first COF, and an eclipsed arrangement, that found in hexagonal boron nitride, for the latter one.

Similarly to MOFs, covalent-organic counterparts present high-surface area being suitable for storing or capturing relevant gases. First applications were focused on this feature.[31,32] Due to their robustness and thermal stability, post-synthetic modification is also possible for COFs. Ding *et al.* prepared a two-dimensional COF with a 1.8 nm-wide pore which can capture metal ions through bi-dental coordination to nitrogen atoms disposed in the pores. It was demonstrated that this structure can be loaded by Pd^{2+} ions after its immersion in a $Pd(OAc)_2$ solution, establishing possible catalytic applications of COFs.[33]

However, the most relevant feature of covalent-organic frameworks from which

the study of these materials has increased enormously in recent years is their high intrinsic electronic mobilities. That, together with their structural versatility, have positioned two-dimensional COFs as a novel organic semiconductor component to be included in devices. More details will be given in Section 2.3, when an introduction about molecular electronics will be presented.

An additional definition is necessary in order to cover all aspects that this thesis will discuss. Covalent and metal organic frameworks have been synthesised so far, in many different forms: either in two or three-dimensional systems, yielding layered crystals, monolayers or multilayer forms. Another terminology exists, that refers to ultrathin two-dimensional materials, or equivalently to nanosheets. Such systems have a thickness of the order of a few atoms, overall thinner than 5 nm, and a lateral size from 100 nm to few micrometers.[34] Nanosheets and single-layer sheets have stimulated considerable interest recently, due to their superior flexibility, convenient interfacing with other materials, and possible electrical manipulation with electrostatic back-gates in field-effect transistor geometries. We will specifically discuss the synthesis of these important materials when addressing interfacial reactions in Section 2.6.

2.3 Molecular electronics

Molecular electronics is considered as a branch of nanotechnology and nano-electronics that studies and exploits molecular building-blocks for the fabrication of electronic components of devices. The onset of the miniaturization of these components began to gain relevance from the 60's. However, this new field strongly rose in the late 90's when lithography-based technologies were approaching the limits of their capabilities due to several problems: need of ever-thinner gate oxides, short channel effects, doping fluctuations and an increase of difficulties and expensive lithography processes. The growth in complexity, compactness and versatility in device functions in a minimum space and weight, constituted one of the major technological advances of the epoch. This tendency has been described since 1965, by the co-founder of Intel, Gordon E. Moore. He foresaw an increase of twice the total number of components per chip for each year over the next decade, laying the basis for what is now known as Moore's Law.[35] The real tendency, over the past 50 years, has been a double number of transistors approximately every 18 months. What really made possible the explosion of circuits complexity over the decades was the shrinking size of the transistors (from millimetre scale in 1940 for a typical transistor to few tens of nanometres in size in 2010). As a response to the limitations found by lithography-based devices and in foreseeing to extend the validity of Moore's law, the field of

molecular electronics started to be in the spotlight of the scientific community. It is considered that the idea of molecular electronics was conceptualized in 1999 by Mark A. Reed.[36]

The atomistic or molecular-scale technology associated to molecular electronics may become a new alternative device-building technology. In this context, reticulated systems have well-suited aspect ratio to be integrated in devices, but several severe limiting issues regarding their use as such remain. Among these issues, they indeed should be scalable up to large-areas with as few defects as possible, which call for synthesis close to thermodynamical equilibrium. Other issues include the interconnections with solid state electrodes, usually metallic ones. Also, achieving low resistivity contacts is often difficult. Solving all these issues is expected to open the way to inexpensive, flexible electronics as an alternative to the established silicon-based technologies.

Already in the early 70's, Aviram *el at.* presented semi-quantitative calculations about the feasibility of constructing a very simple electronic device, a rectifier, based on the use of a single organic molecule.[37] A rectifier is an element which converts the alternating current (AC) into direct current (DC). Common solid-states rectifiers are based on the use of p-n junctions, presenting a single electronic transfer direction as an indispensable condition. An organic molecule that will be used as a rectifier, should show p-n junction properties as well. This is possible thanks to the presence of certain substitutional groups on aromatic systems, which can redistribute the total charge of the molecule. Thus, an electron-withdrawing group will create an electron-poor region (p-type), raising the electron affinity of the central ring and making the structure a good electron acceptor. Likewise, an electron-donating substituent will generate an electron-rich aromatic centrer (n-type), lowering its ionization potential and leading to a good electron donor system. This is observed for the molecule shown in Figure 2.4, where the ceto groups (C=O) decrease the π-density of the central ring, whereas the methoxy groups (OMe) produce the opposite effect on the right part. The electron motion direction demanded in a rectifier would require to position, besides the cathode of the device, an acceptor molecule, and close to the anode a donor one, respectively.

The B orbital depicted in Figure 2.4a (LUMO of acceptor part) will receive the electrons from the cathode, which should be totally or partially empty and lie at or slightly above of the Fermi level. When a enough large voltage, $V>0$, is applied for the cathode level to overlap the acceptor level, the electron transfer becomes possible (Figure 2.4b). The way to connect the acceptor-donor parts, will be through a sigma bond, imposing the rectifier properties with an unidirectional electron transfer: from cathode $\rightarrow$ acceptor $\rightarrow$ donor $\rightarrow$ anode. Thus, it is proposed that the current passage

is done through three steps, indicated in Figure 2.3b with 'A', 'B' and 'C'.

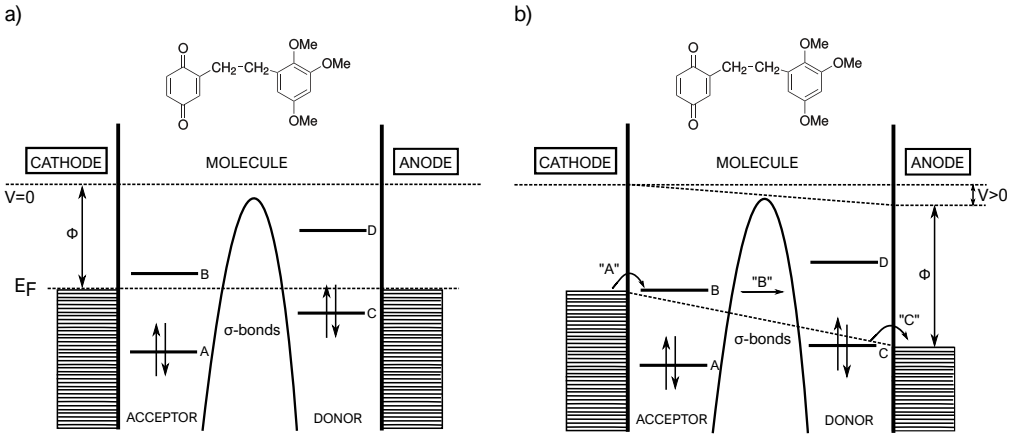

Figure 2.4: Example of a hemiquinone molecule which can act as a molecular rectifier. Energy versus distance diagram of the device built with this molecule. A and C are the HOMO of acceptor and donor parts, respectively, whereas B and D correspond to LUMO. a) Diagram at V=0 and b) Diagram at V>0. Reproduced and adapted from reference 37.

Since these first attempts and studies, the building of new devices based on organic molecular layers have been addressed extensively. Molecular candidates for being part of passive elements (*e.g* wires or resistors) or active parts (*e.g* switching or amplifying), include polyporphyrins, polyphenylenes, polythiophenes and other planar organic polymers with extended π-conjugation along the length of the molecule. A parallel field also emerged with the use of rigid-carbon structures with C_{60} molecules or single-wall nanotubes, even if they do not present the functionalization versatility of the above-mentioned molecules.

A key point to take into account when building a molecular-based device is the connexion of the molecular building-block with the metallic contacts. An efficient way to deal with that is the self-absorption of the molecular species on the contacts. Several advances have been done in the functionalization of molecular end groups with specific chemical components which present high affinity for the metal surfaces. This is the case of terminal thiol moieties, that can self-adsorbed onto gold contacts allowing conjugated oligomers to act as molecular wires in molecular-based electronic devices.[38]

In order to assure the success of a molecular-based device, it is important to choose a suitable link between the molecules. As mentioned above for the case of covalent and metal organic frameworks, the covalent intermolecular interactions are

more robust than their non-covalent counterparts and they assure an efficient electron transport through the bond and hence, the whole system. Much progress has been done on the study of the linkage between molecules that have been deposited onto metallic substrates in highly-controlled conditions, during the past years. The advantage of this approach is double; the substrate-molecule interactions can help for the dispersion of precursors, avoiding the growth of multilayer networks and the near field characterization techniques often employed in these conditions, offer exhaustive studies about the resulting structures and their linkages.

First studies on this matter were carried out by Grill *et al.* when they demonstrated how, by combining carefully chosen molecules with a specific functionalization, it is possible to form covalently bonded nanostructures, with a desired geometry.[39] They chose the square-planar porphyrin molecules as building-blocks and Au(111) single-crystal surface as a substrate. They designed different substituted porphyrins functionalized with one, two or four bromine atoms, to be removed by thermal treatment. Thereby, hierarchical growth of complex nanostructures can be achieved. Porphyrins with only one bromine atom, will develop into a single radical after heating up. A new carbon-carbon bond will be generated once two-free radicals are found on the surface, leading to a molecular dimer (Figure 2.5a). Similarly, a bi-substituted porphyrin - with the bromine atoms disposed 180^{o} apart- will derive into two free-radicals which, by combination between them, will generate linear chains (Figure 2.5b). Finally, a tetra substituted porphyrin will present four possible active sites after thermal activation, which will link into two dimensional networks (Figure 2.5c). An experimental dI/dV curve taken at the connexion between two molecular units reveals the presence of a peak around 3 eV confirming the presence of a covalent bond.

So, in general terms, the successful fabrication of molecular electronic devices lays on the control of a wide variety of parameters:ent leaving behind a radical in their positions (red dots). Then, they can combine by forming carbon–carbon bonds. The shape of the final structure depends on the nu

- The chemical nature and electronic structure of building-blocks, whose alteration upon chemical reaction need to be anticipated.

- The degree of order on the active layer, achieved by the well-choosing of catalytic or patterned surfaces, where molecules are deposited.

- The presence of impurities or dopants in the films, that can be controlled to some extent with catalytic or patterned surfaces, specially under kinetically or thermodynamic control, as it will be discussed in Sections 2.4.2 and 2.4.1.

– The morphology of the final organic films, which is strongly influenced by the initial design of the molecular building-blocks.

– The interface between the active organic layer and the surface that will eventually support it.

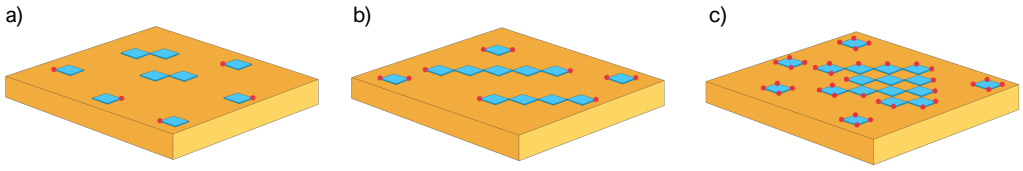

Figure 2.5: Controlled formation of a covalently bonded structure with porphyrin molecules (blue species) on a gold surface. Substituent bromine atoms can be lost after thermal treatment and location of the substituents, so a) depicts the formation of dimers when porphyrins are mono-substituted, in b) linear chains are formed by using bi-substituted porphyrins and c) shows an example of two-dimensional array formation by progressive activation of tetra-substituted porphyrins. Adapted from reference 40.

As previously discussed for the molecular rectifier example, strong donor/acceptor molecules lead to charge transfer phenomena. Such phenomena can involve the surface itself, specially when the substrate is a large electron reservoir, as it is the case with metal surfaces.

Normally, when a molecule is deposited on a surface it can suffer some morphological modifications, which consequently will derive into electrical ones. Depending on the degree of interaction between the surface and the organic molecules, three limit (idealized) cases are usually considered (Figure 2.6).[41] When organic molecules are far away from the surface, we find the ideal Schottky-Mott limit, where no alignment of energy levels happened, as shown in Figure 2.6a. In this case, the inherent surface dipole (which comes from the natural distribution of negative charge density into the vacuum side and the positive one on the bulk side) is not altered. However, when organic species are in contact with the metallic surface, but there is not direct interaction, a vacuum level realignment occurs, as it is depicted in Figure 2.6b. This happens in systems prepared normally in ambient conditions, where the hybridization of molecular and metal orbitals is negligible, often due to an oxide-layer formation. The vacuum level alignment generates injection barriers for electrons (Φ_B^e), and for holes (Φ_B^h). The former is given by $\Phi_B^e = \Phi_m$ - EA (EA: electron affinity) and it describes the energy necessary to inject an electron from the metal into the molecule. Whereas the injection barrier for holes is given by Φ_B^h = IP - Φ_m (IP: ionization potential) and corresponds to the energy necessary to inject an

electron from the molecule into the metal.

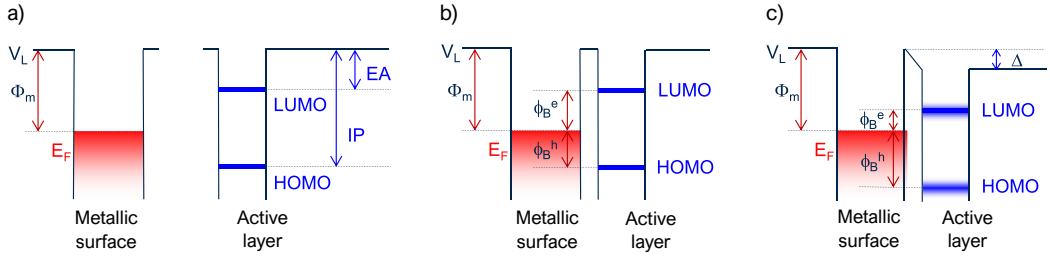

Figure 2.6: Scheme of the energy levels of a metallic surface and an organic active layer: a) when they are far away from each other, b) in contact, assuming vacuum level alignment and c) in contact after the formation of a surface dipole. V_L = vacuum limit, EA = electron affinity, IP= ionization potential, Φ_m = work function of the clean metal surface, E_F = Fermi level of the metal, Φ_B^e = electron injection barrier, Φ_B^h = hole injection barrier, Δ = interface dipole. Taken from reference 41.

In many cases, even for weakly interacting systems, the experimentally determination of these injections barriers yields different values than those expected from a simple vacuum level alignment. When the molecules are in contact with the surface, a re-alignment of electronic levels occurs, as it is depicted in Figure 2.6c. This produces a re-distribution of charge at the interface, hence an interface dipole, Δ. Among all possible factors that can contribute for the interface dipole, the most relevant ones are i) the rearrangement of the electron cloud of the metal surface, due to the repulsion induced by the presence of the electron clouds of the absorbed molecules, ii) the presence of a molecular dipole (permanent or induced by the substrate) and iii) a charge transfer between the metal and the organic layer. In any of these cases, the injection barriers are given now by $\Phi_B^e = \Phi_m$ - EA - Δ and Φ_B^h = IP - Φ_m + Δ.

Charge transfer processes between molecules and substrates can lead to molecular conformation changes,[42,43] substrate reconstructions,[44,45] substrate-mediated interactions[46] and new chemical reactions pathways that otherwise are not observed in solution.[47,48] In summary, a thorough analysis of electronic properties and effects derived of them at the interface, together with an exhaustive study of the interface's geometry, will be essential to understand the physical behaviour of the final device.

2.4 Organic two-dimensional materials

Of importance on the final material's properties is its dimensionality.[49] A representative example is the case of sp^2 carbon materials: 0D fullerenes, 1D nanotubes, 2D graphene and 3D graphite exhibit very different properties. After the isolation of a monolayer graphene sheet for the first time[50] a variety of new inorganic 2D materials emerged (e.g. transition metal dichalcogenides, or boron nitride among others) due to their interesting properties.[34] It turns out that their optical and electronic properties are usually different from their 3D counterparts due to confinement of electrons and because of the absence of interlayer interactions, which can play an important role in determining the band structure. Additionally, other properties can be improved (i.e. mechanical and chemical response) making these new materials candidates for molecular electronics, sensors and optoelectronic devices.

The already mentioned natural curiosity and ability of chemists to create and modify matter launched the interest on organic 2D materials. In particular, first theoretical studies focused on the electronic characteristics of graphyne (a carbon phase which contains planar sheets of a mixture of sp^2 and sp hybridized bonds), put in evidence the interest of 2D polymers with a conjugated back-bone for interesting electrical purposes.[51] Graphyne shown a semiconducting behaviour, with large bandgap, as well as the possibility of tuning its electronic properties with respect to the periodicity and topography. Since then, great attention has been paid to synthetic 2D polymers with well-defined in-plane crystalline structures in the past years.[34] Usually, they present covalent linking between monomers, forming permanent pores of defined size and shape. The bottom-up synthesis of these materials is governed by the control monomer assembly, before and during the covalent bonding process. Two strategies provide such control: thermodynamic and kinetic approaches,[52] which we will explain in details in their corresponding sections (Section 2.4.1 and 2.4.2, respectively). Both of them require rigid and robust monomers, which form directional interactions, driving the formation of specific geometries.

2.4.1 Kinetic control approaches

In kinetic approaches, the polymerization process occurs on a pre-organised two-dimensional assembly, where the bond self-repairing took place (Figure 2.7). This approach is compatible with irreversible reactions or conditions, since when the polymerization occurs (second step in the scheme) the assembly is already ordered.[52]

Preparation of covalent and metal organic frameworks under highly-controlled conditions (*i.e* ultra high vacuum - UHV) is an example of kinetic controlled two-

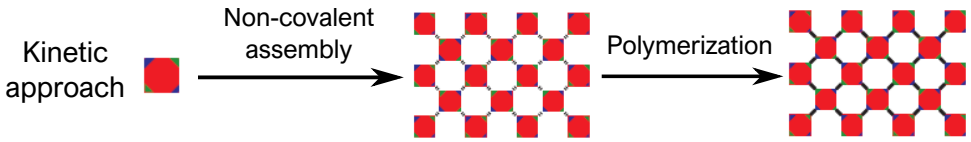

Figure 2.7: 2D polymerization processes under kinetic control. Red squares represent monomers, where blue and green triangles correspond to functional groups. Solid black lines represent covalent bonds formed during polymerization and dashed black lines are non-covalent interactions formed before polymerization. Adapted from reference 52.

dimensional polymerization growth. Many examples of reversible reactions, such as the condensation processes already mentioned in Section 2.2 or other traditional reactions that will be discuss in Section 2.5, have been successful adapted to the UHV environment.[53–56] Typically, during a polycondensation reaction a by-product in the form of a small molecule is produced (*e.g* water, alcohols, and hydrogen halides). The presence of these small "impurity" molecules may affect negatively the polymerization kinetics, altering the reaction mechanism. In order to reduce the effect of these by-products, annealing or working under vacuum conditions are strongly recommended. The feasibility of implementing these condensation reactions was demonstrated for the first time by Zwaneveld *et al.*[53] The already mentioned condensation reaction of benzene diboronic acid molecules by Côté *et al.* under mild conditions,[9] was then demonstrated on Ag(111). A boronate-based covalently bonded nanoporous was formed, composed by five-, six-, seven- and eight-membered rings.[53]

This seminal work established the potential of surface science approaches to control and scrutinize the chemical and physical processes that occur when molecular building blocks react to form bonds and extended networks. Understanding the atomistic processes requires well-defined systems and controlled conditions. For these reasons, atomically-clean single crystals are commonly employed as a reaction substrate. Pressures of the order of value of $\sim 10^{-10}$ mbar are kept during reaction processes, to limit the amount of surface contaminants. Also, the lack of solvents reduces the interactions and interferences between the molecular building blocks. The progress of the surface science field has been boosted by the expansion of surface science techniques such scanning probe microscopies, photoemission spectroscopies and diffraction, which along with theoretical methods give fundamental and fine insights about on-surface reaction mechanisms,[57,58] including the formation of intermediate species, the role of the substrate,[59] and molecular diffusion among other effects. More details about the surface science techniques employed in this thesis are given in chapter 3.

As noted, the surface can act as a template for the growth of two-dimensional networks. Specially, metallic surfaces are of the great relevance, all the more as they can have desirable catalytic effects.[60] They can kinetically enhance reactions by reducing the activation energy barriers. This catalytic behaviour is founded on the ability of the metallic surface to create bonds with the molecules. Once the molecules absorb on it, strong or weak interactions can be established with the surface, which additionally has strong influence on the surface diffusion of the molecules. Then, the surface can ease the cleavage of some intermolecular bonds and help forming new ones when the new chemical products are created.

The catalytic activity greatly depends on the electronic structure of the metal surface, in particular on its *d*-band configuration. Upon absorption, the electronic states of an adsorbed molecule and of the metallic surface interact. The Newns-Anderson model plots three different regimes of adsorbed organic molecules on metal surfaces depending on molecule–substrate interaction strength: i) physisorption, ii) weak-chemisorption or iii) strong-chemisorption.[61,62] Two important parameters are defined in this model, the bandwidth of the metal bands (W) and the hybridization strength (ΔE) between organic-metal orbitals. The latter is obtained by the difference between, the energy of separate molecules and surface and the energy of the hybrid system. The physisorption regime is usually found when weak van der Walls forces govern the molecule–substrate interactions (it is often the case of inert surfaces). In this case, molecular orbitals are similar to those of the gas phase and are not altered by the substrate. A more complex scenario is found for more reactive metal surfaces. For metal surfaces with large bandwidth, W $>$ 10 eV, (*e.g.* Ag and Cu), a W/ΔE $\gg$ 1 ratio can be estimated and a weak-chemisorption regime is considered. This is observed for the case of Ag/perylenetetracarboxylic dianhydride (PTCDA) interface.[63] In the case of narrow *d* metals, W$\sim$ 1 eV, (*e.g.* Ni), a W/ΔE $\gg$ 1 ratio is found yielding to a large hybridization. This is the case for strong-chemisorpted systems, as is observed in H/Ni interface.[64]

The metallic's band structure is composed by a broad *s*-band and a sharp *d*-band. Since the electronic state of the former for all transition metals is the same (filled by only one electron), is the *d*-band which determines the catalytic behaviour of a metallic surface. It is considered that the electronic states of the entire *d*-band of the metal are crucial for controlling the surface reactivity. The density of states at the Fermi level, may shows the electrons that are prone for bonding, and the empty *d*-states above the Fermi level will play an important role in the molecule-surface interaction. Many studies have demonstrated the important role of the substrate in terms of efficient on-surface chemical reactions.[59,65,66] Gutzler *et al.* shown the feasibility of building a two-dimensional network through C–C bond formation

when a metallic substrate was employed. An homolytic rupture of C–Br bonds takes place as a first activation step. Then, after on-surface diffusion of these active species their encounter leads to the formation of a new C–C bond. However, when instead the inert surface of graphite was utilized, no activation occurred, leading to the formation of a non-covalent self-assembled well-ordered network stabilized by hydrogen-halogen bonds.[65]

In this regard, structural surface defects also deserve a word. The presence of steps, vacancies or adatoms change the chemical environment of the adjacent areas, affecting the catalytic activity of the surface.[67,68] This was shown, for instance, in the case of the adsorption of dibromoterflurene molecules on a stepped gold surface.[67] By means of low temperature scanning tunnelling microcopy, the step-edge kinks were identify as the active sites of the surface, where the C–Br bonds are selectively dissociated. Then, thermally induced polymerization led to oligomer chain formation, along the edge steps.

2.4.2 Thermodynamic control approaches

Thermodynamic approaches consist in monomer assembly and polymerization simultaneously, as it is shown in Figure 2.8. They rely on reversible reactions, such as condensation or coordinative processes already mentioned when discussing the formation of covalent and metal organic frameworks. The bond self-repairing of the second step leads to a well-defined and corrected crystalline structure.[52] In a standard reversible reaction, the precursors A and B can react yielding C and D products, which can react together to give the reverse reaction. Thanks to le Chatelier's principle, the control over the reaction conditions (temperature, precursor's or product's concentrations, volume or pressure), drives the equilibrium direction.

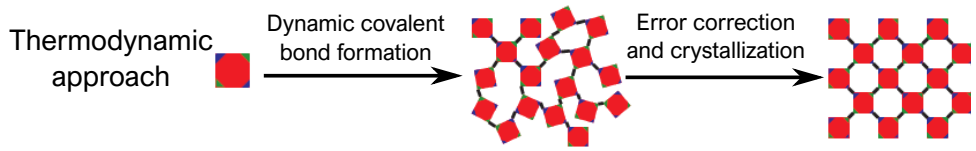

Figure 2.8: 2D polymerization processes under thermodynamic control. Red squares represent monomers, where blue and green triangles correspond to functional groups. Solid black lines represent covalent bonds formed during polymerization and dashed black lines are non-covalent interactions formed before polymerization. Adapted from reference 52.

The mild synthetic conditions employed by Côté *et al.* for the synthesis of the first benzene diboronic acid-based COF, introduced in Section2.2, is a good exam-

ple of synthesis under thermodynamic control. Benzene diboronic acid molecules were heated at 120° C during 72 h in a mesitylene-dioxane solution. This allows the slow dehydration of the molecules and their controlled diffusion due to a low solubility. This strategy allows the nucleation of crystalline material, and also, the close reaction system maintains the presence of H_2O, ensuring the reversible conditions and the crystalline growth.[9] The presence of H_2O during the reaction process changes de Gibbs energy and pushes the equilibrium backward to favour a reverse reaction. This reversibility allows the self-adjustment and self-healing of the system, resulting in the formation of high ordered porous nanostructures. Oxidation-sensitive and low-solubility molecular precursors are not very well-suited to the strategy we just described. Polyfunctional catechols are prone to oxidation and are often sparingly soluble in organic solvents, factors that hinder both, the preparation of useful quantities of functionalized monomers and their incorporation into COFs. Thus, alternative synthetic routes were needed after the blossom of the first synthesis. Spitler *et al.* proposed an acetonide protection (-R'–O–R–O–R') over these sensitive cathecolate groups, yielding to a boronate ester-linked COF, as previous example, but employing more complex precursors.[69] In both cases, the products were in form of insoluble powder, hindering subsequent applications and scalability. Therefore, the methods that yield the synthesis of multilayer or nanosheets in a controlled orientation directly on a support are of great interest.

With these constraints in mind, Colson *et al.* demonstrated that surfaces offer a natural interface to template polymerisation in two dimensions, and performed the condensation reaction done by Côtè *et al.* in the presence of the desired support.[10] They successfully grew oriented COF films on single-layer graphene supported in a variety of supports (polycrystalline copper foil, Si wafers or SiC support), with minor amounts of residual reactants. Interestingly, they observed the formation of crystalline films just after one hour of reaction, while typically the standard reaction lasts 72h.

However, albeit the synthesis describe above yielded crystalline and ordered films, no control in the thickness was achieved. When advanced electronic applications are targeted, a more accurate fabrication method is needed. Mechanical exfoliation processes are a possible route to incorporate layered material into devices, however the lack control on the thickness, and the lateral extension of the material is still limited by chemical synthesis routes. As an alternative, lateral polymerization reactions or, so-called interface reactions, enable the synthesis of not limited length crystals since the polymer or nanosheet is suspended on the interface where they growth. Most relevant interfacial reactions are held at liquid/liquid or air/liquid interfaces. With these techniques the synthesis of two-dimensional polymer monolayers are easily accessible since the polymer suspended at the interface is then transferred to the

desire substrate, depending on the application or characterization mean. Both approaches and examples will be address in Section 2.6.

2.5 Surface mediated of two-dimensional polymerization and chemical transformation

As discussed earlier, metal surfaces have become an important platform for the growth of polymer and are very well-suited for surface science studies. In this section, we will detail a general protocol for polymer growth in ultra-high vacuum conditions as well as the role's surface during on-surface molecular arrangements (in terms of molecule-molecule vs molecule-substrate interactions). Then, several on-surface chemical reactions will be detailed. Finally, specific advantages associated with the use of a metallic surface as a reaction substrate (confinement effect) or by using highly-controlled conditions (reaction control) will be addressed.

Under ultra-high vacuum conditions, the building blocks are deposited by molecular beam epitaxy onto a clean surface. In general, the organic molecules are evaporated from their powder state but alternative deposition methodologies are available for thermolabile species or species which polymerize inside the crucible. Molecular spray deposition is yet another approach, where the desired organic molecule is dissolved in a convenient organic solvent and is then deposited directly on the surface.[70] With this method almost any kind of organic compound can be used avoiding damage or fragmentation. In the case of synthesis of metal organic frameworks or simply formation of coordinated bonds, metallic centres can be supplied by thermal evaporation of high-purity materials. Additionally, some specific metal surfaces, *e.g.* copper or silver, naturally provide metal adatoms coming from the atomic step evaporation or vacancy formation.[71,72]

In general, the two-dimensional arrangement of molecules on solid surfaces is determined by the balance between intermolecular forces and molecule-substrate interactions. In the case of weak substrate-molecule interactions are present, the intermolecular forces will govern the molecular assembly. Planar molecules tend to lay parallel to the surface and bulky molecules, or molecules with voluminous groups, tend to occupy hollow sites of the substrate. When heteroatoms are present in the molecule, stronger molecule-substrate interactions can occur, even if the molecular back-bone is not disrupted. Usually, the molecular absorption occurs where the overlapping between lone electron pairs of the molecule and surface d-states is maximum. In the case of molecules with more than one heteroatom, specific molecular orientations might occur. If the surface is not homogeneous (*e.g.* due

to different chemical compositions or lattice parameters) or the molecule-substrate interactions are really strong (*e.g.* important charge transfer phenomena led by strong donor/acceptor molecules), site selective adsorption might take place and in these cases, chemical transformations can occur.[73]

2.5.1 On-surface chemistry as a tool of creating long-term stable structures

From a practical standpoint, surface functionalization with molecular structures is a route to functional molecular electronics devices (Section 2.3). On a more fundamental level, ultrahigh vacuum conditions allow the synthesis of substances that may not be synthesised in solution due to solubility problems, and sometimes gives access to new chemical synthesis pathways due to surface confinement of the reactants. In this section we will give an overview of the main on-surface chemical reactions which allow the synthesis of new bonds for network growth. The reviewed reactions will be classified into different categories: reactions with carbon–halogen bond cleavage (or dehalogenation reactions), reactions with carbon–hydrogen bond cleavage (or dehydrogenation reactions) and reactions producing water molecules (or dehydration reactions).

Dehalogenation reactions

These reactions involve the cleavage of a C–X (X = F, Cl, Br, I) bond. The high polarity of these bonds makes their rupture easy and so, they have been widely used in classical organic chemistry synthesis. Several well-known reactions which produce new carbon-carbon bonds, are based on these chemical groups. The classical Ullmann coupling reaction, described in 1904,[74] allows the selective formation carbon-carbon bond between two aryl molecules, by a Cu mediated activation of an aryl halide, as shown in Figure 2.9.

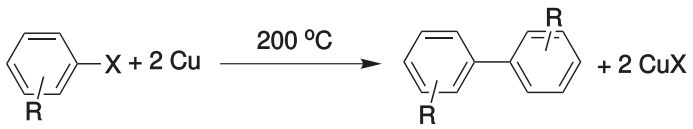

Figure 2.9: Ullmann coupling reaction mediated by copper between two aryl halides. Reproduced from reference 57.

The homolysis of the carbon-halide bond can take place at room temperature, yielding to a single radical. Then, further thermal treatments usually lead to the addition of radicals generating the new (carbon) bond.[39,65,75,76] Although Cu is the catalyst par excellence, Ullmann coupling reactions can be performed with other

metals such as Au,[39,65] and Ag.[77] An important application of this reaction developed in the past years is the graphene-nanoribbons growth.[78,79] The presence of different type of halides in the same molecular structure allow a higher control over the reaction. Due to a different C–halide bond strength, the bond cleavage takes place at different annealing temperatures. This strategy is considered as what is known as a hierarchical synthesis.[80,81] It was demonstrated by Lafferentz *et al.* with a phenyl-porphyrin selectively functionalized by bromine and iodine (Figure 2.10a) and deposited on Au(111) surface.[80]

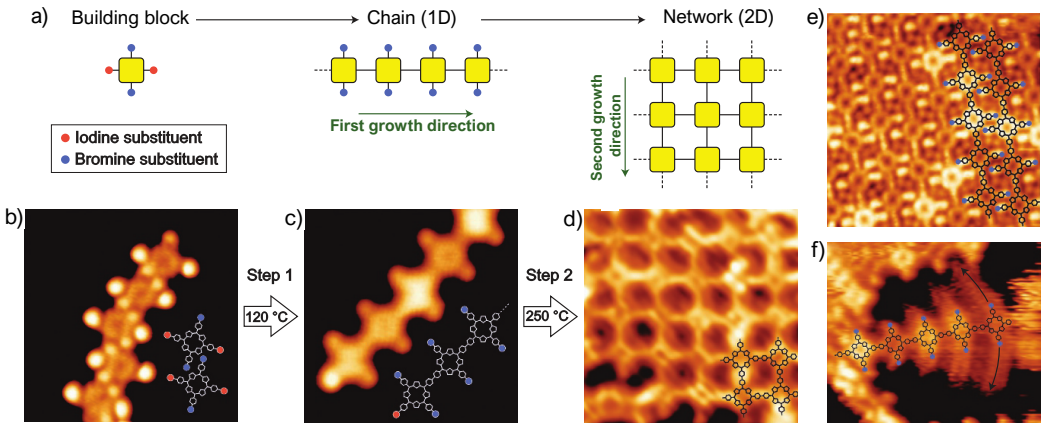

Figure 2.10: a) Two step activation mechanism of the Ullmann coupling using iodine and bromine substituted-porphyrins. Pristine molecules b), form linear chains c) after a first activation step by thermal treatment. After further annealing, an extended two-dimensional network is formed. Taken from reference 80.

In a first annealing step at 120 °C, iodine atoms are cleaved off from the porphyrin structure, whereas the bromine atoms stay intact. This leads to the activation of the first direction growth, with the formation of one-dimensional chain (Figure 2.10a). A second thermal treatment at 250 °C was carried out, producing the C-Br bond cleavage. Now, the second growth direction is activated allowing the cross-linking of previous molecular chains, leading to an extended two-dimensional network (Figure 2.10b).

Likewise, other coupling reactions which generate C–C bonds were proposed by Sonogashira, Heck or Suzuki. All of them are cross-coupling reactions, where two different precursors, A and B, are joined assisted by a metal catalyst, typically palladium. These in solution reactions are extremely useful for generating C–C bonds with highly selective reaction between AB leading to the desired network, while inhibiting the formation of homocoupling products AA or BB, which is often difficult. This was evidenced by Kanuru *et al.* when they presented for the first time the

on-surface Sonogashira reaction on Au(111).[82] The homocoupling products of both reactants, phenylacetylene and iodobenzene, were found on the metal surface alongside with the expected cross-linking product (Figure 2.11-upper reaction). Although the selective cross-coupling was not achieved entirely, the milder synthetic conditions employed with respect to the ones needed in solution, constituted an advance for the accessibility of these kind of reactions. It was few years later, when a full cross-linking on-surface Heck reaction was achieved by Shi *et al.*, that the successful coupling of bromophenyl-diphenylporphyrin to a vinly derivated was demonstrated on a Au(111) surface, by using Pd as a catalyst (Figure 2.11-lower reaction). First principle calculations revealed that the presence of Pd on Au(111) is essential for promoting the high-selective cross-coupling reaction.[83]

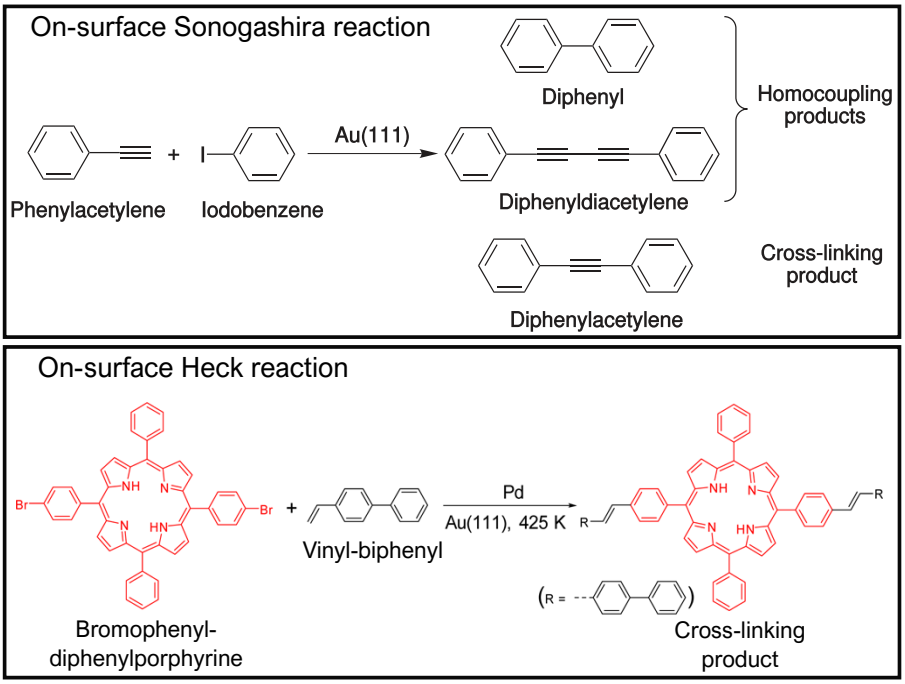

Figure 2.11: On-surface Sonogashira coupling in vacuum on Au(111) and homocoupling products of iodobenzene and phenylacetylene reactants. Reproduced and adapted from reference 82. On-surface Heck coupling on Au(111) leading to cross-linking product as a unique reaction product. Adapted from reference 83.

Dehydrogenation reactions

These reactions involve C–H bond cleavage. They are of valuable interest in classical organic chemistry since they allow to transform alkanes into alkenes (much more

versatile). The small size of hydrogen atom, makes it difficult to track it by scanning tunnelling microscopy or x-ray photoelectron spectroscopy. Mass spectroscopy performed *in situ* during annealing allows to monitor the dehydrogenation process, by tracking the signal of the dihydrogen molecule. Another way to indirectly follow a dehydrogenation process is by analyzing the core-level shift of an specific species when the hydrogen atom is lost by the molecule (*e.g.* the O 1s core-level shift when a carboxylic acid group undergoes to a dehydrogenation, transforming it into a carboxylate group)[84] The energy of a C–H bond is 4.5 eV,[58] which implies that it is quite inert and catalytic-assisted reactions are needed to make it react. A large variety of strategies has been explored for C–H bond activation. One widely exploited approach has been the activation through the use of aromatic groups.[48,85]

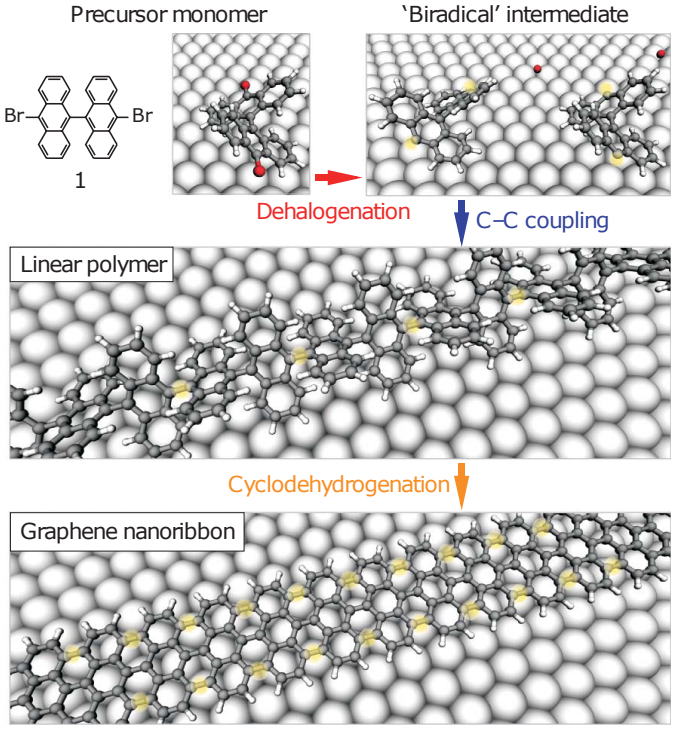

Figure 2.12: Steps for surface-supported graphene nanoribbons synthesis. The dehalogenation of dibromo-bianthryl molecule (1) occurs upon adsorption on Au(111) surface. Linear polymer formation upon first thermal treatment. Finally, the cyclodehydrogenation occurs after second annealing by the loss of hydrogen molecules. Adpated from reference 83.

Cai *et al.* deposited dibromo-bianthryl molecules on a Au(111) surface leading to the formation of biradical intermediates, through Ullmann coupling process (first step in Figure 2.12). A thermal treatment at 470 K allowed their diffusion across the

surface and a radical addition reaction occur, forming a linear chain (Figure 2.12).[85] An additional annealing of the Au(111) substrate, produced the loss of a dyhydrogen molecule and the formation of a new C–C bond. This last step is known as cyclodehydrogenation process, which involves the cyclization of an organic molecule due to C–H bond cleavage.

Soon after, a dehydrogenative C–C coupling reaction of long-chain linear alkanes was proposed by Zhong *et al.*[47] The alkane molecules physisorbed on the Au(110) undergone a C–H bond dissociation. The loss of available hydrogen atoms on the surface shifts the equilibrium towards the formation of new C–C bonds. Zhong *et al.* proposed a low activation barrier for the subsequent C–C bond formation, once the intermediates are formed.

Dehydration reactions

These reactions involve the combination of two or more molecules to form a larger one, and a small molecule is released, like water (herein the dehydration or condensation names). The condensation reactions typically employed for the covalent-organic framework synthesis were already listed in Section 2.2. All of them have been adapted to fit ultra-high vacuum conditions, and the ones involved in the boroxine bond formation were already detailed in the kinetic controlled approaches section (Section 2.4.1). Herein, most relevant examples of on-surface dehydration reaction, which leads to C=N (imine) bond formation, will be discussed.

The interest of these reactions lies mainly on the possibility of incorporating several chemical groups into the final product by using two or more reactants, which is of particular interest when all chemical groups cannot be included in a single molecule. Also, it is noteworthy that the initiation step may require no annealing process and organic molecules may be activated by simply co-deposition. This is the case of the two-component condensation reaction between the dialdehyde and the aliphatic amine chosen by Weigelt *et al.*, shown in Figure 2.13.[86] The reaction was performed at room temperature and close to saturation of the first monolayer of co-deposited reactants on a Au(111) surface. Known as Schiff-base condensation, the last step in which the tetrahedral intermediated is covered into the imine product, is normally catalysed by the solvent (acting as a combined proton donor/acceptor). However, Weigelt *et al.* pointed out a more favourable reaction mechanism in which an intermolecular proton transfer occurs, substituting the solvent's role.

Like boroxine bonds,[53,54,56] the C=N bond is involved in the surface synthesis of two-dimensional polymeric structures, allowing a covalent linking between

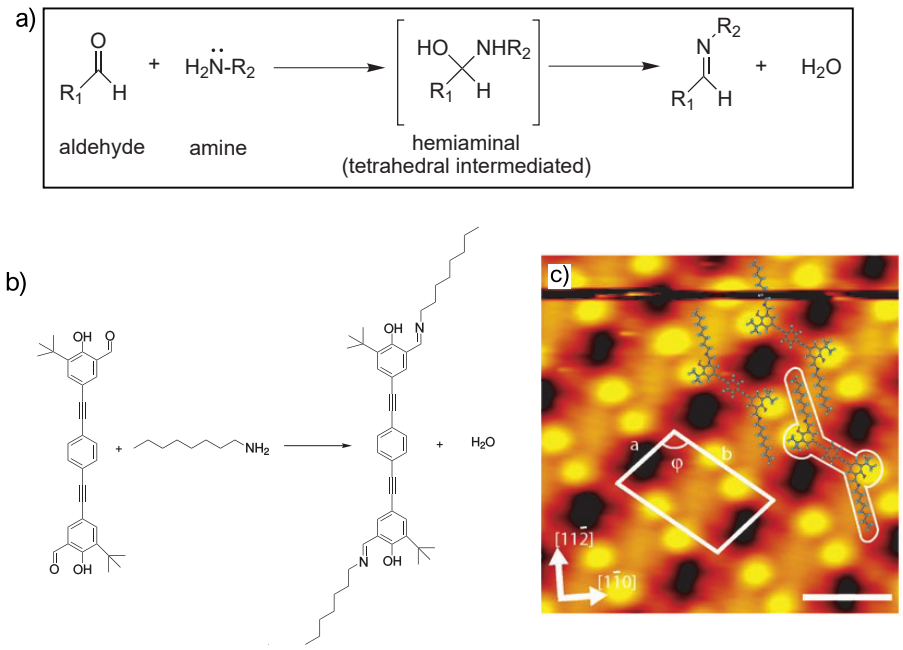

Figure 2.13: Generalized-solution catalysed formation of C=N bond (imine) from an aldehyde and an amine. b) On-surface dehydration reaction of coadsorbed dialdehyde and aliphatic amine on Au(111). c) Laterally ordered diimine structures formed on Au(111) surface at room temperature via Shiff-base condensation. Adpated from reference 86.

precursors, with interesting collective electronic properties as well as high thermal and chemical stability. Later, Weigelt *et al.* synthesised polymeric nanostructures consisting in both, oligomeric chains and networks with pores of about 3-10 nm in dimension by the combination of bi- and tri-functionalized precursors.[87] It is noteworthy that the connectivity of polymeric nanostructures was controlled by adjusting the kinetic parameters during the growth. Two different approaches were tested, in which the trialdehyde was always first dosed onto the surface. Then, a first strategy consisted of the subsequent deposition of the diamine at 120-160 K and the reaction was performed at 400 K. This led to small oligomers linked via imine bonds. The second strategy consisted of depositing the diamine on top of trialdehyde when the substrate was already at 400 K, allowing a higher molecular diffusion for both reactants. This approach led the formation of both, two-dimensional networks and one-dimensional chains.

Similar reactions have been explored also on a variety of metallic surfaces, such as the condensation between the highly reactive acyl chlorides with amines on Ag(111), yielding the corresponding polyamides,[88] or the formation of polyimides on Au(111)

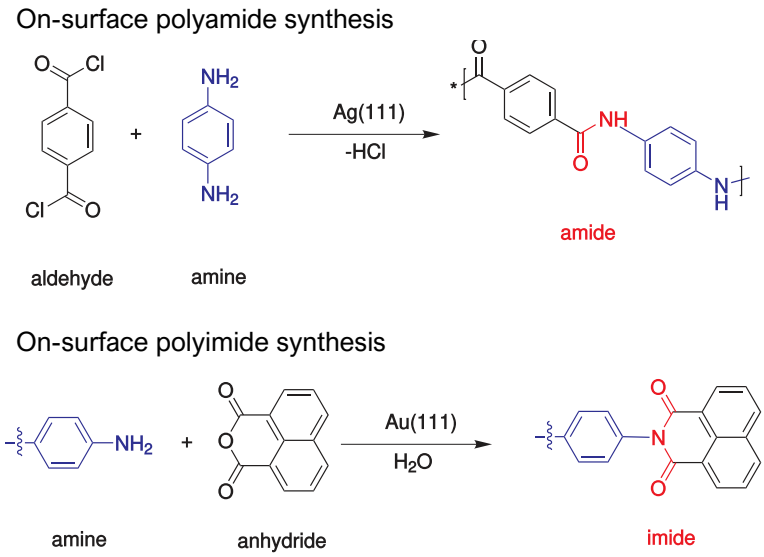

Figure 2.14: Reaction of an amine with an aldehyde and with an anhydride leading to amide and imide products, respectively. Adapted from reference 88, 89.

after the convergence of dianhydride-derivative and di or tri-amino compounds.[89] One- or two- dimensional polymers are obtained depending on the stoichiometry and reactants employed. Associated reaction schemes of aforementioned on-surface reactions are shown in Figure 2.14.

2.5.2 Ultrahigh vacuum conditions for reaction control

Intermolecular coupling reactions on surfaces have demonstrated to be a suitable synthesis method for metal and covalent organic frameworks. The vast variety of possible combinations between organic molecules and/or metallic centres allows to modulate both, the shape and size of the pores as well as the specific features of the final structure. Although well-established chemical reactions are readily adapted to highly-controlled conditions, a fine tuning or reaction conditions is always necessary. Many examples in the literature make references to stoichiometry and substrate temperature regulation in order to get a specific product.[53–55,90–92] Another possible approach is to vary the length of the reactants or the number of substitutional groups on them. With this strategy, it is possible to favour, for instance, the formation of two-dimensional networks rather than one-dimensional chains,[81,87,89] or to tune the pore size of the final network.[53,93,94] Yet another way to control the final product is through hierarchical growth or subsequent activation. In this regard, few examples have been already discussed,[39,79,80] where a well-selected monomer, with different

substitutional chemical groups, and so, different bond strength, are subsequent activated via consecutive thermal steps. This allows the controlling over the direction growth. Further examples can be given.[81,95] Zhang *et al.* synthesised a network with conjugated back-bone under mild conditions by using terminal alkynes.[95] The interesting point of this work is the control over the coupling by substrate temperature, since the deposition of alkyne-molecules on Ag(111) at 170 K, results in their self-assembly; rising the system at room temperature, reduces considerably the molecular coverage, and an annealing at 330 K restores the pristine surface. However, by deposition onto hot Ag(111) at the same temperature, the dimerization and oligomerization is induced, being favoured by further thermal treatments. This hierarchical process demonstrates how sensitive is the alkyne C–H activation and reactivity to subtle changes of the local environment. Also, the mild conditions in which the homocoupling takes place pointed out the catalytic behaviour of Ag(111) surface.

2.5.3 Two-dimensional confinement effects

Confinement to two dimensions appeared as an important benefit of the use of a surface for the creation of covalent structures. The dimensional restriction enables new reaction pathways with respect to other synthetic approaches.[47,48,96,97] This has been shown for the transformation of the four-fold brominated anthrathiophene into pentacene molecule, by deposition of the former on Ni(111) and thermal annealing to 473 K.[96]

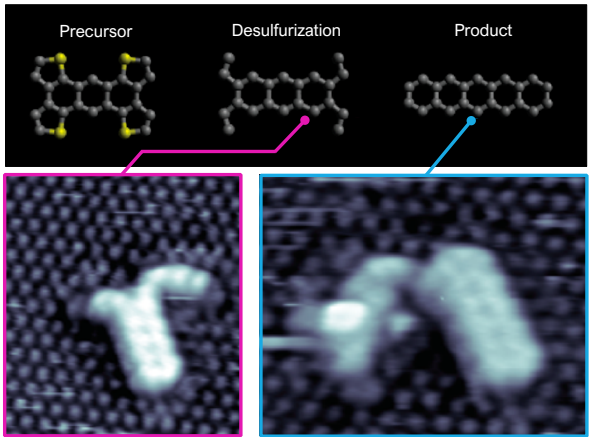

Figure 2.15: Representative STM images of products after deposition of brominated anthrathiophene (precursor) on Ni(111) and annealing at 470 K After desulfurization, elongeted linear features without lateral protrusions are found, which are identified as pentacene molecules. Adapted from reference 96.

In this conditions the reaction mechanism proposed is the dehalogenation followed by a desulfurization reaction. At this step an unsaturated species is formed, which undergoes a dehydrogenation reaction to form pentacene (Figure 2.15). The adsorption of the molecules on Ni(111) not only produces the C–S bond cleavage, but also stabilises the reactive intermediated allowing a posterior intramolecular rebonding leading to a new cycle formation.

An interesting case about the advantages of studying chemical reactions on surfaces is shown by Matena *et al.* They achieved the C–C coupling between N-heterocyclic end molecules (1,3,8,10-tetraazaperopyrene) on Cu(111) after a thermal treatment.[97] The low solubility of this precursor and the high activation barrier associated to the polymerization process have been historically a practical obstacle for its investigation. However, the reduction of molecular degrees of freedom by their adsorption on a surface, leads to the reduction of the polymerization activation barrier, allowing the covalent linkage between these aromatic molecules. This study is a step forward on the understanding of the concatenation mechanism, since it is thought that it occurs through the tautomerization of the N-heterocyclic end units to carbene intermediates (Figure 2.16).

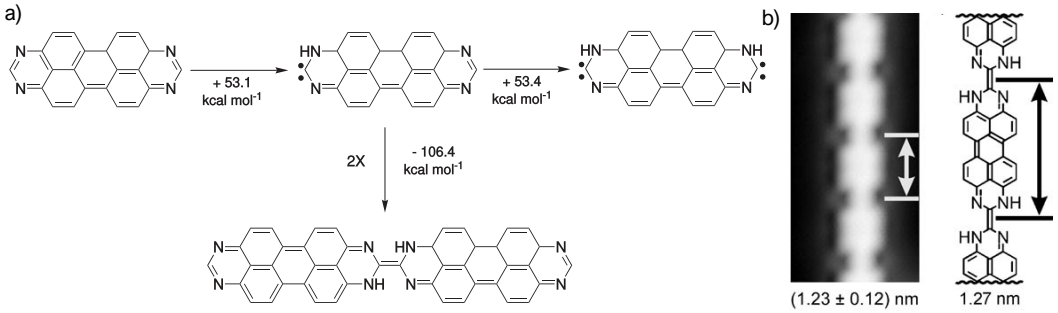

Figure 2.16: a) Single and double tautomerization of N-heterocyclic end precursor (1,3,8,10-tetraazaperopyrene) deposited on Cu(111) leading to the dimerization. b) STM image of a polymeric chain formed on surface by the mentioned precursor and schematic model of the expected structure. Adapted from reference 97.

2.6 Interfacial polymerizations

The necessity to control the thickness of polymer nanosheets and to achieve high structural quality such that, good charge carrier or spin transport, or pure optical properties, is a strong motivation in the field of molecular electronics. The study of on-surface growth performed under well-controlled environment such as a ultrahigh

vacuum chamber is particularly insightful to understand the chemical processes at play during the formation of molecular networks or the metal/molecule contact. In view of material production and applications, obviously more versatile and cheap strategies are desirable. Lateral polymerization reactions are performed at the interface generated between two fluid phases, each hosting a single kind of precursor, and it appears as a more application-compatible approach. The key features of this relatively new approach are: flat and uniform interface whose size can in principle be large, a constant supply of monomers and catalysts from the involved phases and ambient conditions. Since no exfoliation steps are needed, mechanical damage and undesired crumpling or folding of the layers can a priori be avoided. Instead, gentle transfer to virtually any kind of substrate is possible, following the horizontal Schaefer or Langmuir-Blodgett methods.

A Langmuir-Blodgett system is illustrated in Figure 2.17a, where the monomers (grey sticks) are spread at the surface of that contains another kind of monomer or a catalyst (green circles). A thin film is formed in the air/liquid interface, whose compactness can be adjusted by gentle in-plane pressure applied by lateral barriers. Then, once the polymerization reaction is complete, a solid host substrate (chosen, *e.g.* with respect to the application or characterization to be made) is approached to the interface. Figure 2.17a (3-4) illustrates the horizontal Schaefer transfer method, where the substrate is approached from the top until the interface. Once the contact of the polymeric film and the substrate is reached, the latter is smoothly withdrawn and thus, the synthesized layer is lifted off from the interface.

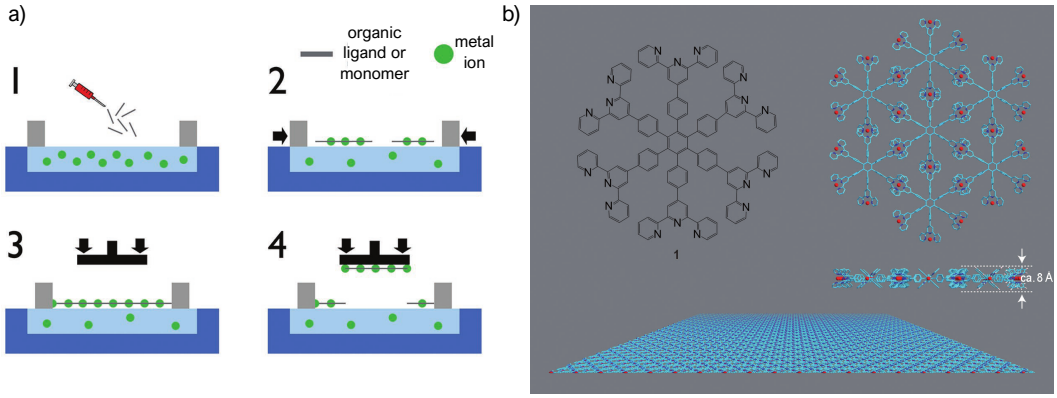

Figure 2.17: a) Cartoon of two-dimensional lateral polymerization at air/liquid interface. Adapted from reference 98. b) Chemical structure of monomer used by Bauer *et al.* and representation of the expected two-dimensional organometallic network (metal ion red, C turquoise, N blue). Taken from reference 99.

First lateral polymerization reactions where demonstrated by Bauer *et al.*, when they reported the first free-standing organometallic monolayer sheet prepared at air/liquid interface.[99] Figure 2.17b shows the chemical structure of the monomer that they employed, consisting of a hexafunctional terpyridine structure, which was specifically designed for this purpose. The (nano)sheet was expected to be formed at the air/water interface by deposition of the monomer 1 onto the water phase which hosts a metal salt. The polymerization reaction is based on the metal complexation of the terpyridine groups of two adjacent monomers. For this thermodynamically-controlled reaction, experimental conditions have been adjusted in order to adapt the reaction pathway (*i.e.* variation of metal ions/salts and their concentration, pH values, surface pressure, temperature of liquid phase and also how to deposit the monomer onto the surface and the metal ions into the liquid). The monomer design is of utmost importance to limit parasitic interactions between molecules or with the liquid phase that would promote competitive reaction pathways and hence would reduce the polymer stability and degree of order.[100] An important development was done in this direction by Payamyar *et al.* who used an amphiphilic monomer (having both, hydrophobic and hydrophilic parts) for an air/liquid interfacial reaction.[100] Thanks to this strategy, the hydrophobic part stands upright on the interface driving the molecular packing orientation.

2.6.1 Extended π-conjugated polymer nanosheets at interfaces

The polymer electrical conductivity stems from either, conjugated double bonds along the back-bone or aromatic chemical groups, linked together or with the carbon back-bone through covalent bonds. Undoped π-conjugated polymers have their Fermi level crossing the conduction band since one of the four electrons which compose the carbon valence band remains unpaired (belonging to p_z orbital). The alternation on single and double carbon bonds along the polymer, generates an overlap between p_z orbital allowing the delocalization of unpaired electrons over the whole system. However, if there are no charge carriers within the polymer structure, this will not be conductive. Most organic conjugated polymers do not have intrinsic charge carriers. Therefore, external charge carriers should be introduced to the polymers to make them conductive. When an electron is removed from the valence band by oxidation (p-doping) or is added to the conducting band by reduction (n-doping) does the polymer become highly conductive. By this way the conduction (valence) band ends up being partially filled (unfilled) and a radical anion (cation) is formed. These charged species are commonly known as polaritons and their formation causes the injection of states from the bottom of the conduction band and top of the valence band into the band gap.[101]

Several post-synthetic alternatives are available for doping polymers: Redox or electrochemical reactions and photo-induced doping. Alternatively, the conductivity may be increased by designing special monomers comprising well-suited heteroatoms or by using synthesis schemes that involve the formation of organometallic reticulation nodes. Neutral conjugated polymers with a small conductivity, typically in the range of 10^{-10}–10^{-5} S cm^{-1}, can be converted into semiconductive or conductive states with conductivities of 1–10^{4} S cm^{-1}.[102]

Lateral polymerization at interfaces produces nanosheets and in some cases monolayers (the thickness of a single molecule). The gentle transfer is thought to only marginally alter the intrinsic electrical conductivity. This is of paramount importance in view of their application to electronic and optoelectronic purposes.[98,103–106] The first interfacial synthesis of a π-conjugated organometallic nanosheets was reported by Kambe *et al.*[103] The polymer comprised nickel bis(diothiolene) units which were formed by a coordination reaction between benzenehexathiol molecules and nickel(II) acetate. The planar and three-fold symmetric configuration of the ligand alongside with its multi-chelating character drive the organization of the units leading to a sixfold symmetry. Additionally, Ni ions adopts a d^8 electronic configuration with, as the more favourable configuration, square-planar coordination. The strong charge delocalization among the metaldithiolene rings results in a well-developed π-conjugation.

Two routes were explored, one synthesis at air/liquid interface and another one at liquid/liquid interface. In the former synthesis, the benzenehexathiol is dissolved in an organic solvent which is gently spread using a microsyringe on top of an aqueous phase where the Ni(II) acetate is dispersed. By this method, a nanosheet of 0.6 nm was synthesised after 2 h of reaction at room temperature and in Ar atmosphere, in which the organic solvent was evaporated. Then, it was transferred onto a graphite surface (HOPG) for full characterization. An additional synthesis at liquid/liquid interface was carried out aiming at the formation of a thicker nanosheet, hence better suited to a comprehensive analysis of the crystallinity and composition. In this case, the organic phase was first overlaid with pure water. The difference in density makes that the organic phase stays in the bottom and leaving the thin layer of pure water on top. Then, the aqueous phase which contains the ion metal was smoothly added on top of the organic phase, allowing a calm liquid-liquid interface. With this approach, a microsheet with $\sim$100 μm lateral size and 1-2 μm of thickness was obtained. The redox states for both, micro and nano-sheets, were analysed and it was found that they can be switched from 0 to -1 by means of chemical reduction with a sodium salt. Finally, in a two-electrode configuration, the electrical conductivity of both systems was measured. It was found that the as prepared micro-sheets gave a conductivity of 0.15 S cm^{-1} at 298 K, while after

reduction with the sodium salt, the conductivity dropped to 6.7×10^{-3} S cm^{-1} at the same temperature. The multivalence states (0/-1) in the microsheet contributes to a higher conductivity.

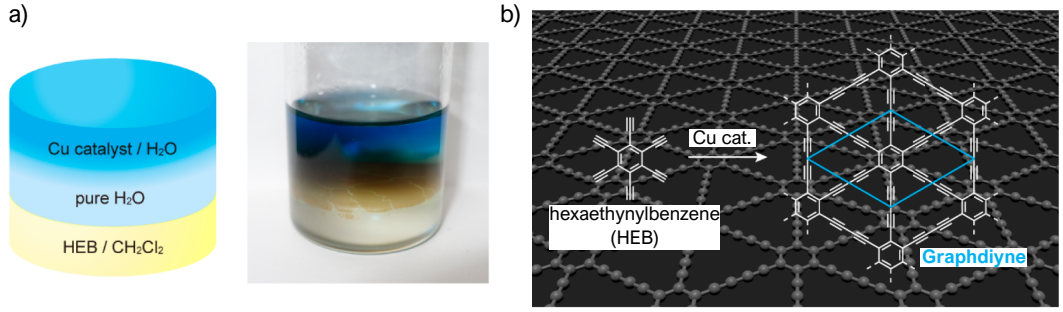

Figure 2.18: a) Cartoon and picture of two-dimensional lateral graphdiyne polymerization at liquid/liquid interface. Hexaethynylbenzene monomers (HEB) are dispersed in dichloromethane (CH_2Cl_2) and the copper catalyst in the upper aqueous phase. b) Chemical structure of monomer used by Bauer *et al.* and representation of the expected two-dimensional organometallic network. Adapted from reference 107.

Interesting advances in the synthesis of polymer nanosheets with fully carbonated back-bones have been done more recently by Matsuoka *et al.* A highly crystalline monolayer ($<$ 3 nm) of graphdiyne was obtained by air/liquid interfacial homocoupling reaction between, hexaethynylbenzene (HEB) (see structural model in Figure 2.18b), catalysed by copper ions present in an aqueous phase.[107] The synthesis procedure is similar for the one shown in Figure 2.17. After 24 h the nanosheet was invisible to the naked eye, but it was successfully transferred to various substrates for its characterization. Similarly, the synthesis of a thicker (24 nm) graphdiyne nanosheet were accomplished at liquid/liquid interface, in the form of a dark brown film (Figure 2.18a). Its insolubility already indicated that its back-bone is π-conjugated. Spectroscopic characterization (X-ray photoemission spectroscopy) confirmed the good expected crystallinity of both polymer sheets, that is required to account for the ratio of two observed between the sp and sp^2 contributions to the C 1s core level spectra. The calculated carbon/oxygen ratio for the monolayer was 0.09, lower than the 0.2 value calculated for the ticker graphdiyne sheet grown at liquid/liquid interface. The latter in turn was in the range of values for graphdiyne grown by other methods ($\sim$ 0.2) or other carbon-based materials grown by CVD. A low oxygen defect level is crucial for the good performance of carbon-based materials. Raman spectroscopy confirmed the presence of conjugated diyne linkages, as well as the D and G peaks expected for graphdiyne materials.

The wide variety of materials that can be synthesized at interfaces is a good

illustration of the versatility of lateral polymerization synthesis. As properties improve, the next step is the scalability of the process. As discussed in the Section 2.1 devoted to molecular self-assembly, spontaneous molecular re-organization is of utmost relevance for process scalability since a low energy investment is required and low wastes are generated. Following the same argument, the scalability of lateral polymerization will be more favourable if bond formation is based on some spontaneous and reversible process. In this respect, dynamic covalent chemistry is an interesting tool which allows the synthesis of polymeric nanosheets with robust and stable structures in ambient conditions.

2.6.2 Dynamic covalent chemistry: a self-repairing methodology for polymerization growth

Dynamic covalent chemistry embraces chemical reactions which are carried out under thermodynamic control conditions. Covalent bonds are formed and broken, and finally reformed continuously while the reaction progresses. Historically, organic compounds synthesis was dominated by irreversible reactions where reactants were designed to follow a specific reaction pathway yielding a product. The irreversible nature ensures that once the product is formed, not further transformations will be produced (at least under the same conditions). Reversible reactions were already shortly defined in Section 2.4.2 devoted to thermodynamic control reactions. The products formation and proportion under thermodynamic conditions are governed by their relative stabilities (*i.e.* $\Delta G_B > \Delta G_C$) and not by the relative barrier activation energies of transition states (*i.e.* $\Delta G_B^{\ddagger} > \Delta G_C^{\ddagger}$) as it is shown in Figure 2.19a. For a dynamic reaction, the change in free energy during the reaction must be favourable, that is a ΔG^0 negative in the following equation: $\Delta G^0 = \Delta H^0 - T\Delta S^0 = -RTlnK$. Thus, control over the products can be achieved by either introducing certain features into the starter monomers which stabilize the desire product (*e.g.* steric, electrostatic effects) or by driving the reaction equilibrium (following le Chatelier's principle in a number of external factors such as temperature, pressure, concentrations, impurities, and so on) towards the formation of the desired product.[108]

Some features are in common between dynamic covalent and supramolecular chemistry. Both involve reversible processes and the products formation are under equilibrium conditions. However, some major differences exits for instance, the kinetics of both processes. Dynamic chemistry is generally slower than supramolecular chemistry and to accelerate the process catalysts are usually employed. The use of a catalyst gives the additional advantage to possibly adjust the reaction kinetics towards a specific product, for instance by stopping the evolution of the system at a given stage of the overal reaction.[108]

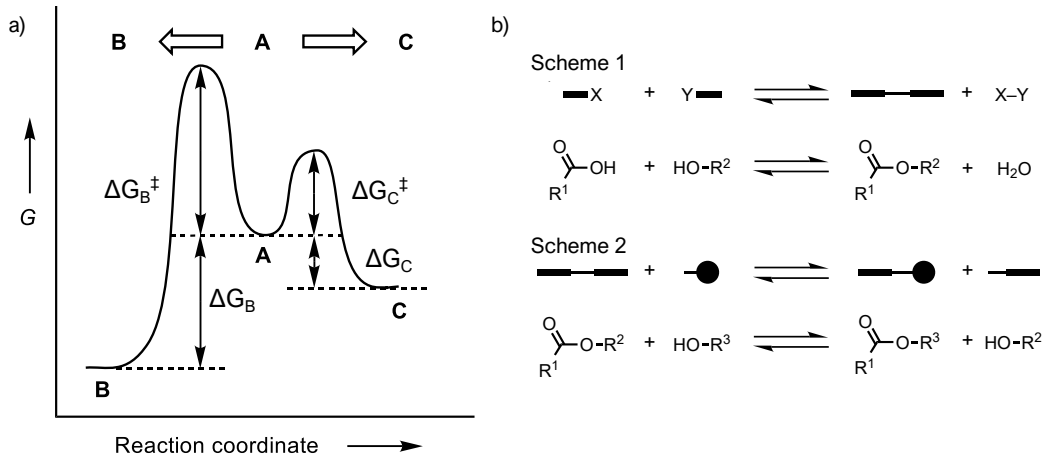

Figure 2.19: a) Free energy profile illustrating kinetic (A ⟶ C) Vs thermodynamic (A ⟶ B) control of the product distribution. b) Two possible types or reversible reactions. Scheme 1 involves the formation of a new type of bond and Scheme 2 shows a direct exchange reaction. Adapted from reference 108.

Two possible categories of reversible reactions can be considered regarding the bond formation mechanism. The corresponding reaction schemes are shown in Figure 2.19. Scheme 1 refers to reactions in which the formation/scission of the reversible bond leads to the formation of a new type of bond. Usually it involves the formation of a condensation product with loss of a small molecule (*e.g.* condensation reaction between a carboxylic acid and an alcohol leading an ester new bond). Scheme 2 represents a direct exchange reaction where the new bond formed is of the same type in both starting materials and products (*e.g.* trans-esterification reaction; from one ester and one alcohol, different ester and alcohol products are generated). This requires the use of a catalyst, which helps to initialise and/or speed up the reaction. In the following, we will be focused on a specific reversible bond chemistry based on the formation of imine covalent bonds (C=N); its characteristics and synthesis at air/liquid and liquid/liquid interfaces.

2.6.3 Dynamic imine chemistry involved in polymerization reactions at interface

Dynamic imine chemistry is represented by the reversible imine bond (C=N) formation, which takes place between an amine and aldehyde (Figure 2.20). It is involved in the Schiff base condensation reactions which produce the famous Schiff's bases family compounds. A general Schiff condensation occurs between a carbonyl group

(*e.g.* aldehyde groups) and an amino group with the loss of a water molecule. Constitutionally, the products look like the structure of Schiff's bases (Figure 2.20), where R is an aryl group, R_1 is a hydrogen atom, an alkyl or an aryl group, and R_2 is an alkyl or aryl group (without H atom). The reaction is acid-catalysed, and the equilibrium is usually controlled by removing water that forms as a by-product (physically, in a Dean-Stark apparatus, or by adding a drying agent).[109]

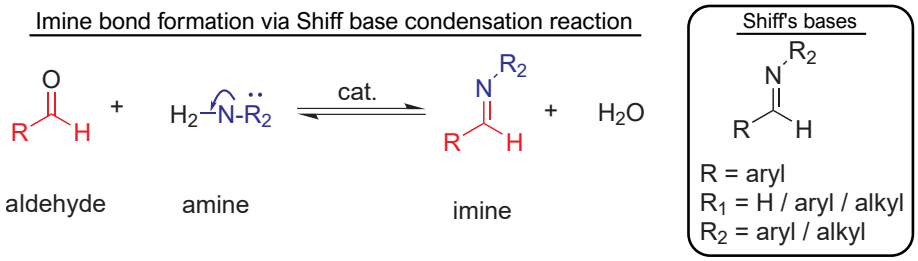

Figure 2.20: Imine bond formation via Schiff base condensation reaction between an aldehyde and an amine molecule. Inside the box a general structure of Schiff's bases is shown. Adapted from reference 109.

The imine bond formation is special, since not all covalent bonds are capable of being formed, broken and reformed under equilibrium control and relatively fast. Also, the chemistry behind the imine bond allows that once the desire imine is formed, still is possible to 'fix' it, by reducing the imine bond to a secondary amine function, trapping the product in a kinetic manner. An illustration of its versatility is the wide variety of exotic molecules and complex structures that have been synthesized in the past years (*e.g.* self-sorting systems, molecular motors, configurational switches, MOFs, COFs, molecular cages, and so on).[109,110]

Two significant works were published almost simultaneously from Sahabudeen *et al.* and Dai *et al.* in 2016. Both synthesised two-dimensional conjugated polymers at air/water and/or liquid/liquid interfaces via dynamic imine chemistry.[111,112] Dai *et al.* approach lays in the thoughtful monomer structures which facilitate the polyimine condensation at an air/liquid interface. The targeted imine-linked two-dimensional covalent monolayer displayed hexagonal pores, as it is shown in Figure 2.21a. The structure will be formed by linkers, composed by terephthaldehyde molecules (1), and reticulation nodes, which will be constituted by a three-fold symmetric amino phenyl-benzene molecule (2). The latter also bears three hydrophobic n-hexyl groups. Once the monomer 2 is spread on top of the liquid phase, n-hexyl groups will stand up on the surface (*i.e.* pointing into the air), while all the phenyl rings will stay in the interface. By this strategy, the triamine (2) and dialdehyde (1) molecules will orient themselves facilitating the imine bond formation. The success

of the interfacial reaction carried out at ambient conditions overnight was demonstrated by Raman spectroscopy. Both, the existence of imine bonds and the absence of end groups (aldehydes and imine ones) were evidenced. By tapping-mode AFM, the monolayer thickness of the poylyimine structure was assessed to about 0.7 nm.

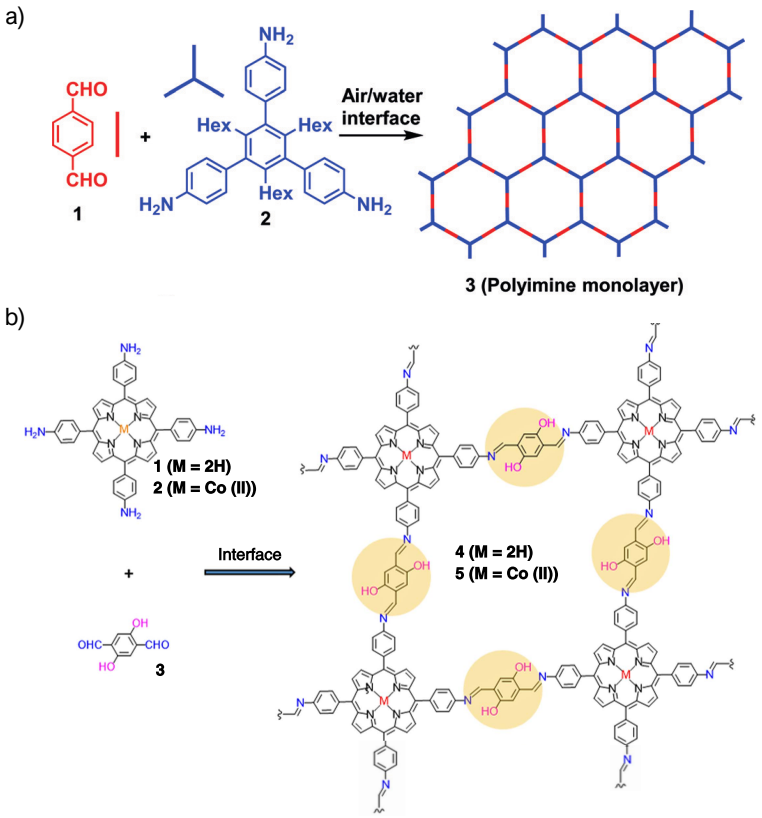

Figure 2.21: a) Two-dimensional synthesis of polyimine network by using terephthalaldehyde (1) and 1,3,5-trihexyl-2,4,6-tris(4-aminophenyl)benzene (2) at air/water interface under ambient conditions. Taken from reference 111 b) Two-dimensional synthesis of polyimine network by using 5,10,15,20-tetrakis(4-aminophenyl)-21H,23H-porphyrin (1) or 5,10,15,20-tetrakis(4-aminophenyl)-21H,23H-porphyrin-Co(II) (2) and 2,5-dihydroxyterephthalaldehyde (3) at an air–water and water–chloroform interface, respectively. Taken from reference 112.

The imine polymeric reaction designed by Sahabudeen *et al.* uses monomers whose structure was designed to give superior robustness and stability to the final polymer (and not to improve the synthesis process itself).[112] Careful choice on the linker (2,5-dihydroxyterephthalaldehyde, (3)) and reticulation node (monomer 2) was done (see chemical structures of monomers 1 and 2 in Figure 2.21b). Here, the

presence of hydroxyl groups in the adjacent position with respect to the aldehyde will introduce an additional stability trough an internal H-bond once the imine bond will be formed. The two-dimensional monolayer network (0.7 nm thickness) grown at an air/water interface was the size of a 4-inch wafer and presented an outstanding mechanical robustness with a Young's modulus of $\sim 267 \pm 30$ GPa. This value is on the same order of graphene ones (40-1000 GPa). A proof-of-concept validation was done on the monolayer when it was integrated in a thin-film transistor as active semiconductive material. A mobility value of 1.3×10^{-6} cm^2 V^{-1} S^{-1} was measured, confirming that the π-conjugation of the polymer was kept and the potential of these synthetic two-dimensional polymers to be used as semiconducting material under ambient conditions.

A parallel experiment was carried out at an liquid/liquid interface, combining monomer 2 and 3 yielding a two-dimensional multilayer network. In this case, the difference with respect to previous reaction is the coordination of cobalt atoms to four nitrogen atoms of porphyrin structure, yielding a direct functionalization of porous channels in the multilayer polymeric system. These Co–N_4 sites can serve as active sites for electrocatalytic hydrogen generation from water.

2.7 Main applications

Undoubtedly, the envisaged main application of synthetic two-dimensional materials, regardless of their chemical bond nature or synthetic process is the molecular electronics. As discussed extensively in Section 2.3, their semiconducting behaviour and their inherent metallic conductivity are essential features for their incorporation in optoelectronic[15,113–115] and electronic devices.[103,105,107,112,116–118] The ultrathin nature of these semiconductors makes them resistant to short-channel effects while having high flexibility. Besides, the surfaces of layered two-dimensional nanomaterials are free of dangling bond, which alleviates the surface scattering effects.

In this context, many contributions have been done by Nihishara's group creating functional bottom-up nanosheets, including electrically conductive nickel bis(dithiolene) nanosheets.[103,104] Same authors synthesised a photoactive complex nanosheet built by dipyrrin units and zinc(II) ions through an air/water interfacial reaction.[15] The bis(dipyrrinato)zinc(II) complex act as a network's linker and also presents strong absorption in the visible and near-infrared region. The photoelectric conversion capacity of this photoactive layer was demonstrated by decorating a transparent SnO_2 working anode and its implementation in a three-electrode electrochemical cell. Anodic current response was measured when the SnO_2 electrode was irradiated with 500 nm light and no response was observed using light at $\lambda < 400$ nm or

$\lambda > 560$ nm. With this study they demonstrated the first photofunctional bottom-up nanosheet based on bis(dipyrrinato)zinc(II) complex. Simultaneously, Takada *et al.* reported on a electrochromic bottom-up nanosheet.[113] The electrochromism consists on the material's colour or opacity change while applying an external voltage. In this work, metal complexes nanosheets comprising three-fold symmetric terpyridine ligands and Co(II) and Fe(II) ions. Taking advantage of the fast and robust redox activity of the bis(terpyridine)metal complex units, quick and reversible electrochromic properties of multi-layer nanosheets were demonstrated when they acted as active layers on a device. Both, Fe(II) and Co(II) complex nanosheet were placed on either side of a pair of transparent indium tin oxide (ITO) electrodes and an external voltage of + 2V was applied. By this, Fe-based nanosheet was oxidized and Co-based nanosheet was reduced and a visual change in both nanosheet's colour happened. Then, by applying an external voltage of + 1V a reduction and a re-oxidation of oxidized Fe-nanosheet and reduced Co-based one, respectively, took place. By the last redox reaction, the original colours of both complex nanosheets were recovered. This study suggests the potential application in eletrochemical devices such as colour displays and electric paper.

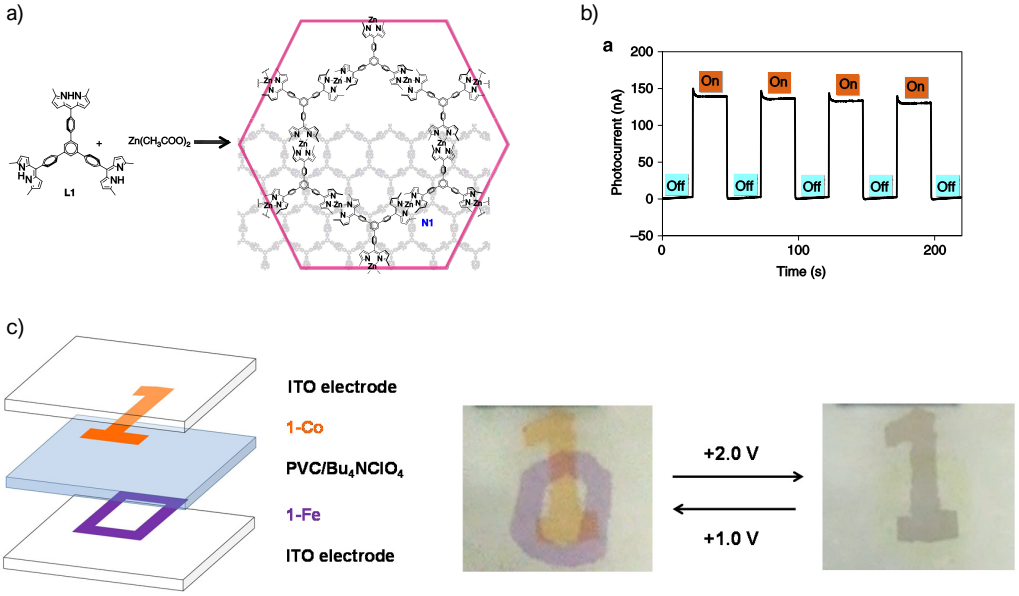

Figure 2.22: a) Chemical structure of three-fold dipyrrin ligand and the bis(dipyrrinato)zinc(II) complex nanosheet. b) Typical anodic current response on irradiation of aSnO_2 modified electrode with a bis(dipyrrinato)zinc(II) complex nanosheet. c) Structure of the electrochromic device built by bis(terpyridine)Fe(II) and Co(II) complex nanosheets, and the operational process by applying external voltages. a), b) taken from reference 15 and c) taken from reference 113.

Additional advantages are offered by the possibility of a wide tailoring of their properties, either thanks by the network's dimensionality, or by the chemical properties included from the building blocks. Theoretical works indicated that the bandgap of 2D COF's can be significantly tuned by the crystalline size, and is much narrower than their 1D polymer counterpart.[119]

The different available synthetic routes and the control of their thermodynamics and/or kinetics are essential for optimizing the quality and size of single-crystalline domains, as we already discussed in the previous sections. Apart from their semiconducting behaviour or metallic conductivity, important features regarding mainly covalent and metal organic networks have been highlighted. Their high chemical and thermal stability and their extraordinary morphological and compositional tunability have made these materials the focus of the attention in applications as sensing,[32,76,120–123] catalysis,[33,112,124–126] and energy storage and/or conversion,[76,127–130] among others.

Ultrathin 2D materials have been widely used as part of sensing devices for the detection of various specific chemical or biological species (*e.g.* gas molecules, toxic ions, chemical molecules and biomolecules). These systems need of high sensitivity, selectivity and stability in a given environment as well as fast detection. The responsiveness toward incoming guest molecules, resulting in changes in their physical and chemical properties. First selectively sensing of nitro explosives (*e.g.* trinitrophenol molecules) based on a metal organic material was reported by Nagarkar *et al.*[123] They reported that the electrostatic interactions formed between the strong acidic proton of the trinitrophenil molecule and the specific basic sites located in the pores, yield to an electron and energy transfer to the MOF. This produce a strong quenching of the network fluorescence.

As it has been already mentioned in the course of this chapter, covalent and metal organic frameworks present superior potential in absorption, gas storage and specially in catalysis than amorphous porous materials. The first example of design, synthesis, and application of an imine-linked COF material for catalysis was reported by Ding *et al.*[33] As in other solid catalysts the imine-linked COF designed by the authors showed the main characteristics that a good catalyst material must present; high stability to thermal treatments, water and most of organic solvents, and the incorporation of catalytic active sites in its structure. Previously, it was demonstrated that the nitrogen atoms which are part of the imine-bonds are willing to coordinate with a variety of metal ions. Accordingly, a specific arrangement of ligands was expected whereby eclipsed nitrogen atoms of adjacent layers were disposed ∼3.7 Å far away. Then, the structure was functionalized by a palladium-complex ($Pd(OAc)_2$) which can takes part catalysing the Suzuki–Miyaura coupling

reaction, an important reaction for the formation of C–C bonds. The excellent catalytic activity of imine-based Pd-functinalized COF was demonstrated by the broad scope of the reactants and the excellent yields (96–98%) of the reaction products, together with the high stability and easy recyclability of the catalyst.

Much effort has been employed also on the applications of highly-porous materials in electrochemistry, mainly focused on clean energy applications, including hydrogen production and storage, fuel cells, lithium-based batteries and solar cells. The metal ions present on the structure of these materials can act as an active redox sites for electrochemical processes. When these materials are employed for lithium batteries purposes, they take care of the lithium-ion immobilization and store inside of their permanent pores. Li storage occurs through reversible conversion reactions in which the metal centrer of the original MOF structure is exchange by Li-ions. Upon de-lithiation the lithium formated MOF comes back to the original state. This process is what allows the long-term cyclability of the structure. Saravanan *et al.* investigated the performance of a family of transition metal COF which exhibited a high reversible capacity of 560 mA h g^{-1} for more than 60 cycles at 60 mA g^{-1}.[131]

3 Experimental Methods

Most relevant aspects of each experimental technique and theoretical methods used during the thesis will be addressed in this chapter. It is divided into two parts. Section 3.1 encompasses the ultra high vacuum methods and theoretical calculations associated to the study of absorbed molecules on copper surface that is described in chapter 4. Section 3.2 contains a brief summary of the experimental techniques employed in the study of the suspended polymer nanosheet synthesised at a liquid/liquid interface, which is detailed in chapter 5.

Contents

3.1 Ultra-high vacuum (UHV) techniques

Ultrahigh vacuum technology is at the heart of modern surface science methodologies. It provides a framework for high sensitivity and resolution characterizations of ultra-clean samples. Surface science techniques are, to a large extent and at least as regards the present work, largely established. They are implemented in laboratory facilities and at synchrotron sources.

We can classify surface science experimental techniques into three main families with different scope and very complementary capabilities: microscopies, spectroscopies and interference-based techniques.

Microscopy techniques provide information on the lattice structure, morphology, and topography of surfaces and small objects deposited on them. In some cases they give additional local spectroscopic information. Extremely high spatial and sometimes energy resolution can be obtained with these techniques, yet the interpretation of the data can be complicated by the concomitant expression of several effects or by the interaction of the microscopic probe with the sample.

Spectroscopy techniques give information about the electronic, vibrational, or magnetic properties of the sample, in some cases with chemical sensitivity. They can, for instance, help to elucidate the conformal adsorption of molecules on a surface. The information is generally averaged at a macroscopic scale, which complicates the analysis, and often somewhat conductive samples are required. Synchrotron radiation is sometimes employed to achieve high energy resolution analysis.

Interference-based techniques exploit the ondulatory behaviour of electrons or photons to characterise the local or long-range structure and chemical compositions of a sample. We disregard this class of techniques in the following, since we have only marginally used them in the course of our work.

A combination of different techniques among the aforementioned families will give us a complementary information allowing a comprehensive analysis of the samples we have prepared.

3.1.1 Experimental set-ups

A large part of our work has been performed in ultra-clean conditions, using well-defined metal surfaces and deposition of molecules controlled at a level well below one molecular layer. Three different UHV set-ups have been employed.

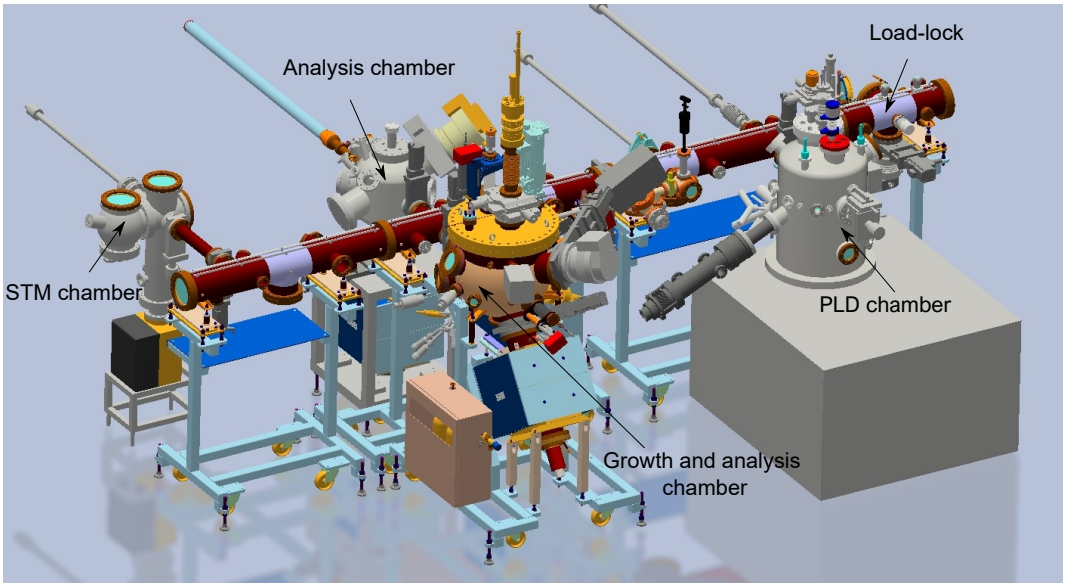

Figure 3.1: Multi-purpose UHV system at Néel Institute. It encompasses four chambers (STM, analysis, growth and analysis and PLD chambers) connected by a tunnel also under UHV conditions. Samples are introduced via a load-lock system which is connected to the tunnel.

Part of the experiments that make up this thesis have been done in the multi-purpose UHV system located at Néel Institute (Grenoble). It is composed by four UHV chambers connected between them by a tunnel also held under ultra high vacuum conditions (Figure 3.1). This system is equipped with a room-temperature Omicron scanning tunneling microscope (RT-STM), which is isolated in one of the four chambers and works in a base pressure in the low 10^{-11} mbar range. The main chamber where both, growth and analysis can be performed, is equipped with metal Tectra dual electro beam and molecular Kentax two-cell evaporators, an Ar^{+} ion sputtering gun, for surface preparation. It also has a REG-30 Electron Devices reflection high-energy electron diffraction (RHEED) system which provides structural surface information, a quadrupole mass spectrometer that analyses the composition of the residual gases in vacuum, an a quartz microbalance measuring deposition rates and a variable temperature sample manipulator with a working temperature range from 100 to 1000 K. The base pressure of this chamber is 5×10^{-10} mbar. The analysis and the PLD (pulsed laser deposition) chambers have been used sporadically during this work, mainly for storage, surface preparation and analysis purposes.

Two 3-week measurement campaigns have also been done at the ESISNA group

of the Materials Science Institute of Madrid (ICMM-CSIC), in close collaboration with Dr. Carlos Sánchez-Sánchez and Prof. José Ángel Martín-Gago The UHV system used during these experiments (Figure 3.2),presents a home-made molecular evaporator which was employed for depositing the desired molecules onto an atomically-clean sample held on a heating stage (273-873 K). The main characterization techniques employed in this chamber were a variable-temperature Flow-cryostat STM from SIGMA Surface Science, for scanning the surface samples, and a low-energy electron-diffraction (LEED) Scienta Omicron system, for checking surface cleanliness before the molecular deposits.

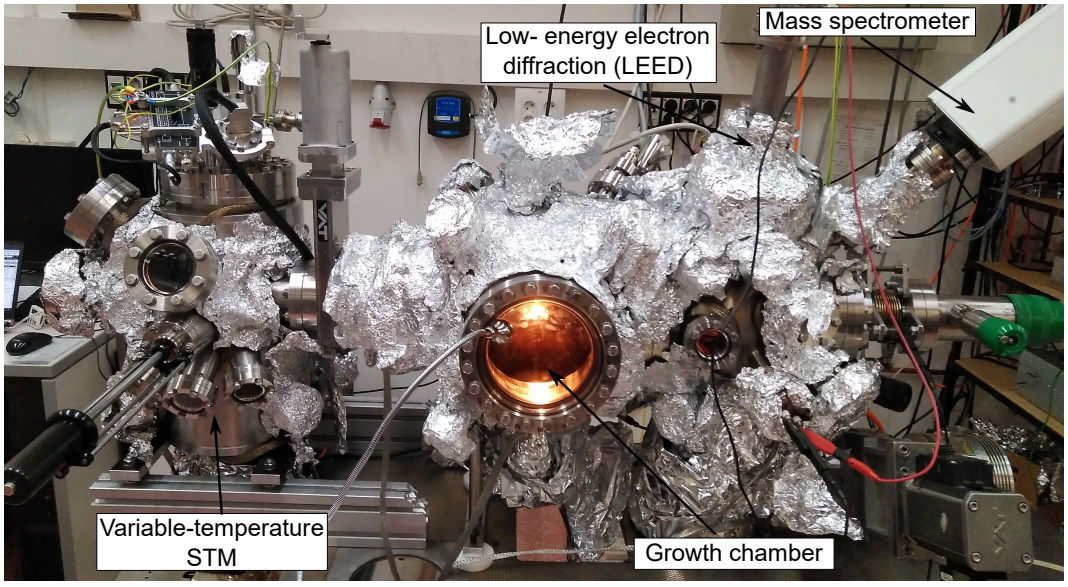

Figure 3.2: UHV chamber at ICMM-CSIC, equipped with variable-temperature STM, LEED and mass spectrometer for quality vacuum control. It is also equipped with a home-made molecular evaporator.

Complementary characterization with X-ray photoemission spectroscopy (XPS) and Near-edge X-ray absorption fine structure (NEXAFS) techniques was performed in the framework of a collaboration. These measurements were carried out in the UHV system located at ALOISA-beamline of Elletra synchrotron facility (Trieste, Italy) by Prof. Martín-Gago and supported by Dr. Luca Floreano, Dr. Alberto Verdini and Dr. Albano Cossaro.

3.1.2 Substrate preparation

For our experiments, we have used a copper single crystal substrate (purchased at SPL), with (111) orientation and 99.9999% purity. When a sample is introduced for the first time into a UHV system, it is first degassed by moderate annealing during few hours (actually, until the pressure of the systems gets down to the low 10^{-8} mbar range).

Surface cleaning

After this degassing step, the surface of the sample is prepared aiming at the lowest possible amount of contaminants on the surface and the largest possible atomically-high flat terraces. The sputtering step consists in the bombardment of the surface substrate by accelerated Ar^+ ions. Then, an annealing process is needed to let the surface atoms reorganize in its most stable reconstruction. The acceleration voltage, temperature and time parameters employed for the surface preparation must be adjusted to each UHV chamber and substrate, so no universal recipes exist. In order to optimize the cleaning protocol, diffraction techniques (RHEED and LEED) together with STM measurements are usually employed. Sharp diffraction patterns free of parasitic phases are sought for. Then, STM images showing $\geq$ 100 nm-wide terraces, with no or few surface pollution is the final criterion to decide whether the surface quality is acceptable for further experiments. The preparation recipes of Cu(111) single crystal employed in the UHV system at Néel Institute consists in:

1. Surface bombardment with Ar^+ with 0.8 keV ion energy for 30 min with an ion current of typically 23 mA.

2. Annealing up to 620 K-670 K for 10 min.

The monitoring of the surface temperature was done with a Keller infra-red pyrometer, with emissivity set to 0.1. For the preparation of the copper substrate is essential to do not overcome the maximum temperature of 670 K since sulphur atoms, which typically are hosted in the bulk, would otherwise migrate to the surface. These absorbed ad-atoms can be easily recognized in STM by the presence of 'dark-holes' decorating the surface.

The surface cleaning process described above will be necessary every time before any (organic/inorganic material) deposit. More than one combined sputtering/annealing cycle is required if the single crystal has not been used for a while, even if it has been stored under vacuum.

Organic molecules deposition

Three molecular evaporators have been used during our experiments. A commercial Kentax two-cell evaporator designed especially for materials with a maximum sublimation temperature of 923 K at Néel Institute and a couple of home-made evaporators based on tantalum envelopes at ICMM-CSIC and at the ALOISA beamline. The evaporators employed in most experiments are shown in Figure 3.3.

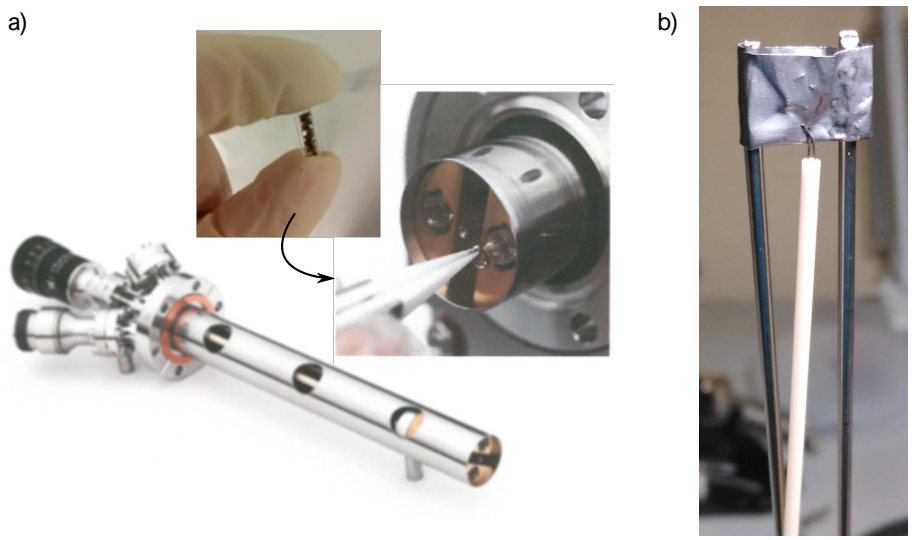

Figure 3.3: a) Commercial Kentax two-cell evaporator used at Néel Institute and b) home-made evaporator based on tantalum envelope spot-welded to two stainless steel rods used in ICMM-CSIC.

The Kentax evaporator has two cell-pockets where low thermal capacity crucibles (*i.e.* made by quartz) are inserted (Figure 3.3a). Two different organic molecules can be loaded in the UHV chamber simultaneously, and be deposited selectively thanks to a specific power supply which controls the heating of the pockets. For a simultaneous molecular evaporation, two power supplies are needed. Induction heating is done by tungsten coils which enclose the quartz crucibles. In our system, the heating temperature is regulated by a controller in the power supply which tunes the current applied to the tungsten coils. Even though the two cells of the evaporator have independent tungsten coils, both crucibles are cooled down using water during operation, so that the unusued cell is not heated by the neighboring coils. The home-made evaporator, shown in Figure 3.3b, is made of a tantalum envelope where the powder to deposit is loaded. It is spot-welded to two stainless steel rods fixed to a feedthrough. Also a K-type thermocouple is spot-welded to the tantalum envelope to measure the evaporation temperature. The envelope is heated

by circulating a current through it (typically from 5 to 13 A).

Just like any new element introduced for the first time in the UHV chambers, the evaporator and the molecular powder need to be degassed prior to use. The molecular evaporator installed at Néel Institute is naturally baked out after every opening of the chamber to the air. This bake-out consists on the external heating of the evaporator through heating tapes while the pumps are working. With this procedure, most pollution adsorbed on the elements installed in the chamber and in the walls are desorbed and pumped out of the system. Additionally, the evaporator is equipped by internal heating heads (enclosing the tungsten coils) which allow to make a local bake out. This process should be applied several hours (or overnight) and it is followed by the degassing of the molecular powder. The latter consists in progressively heating the powder allowing the airborne species and residual chemical traces from chemical synthesis reaction and purification to be removed before the evaporation of the organic molecules. This step is crucial since the cleanest molecular deposit is necessary.

The evaporation protocol is slightly different whether the evaporation temperature is known or not. If the evaporation temperature is known, because of previous molecular calibration on the system or because the molecule is well-known, the powder is gently heated up respecting always the maximum upper pressure limit in the chamber of 10^{-7} mbar. Once the powder reaches its evaporation temperature, the degassing lasts until the pressure of the chamber downs to 5×10^{-9} mbar. As from this minimal pressure value, the molecules are decently clean and first attempts for their deposition on the desired substrate can be made. When new organic molecules are handled, this process is not as straightforward since the evaporation temperature is not known, and even more critically, their degradation temperature either (it may be close to the evaporation temperature). In this case, the pressure monitoring is essential since it can help us to detect when the molecules start evaporating. However, the most useful and efficient way to: i) find the evaporation temperature of the molecule and ii) degass the molecular powder, is to follow the deposition rate by using a quartz microbalance located in face of the evaporator outlet. This configuration is shown in Figure 3.4. A rate of 1 Å/min was sufficient and convenient in our experiments.

At ICMM-CSIC, the evaporator degassing is done exclusively by external heating tapes when the evaporator is introduced in the chamber, and the protocol for degassing the molecular powder is the same as explained before. In fact, the configuration shown in Figure 3.4 is the one used during the two measurement campaigns at ICMM.

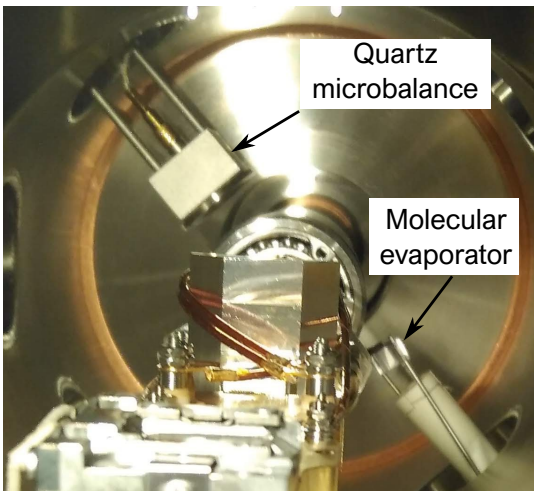

Figure 3.4: Picture of the configuration adopted at ICMM-CISC for controlling the evaporation rate. The molecular evaporator is installed in front of the quartz microbalance at a distance of 10-12 cm.

The next step is the deposition of the molecules onto the desired surface, in our case, on Cu(111) single crystal freshly and atomically cleaned. In Figure 3.5, the deposition configurations employed at Néel Institute and at ICMM-CSIC laboratory are shown. In both cases the evaporation rate was calibrated by means of STM, whereas at ALOISA beamline, this was achieved by quartz microbalance since no access to a STM system was possible. During the deposition process, the distance between the evaporator's head and the substrate is crucial, since the flux density decreases with the square of the distance from the source. A large evaporator-substrate distance was in fact one of the difficulties found during the experiments done at Néel Institute since the working distance of our set-up was out of the recommended values of 8-12 cm. To overcome this issue, the temperature evaporation or the exposition time can be increased, rising in both cases the molecular dose which arrives at the surface.

During this thesis we have deposited the 2,3,6,7,10,11-hexahydroxy-triphenylene molecule on Cu(111). It evaporates at 540 K and the average pressure during the deposition was $\sim 2 \times 10^{-9}$ mbar. More details about its structure, purification process and its interest as a molecular building blocks for polymer synthesis is given in chapter 4.

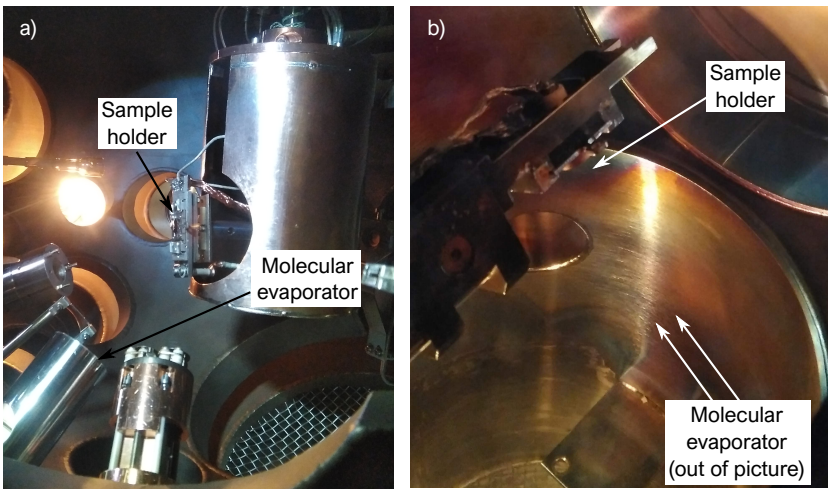

Figure 3.5: Pictures of deposition configuration used at a) Néel Institute and b) ICMM-CSIC laboratory (where the molecular evaporator head is out of the image and the pair of arrows mark the virtual molecular flux direction).

3.1.3 Scanning tunneling microscopy (STM)

Scanning tunneling microscopy is one of the practical applications of quantum mechanics. Invented by G. Binnig and H. Röhrer while working for IBM research laboratory in Zürich (Switzerland) in 1982,[132,133] this instrument revolutionized surface science. An elementary introduction to this technique is given in the following, and further information can be found in dedicated books and reviews.[134,135]

Working principle

The working principle of the scanning tunneling microscopy technique is based on the quantum tunneling effect. From a classical point of view, the tunneling effect could be compared with throwing a ball against a wall expecting a non-zero probability to find the ball beyond the wall. This probability is of course zero in a classical world, and the only way the ball can be found on the other part of the wall is to give it sufficient kinetic energy to cross the (gravitational) potential energy barrier represented by the height of the wall. In a quantum world, the wall is now a potential barrier and the ball an electron. From the same principle as in the classical theory, we could think that the electron can not pass over the potential barrier if its energy is lower than the potential energy or the barrier. However, owing to the wave nature of the electron, there is a non-zero probability that the electron passes through the potential barrier to the other side, by tunneling effect. A pictorial representation of it is shown in Figure 3.6.

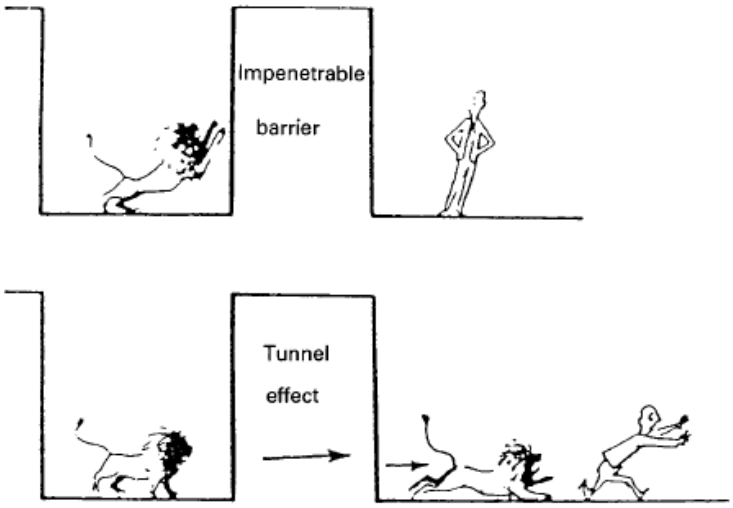

Figure 3.6: The difference between classical theory and quantum theory, illustrating tunneling through a potential barrier. Taken from reference 134.

The electron tunneling probability can be calculated for instance in the case of a one-dimensional potential barrier using the time-independent wave functions as a solution of the time-independent Schrödinger equation for the electron. A more advanced treatment, relying on Bardeen's tunnel current formalism, is often used to describe the tunnel junction.[136] It states that the current tunneling between two conductors separated by a thin insulator can be described by considering the overlap of the tip and sample wave functions. This current depends exponentially on the tip-sample distance, d:

$$I_t \propto exp(-2\kappa d),\ with\ \kappa = \sqrt{\frac{2m\phi}{\hbar^2}} \tag{3.1.1}$$

with m the electron free mass, and ϕ the work function of the tip and sample (for simplicity the work functions of the tip and of the sample are assumed to be equal). In fact, is this strong (exponential) dependence of the current tunneling with the tip-surface distance, that makes STM so sensitive and extremely interesting for high (lateral and height) spacial resolution, in the order of tenths of an angstrom.

Experimental set-up

From the experimental point of view the probe tip, which is often made of W or of a Ir/Pt alloy, scans the metallic surface separated by some angstroms. As it is shown in Figure 3.7, the tip is attached to a piezodrive stage, which consists of three different piezoelectric transducers (one for each direction, x, y and z). Upon applying a voltage, the transducers expand or retract, allowing the smooth movement of the tip on the surface. In these conditions the tip and sample wave functions overlap, and by applying a bias voltage a tunneling current is generated, as it is deduced from equation 3.1.1. This current is converted to a voltage by the current amplifier, which is compared with the reference value. The difference is used to drive the z piezoelectric: if the tunneling current is larger than the value of reference, a voltage applied to this piezo tends to withdraw the tip from the sample surface, and *vice versa*. The tip scans the surface in the xy plane, so a two-dimensional plot with equilibrium z values is performed and stored in the computer.

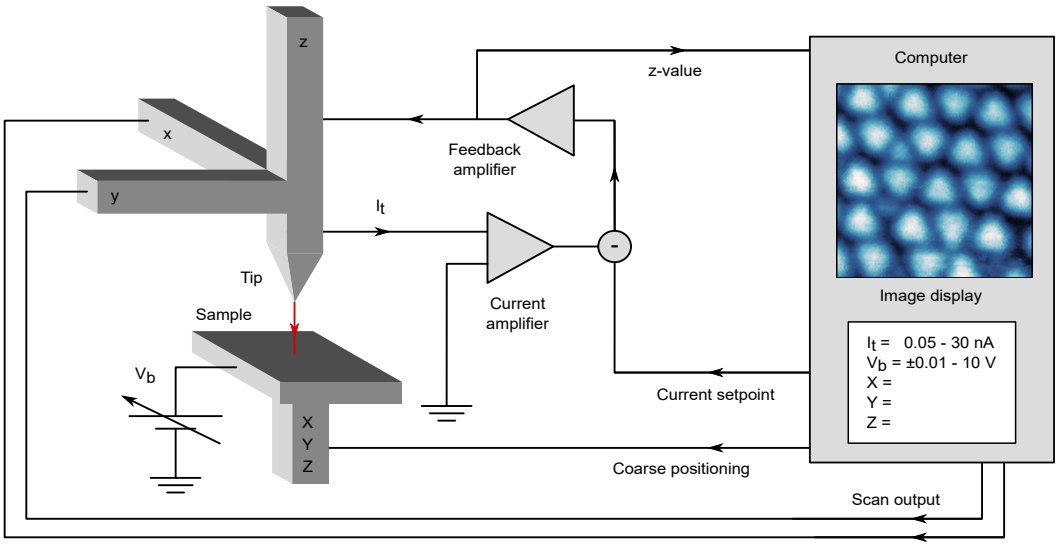

Figure 3.7: Schematic representation of the STM system, showing the measurement cycle working. Reproduced and adapted from reference 137.

With this description it may seem that an STM image only represents the surface topography. Nevertheless, the measured topography may sometimes be only (or partly) apparent. The overlap of the tip and surface wave functions is indeed directly related to the density of states of the tip-sample system. This means that the STM images are a convolution of both, the surface topography and the local density of states (LDOS) of the system, making the STM image interpretation by

no means straightforward.

The STM measurements presented in this thesis have been carried out in two different set-up:

- A commercial room-temperature STM: Omicron UHV-STM 1, with an electrochemically etched tungsten tips at Néel Institute.
- A commercial low temperature STM: Flow-cryostat STM from SIGMA Surface Science. The images were acquired at a temperature of 79 K, with an electrochemically etched tungsten tip at ICMM-CSIC.

The measurements were performed in constant current mode and the bias was always applied to the sample (*i.e.* for positive bias, the tunneling current flowed from the tip to the sample). The images were represented and filtered with the Gwyddion software.

3.1.4 X-ray photoelectron spectroscopy (XPS)

X-ray photoemission spectroscopy (XPS) is an electronic spectroscopy based on the photoelectric effect (discovered by H. Hertz in 1887) and it consists in analysing the energy of the emitted photelectrons, whose kinetic energy is directly measurable. It is a surface sensitive technique, since it probes a sample depth between 5-20 Å. Some basic working principles are detailed in this section and further information can be found in specialized books.[138,139]

Working principle

This technique employs photons as incident irradiation and depending on their energy, valence bands or core-level states can be probed. For the former regime a lower incident energy is required, so photons in the UV-Vis region can be employed– this is the domain of ultraviolet photoemission spectroscopy (UPS). In order to gain access to the sample's core-levels a more energetic incident radiation is required, and X-ray photons are employed, giving the name to the technique (XPS).

The diagram shown in Figure 3.8 illustrates the photoelectric effect process. During the sample irradiation with a photon beam ($h\nu$), a fraction of incident photons is absorbed. When the incident radiation is higher than the ionization threshold, electrons from the atomic core-levels can be promoted into the vacuum (overcoming the material's work function, Φ), with a specific kinetic energy (E_K). Since the binding energy (E_B) of these electrons depends on the chemical element and the

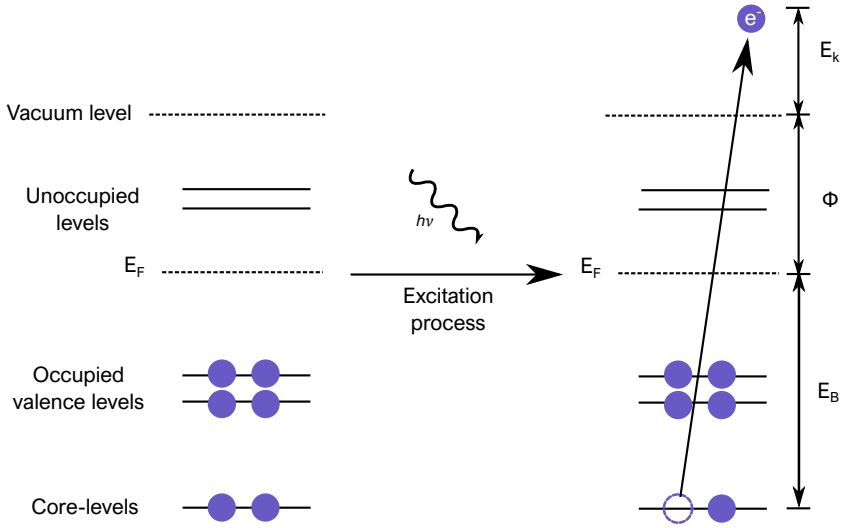

Figure 3.8: Schematic representation of the photoelectric effect. The photon irradiation of an atom in equilibrium with energy above the ionization potential can eject an electron from a core-level state. The difference between the incident energy ($h\nu$) and the binding energy related to the photoelectron (E_B), and the materials' work function (ϕ) is represented by the kinetic energy (E_K) of the detected electron. Reproduced and adapted from reference 140.

core-level which it comes from, and the chemical environment which surrounds the atom, it is considered as a footprint of the ejected electrons. So, the difference between the energy of the incident radiation, the material's work function and the binding energy of the detected electron is its kinetic energy:

$$E_K = h\nu - \Phi - E_B \tag{3.1.2}$$

An XPS experiment consists in counting the number of detected photoelectrons as a function of their kinetic energy. The XPS experiments are done at different energy regions depending on the element and the core-level we want to probe. For a more efficient excitation process, monochromatic and intense X-ray radiation is desirable, so high-resolution XPS measurements are commonly acquired in synchrotron facilities. The photon flux is indeed orders of magnitude higher at synchrotron facilities than it is with lab-scale X-ray sources. Also, synchrotron radiation presents great level of polarization (linear, elliptical or circular), high collimation (*i.e.* small angular divergence of the beam) and wide tunnability in energy by monochromatization (around some meV).

It is noteworthy that considerable attention has been taken to try to understand

the origin of core electron binding energy shifts (or chemical shifts) in photoemission spectroscopy. In general terms, this origin is *a priori* quite simple: the molecular charge redistribution of the system. However, it is exactly what makes its understanding and study complicated. The photoelectron's binding energy is based on the element's final state configuration, which consists on the core-hole created by the photoelectric effect and the surrounding electrons in their initial orbitals. It exists many final state effects which are connected to these chemical shifts, which in turn, have direct consequences on the XPS resolution (since it affects to electronic lifetimes). Some details will be given here, based on the exhaustive study done in reference 138. Among the most common effects are the charge redistributions induced by electronegativity differences between elements, spin orbit splitting of electronic levels which produces the multiplet splitting of the XPS peaks, and multi-electron excitations during the photoemission process, which can produce shake-up or shake-off effects and so, additional peaks. Another effect has a strong, sometimes prominent influence: the relaxation effect. It consists in the rearrangement of the electrons around the K-hole which is just created. This effect must not carry large spatial changes in the molecular orbital, but its influence on the binding energy can be important. Additionally, in the case of the substrate, Fermi level electrons can compensate the hole-core just created, which is known as the screening effect.

Experimental set-up

The X-ray photoemission spectroscopy (XPS) experiments were performed at the ALOISA beamline, at Elettra synchrotron (Trieste-Italy)[141] by Prof. Martín-Gago with the support of the local researchers. Three different phases have been analysed by *in situ* XPS: a multilayer phase of the HHTP molecules on Cu(111) substrate, a sub-monolayer phase of molecules just after being deposited at room temperature and a sub-monolayer deposit after an annealing at 530 K. The XPS spectra were recorded at the C 1s, O 1s and Cu 3p core-level regions for all phases and the photon energies used for the XPS high-resolution spectra were 650 eV for O 1s region and 400 eV for C 1s one. Absolute energy calibration was obtained by simultaneous acquisition of the drain current of the last refocusing mirror (Au coated). By this process, the measured XPS spectra were normalized, at first instances, for any fast fluctuations of the synchrotron beam. All spectra have been analysed by least-squares fits to obtain more details about the chemical states at each phase. We have used Voigt functions with fixed full width half maximum values for the Lorentzian components of 0.2 eV for C 1s and 0.3 eV for O 1s core-levels, respectively. The refined values of the full width half maximum for the Gaussian component of the Voigt functions used were in the range of 0.5-1.2 eV. A Shirley-type background has been considered and removed and all spectra have been calibrated with respect to

the Cu 3p reference-peak located at 75.1 eV. Also, the spectral intensities of sub-monolayer deposits (before and after annealing) have been normalized with respect to the intensity of the Cu 3p peak. For fitting the data, we used a code written for Igor (developed by Francesco Bruno, ALOISA beamline, Laboratorio TASC, CNR-IOM).

3.1.5 Near edge X-ray absorption fine structure (NEXAFS)

When performed with soft X-rays and with specific detection schemes near edge X-ray absorption fine structure is a surface sensitive technique which is considered an inner-shell spectroscopy since incident X-ray radiation interacts primary with deep-core electrons rather than valence ones. Main characteristics will be summarized here on the basis on some reviews and books.[142,143]

Working principle

When a sample is irradiated with X-ray ($h\nu$ energy) photons, different process can take place:

1. If $h\nu >$ ionization potential, photoelectrons can be emitted, and for instance an XPS experiment can be performed.

2. If $h\nu \leq$ ionization potential, absorption may occur.

3. If $h\nu \ll$ ionization potential, then no absorption is possible.

In a NEXAFS experiment, during an absorption process (case 2 listed above), core-level electrons are promoted into the unoccupied or available states above the Fermi level (Figure 3.9).

In this excited state, a core-hole is created, which can be filled by de-excitation of other core-level electron. This de-excitation process can be accompanied by a photon release (fluorescence emission) or by the ejection of a third electron from the core-level (Auger process). The photoemission cross-section for elements with Z$<$ 90 is much higher for Auger process than for fluorescence. Taking advantage of this, the NEXAFS technique monitors the kinetic energy of the Auger electrons which are ejected from the sample.

NEXAFS is an element-specific technique, and informs on the unoccupied electronic states of the probed element. When the incident photon energy reaches the

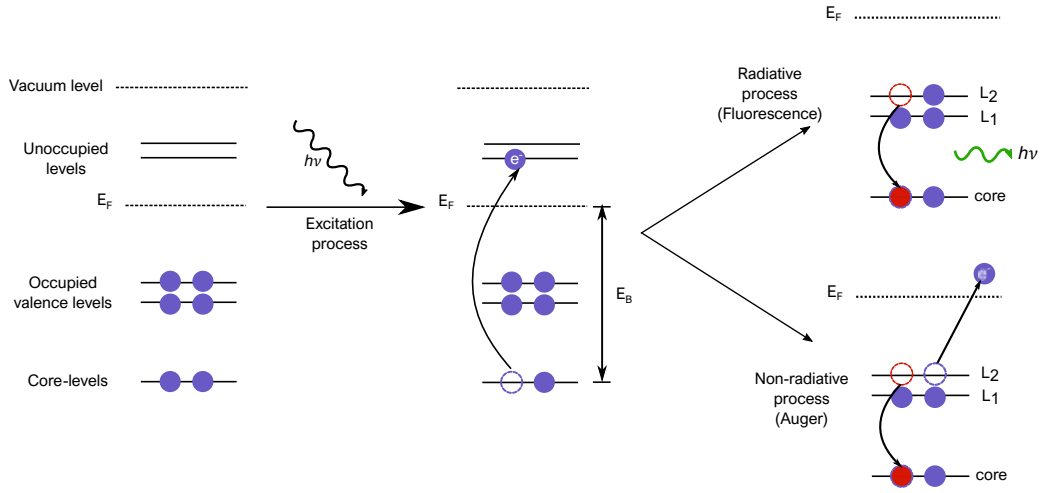

Figure 3.9: Schematic representation of the steps involved in the absorption process during a NEXAFS experiment. On the left, the target atom, in its ground state, is irradiated with X-ray photons, and one core level electron is excited to an unoccupied state (middle diagram). The atom can be de-excited through a radiative process (fluorescence) or through a non-radiative process (ejection of an Auger electron). In NEXAFS, the kinetic energy of the latter electrons are monitored.

absorption edge of the element, a specific transition between a core-level and a unoccupied state occurs which is apparent in the NEXAFS spectra as a peak.

There are three different modes of recording NEXAFS, depending on the kinetic energy (E_K) of the Auger electrons:

- Auger yield. Only Auger electrons of a certain E_K are monitored (there is a risk of loss of information).
- Partial yield. All electrons beyond certain E_K are monitored (the background level is higher due to inelastic processes, but less information is lost).
- Total yield. All the electrons, whatever their E_K, are monitored (quite complex spectra, since a lot of information is recorded).

NEXAFS spectra of organic compounds are composed by two different regions: i) the π^* region, which appears at lower photon energy (E_{ph}) values and comprises information on the transitions of core-level electrons to π character orbitals, ii) the σ^* region, which appears at higher photon energies and includes information on the transitions of core-level electrons to σ character orbitals. Remarkable observations can be done from NEXAFS chemical shift of a specific K-shell region since the electronic transitions are sensitive to electronic charge transfers (from the surface

to the molecular species or *vice versa*), charge reorganization or re-hybridization of the molecule upon absorption on metal surfaces or simply to molecule-substrate interactions.

Moreover, due to the strong directionality of the molecular orbitals, the geometry of the system (*i.e.* angular orientation of absorbed species on the surface) can be analysed by using different polarizations of the X-ray beam. The resonance generated by the interaction corresponding to the electric field corresponding to the incident radiation and, for instance, the orientation of a given molecular orbital varies like the dot product of the two vectorial quantities. As it is shown in Figure 3.10 (upper panel) perpendicular polarized light (or 'p' polarized) is expected to present a maximum resonance with molecular orbitals which are perpendicular to the surface. In this case, a maximum value of the dot product, hence a peak in the spectra, is obtained for electronic transitions involving π out-of-plane orbitals. In this configuration, no contribution of in-plane orbitals will appear in the spectra, since it corresponds to a zero value for the dot product. Conversely, probing the sample with parallel polarized light (or 's' polarized) will present a maximum resonance with in-plane or parallel molecular orbitals, yielding a maximum absorption response whereas perpendicular molecular orbitals will not be probed.

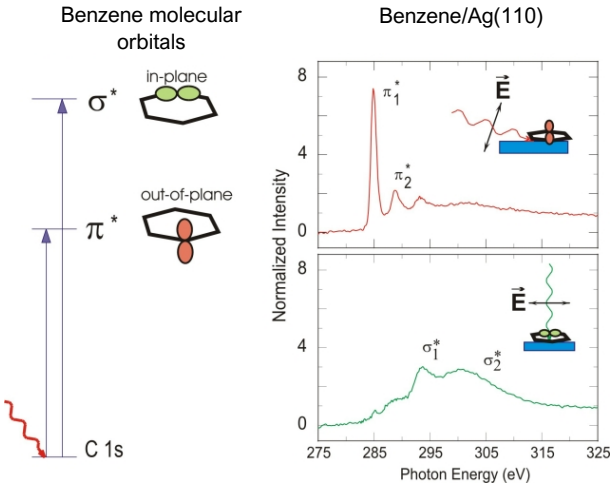

Figure 3.10: Schematic representation of the benzene molecular orbitals, indicating their geometry (left part) and NEXAFS spectra obtained for benzene deposited on Ag(110) (right part), by using p-polarized light (upper panel) and s-polarized light (lower panel). Taken from reference 144.

Experimental set-up

Similarly to the XPS experiments, NEXAFS measurements were performed at the ALOISA beamline at Elettra synchrotron in Trieste.[141] The analysis was done in only two out of three samples (in multilayer and in sub-monolayer samples before annealing) due to a beam interruption which prevented the analysis of the third sample. Polarization-dependence NEXAFS measurements were performed at O and C K-shell ionization thresholds in partial electron yield by means of a full aperture detector (channeltron) in front of the sample with an electrostatic high-pass-filter set to -200 V in order to reject secondary electrons. NEXAFS spectra were acquired in transverse electric (or s-polarization) and transverse magnetic (or quasi p-polarization) polarization by rotating the sample around the photon beam axis while keeping the grazing angle fixed to 6^o.

3.1.6 Density functional theoretical calculations

Density functional theoretical (DFT) calculations have been used for the last decades for quantum mechanical simulation of the structure, electronic, and magnetic properties. Here, the basic concepts underlying of this theory are summarized, based on the reference 145.

Fundamental basis

For the ground state energy calculation of a collection of atoms, the time-dependent, non-relativistic, Born-Oppenheimer approximated Schrödinger equation ($\hat{H}\Psi = E\Psi$) is solved. $\hat{H}$ is the Hamiltonian operator, Ψ corresponds to the wave function of the described system and E corresponds to its associated ground state total energy. The Hamiltonian operator consists of a sum of operators which correspond to the kinetic and the potential energies of the system and can be expressed as follows:

$$\hat{H} = \hat{T} + \hat{V} = \frac{-\hbar^2}{2m}\hat{\nabla}^2 + \hat{V}_{\text{ext}} + \hat{V}_{\text{e-e}} \tag{3.1.3}$$

where the $\hat{T}$ is the kinetic energy of the system, the $\hat{V}_{\text{ext}}$ corresponds to the external potential and the electrons-nuclei interactions in a solid, and $\hat{V}_{\text{e-e}}$ corresponds to the electron-electron interaction.

The direct resolution of the Schrödinger equation implies the determination of the 3N dimensional wavefunctions of the system. This task has a high computational cost requiring a flexible description of the wavefunction's spatial variation. This is all the more critical as complex systems, such as molecules on surfaces are considered.

A solution to limit the computational cost is to exploit the fact that all terms of the Schrödinger equation are functionals of the charge density (ρ) of the system, so that the energy functional can be defined as follows:

$$E[\rho] = T[\rho] + V_{\text{ext}}[\rho] + V_{\text{e-e}}[\rho] \tag{3.1.4}$$

The external potential encompasses ion-electron interactions and can be computed within the Born-Oppenheimer approximation. However, the kinetic energy and e-e- interaction potential terms are unknown and estimating them requires approximations. In this respect, Kohn and Sham proposed the introduction of a fictitious system of N non-interacting electrons in order to describe the kinetic energy. Now, instead of building the system with wavefunctions they propose to do it in terms of one-electron orbitals (ϕ_i). Also, the e-e potential energy term was proposed to be calculated in terms of classical Coulomb interaction, or Hartree energy. Nevertheless, these assumptions carry some errors which must be included in the total energy calculation, under the form of the exchange-correlation functional term ($\mathrm{E_{xc}}$). Assuming these approximations and the correction term in equation 3.1.4, the total energy functional is now defined as:

$$E[\rho] = T_{\text{s}}[\rho] + V_{\text{ext}}[\rho] + V_H[\rho] + E_{\text{xc}}[\rho] \tag{3.1.5}$$

where, $E_{\text{xc}}[\rho] = (T[\rho] + T_{\text{s}}[\rho]) + (V_{\text{e-e}}[\rho] - V_{\text{H}}[\rho])$.

One of the major difficulties is to calculate the exchange-correlation term. Additional approximations are necessary for this purpose. One of these approximations is the local density approximation (LDA) which assumes a homogeneous electron gas where the electron density depends on the position ρ(r). Now, the exchange correlation term is a function of only the local value of the density. However, this method is only relevant for very homogeneous systems and in general, underestimates the interatomic distances and overestimates the binding energies. In this sense, the generalised gradient approximation (GGA) gives a more accurate binding energy values since it describes the exchanges correlation term in terms of local value of the density and its variation (or gradient) with the position. This approximation is more suitable for inhomogeneous systems and popularized density functional theory calculations in condensed matter physics and chemistry.

Theoretical methods and structure modelling

Calculations shown in chapter 4 have been performed in the framework of density functional theory by Dr. José Ignacio Martínez, from ESISNA group of ICMM-

CSIC (Madrid-Spain). In a first step, we have carried out a preliminary DFT analysis of the HHTP molecules in different dehydrogenation steps of its terminating OH groups: i) pristine (no OH group dehydrogenated), ii) with three alternating dehydrogenated terminating OH groups, and iii) with all the OH molecular groups dehydrogenated, in order to obtain reasonable starting point geometries. We have obtained optimized molecular structures using the GAUSSIAN09 code[146] within the B3LYP/cc-pVTZ level of theory implemented in periodic boundary conditions.[147–149]

On the basis of the preliminary optimized molecular structures we have constructed the different interfacial models described in this study: dilute phases of the HHTP molecule on the Cu(111) surface in its three dehydrogenation steps, in different supramolecular organizations and in the case of defect structures involving Cu adatoms. We have fully optimized a large battery of all these starting points (studying all the non-equivalent on-surface locations and orientations) with the QUANTUM EXPRESSO plane-wave DFT code.[150] We have carried out simultaneous full lattice/cell and structure optimizations for the different interfacial configurations. The calculations account for an empirical efficient vdW R-6 correction (DFT+D2 method[151]) to include dispersion forces (van der Waals). We have used the GGA-PBE functional to account for the exchange-correlation (E_{exc}) effects.[152] Ultrasoft pseudopotentials have been used to model the ion-electron interaction within the H, C, O and Cu atoms.[153,154] The Brillouin zones have been sampled by means of optimal Monkhorst-Pack grids.[155] The one-electron wave-functions are expanded in a basis of plane-waves with an energy cut-off of 450 eV for the kinetic energy, which has been adjusted to achieve sufficient accuracy to guarantee a full convergence in total energy and electronic density. All the atomic relaxations were carried out within a conjugate gradient minimization scheme until the maximum force acting on any atoms was below 0.05 eV $Å^{-1}$. Cell-shape/size relaxations have been carried out with two different algorithms: a damped dynamics and a bfgs-like relaxation.[156–158] These different approaches, tested for different interfacial configurations, provide very similar results for cell-shape and lattice parameters, as well as similar frequencies for the internal vibrations and for the cell oscillations.

The Cu(111) surface was modelled in a repeated slab geometry: (i) a slab of four physical Cu(111) layers with a minimum distance of about 20 Å of vacuum between neighbouring cells along the axis perpendicular to the surface; as well as (ii) full periodic boundary conditions representing an infinite Cu(111) surface. For the full geometry optimizations only the two bottom Cu physical layers were kept fixed.

3.2 Polymer nanosheet characterization

The characterization techniques employed for the analysis of the morphology, structure and bond formation of the polymer nanosheet are summarized in this section. The associated results and the synthesis protocol are detailed in chapter 5.

3.2.1 Optical microscopy and ultra violet-visible spectroscopy

Ultra violet-visible (UV-Vis) spectroscopy is widely used for structure resolution of organic compounds, in combination with other techniques such us infrared spectroscopy or magnetic nuclear resonance. It studies the absorption of electromagnetic radiation between 190 nm to 400 nm (UV region) and between 400 nm to 800 nm (Vis region). Photon absorption promotes electrons from an occupied molecular orbital (σ or π character) to an unoccupied molecular orbital of greater potential energy (σ^* or π^* character), hence the technique allows to probe the formation of specific bonds involving these orbitals. It commonly provides information about π-electron systems, conjugated unsaturations, aromatic compounds and conjugated non-bonding electron systems. UV-visible spectra were collected using an UV-Vis Spectrophotometer Lamba 900 (PerkinElmer) apparatus. UV-Vis spectra on synthesised monomers in powder as well as on thin polymer nanosheets deposited on quartz substrates were acquired to follow the progression of the reaction. All these experiments were performed at FEMTO-ST laboratory by Dr. Frédéric Cherioux.

Optical microscopy is the technique we have used at first instance just after the deposition of the polymer nanosheets onto different substrates. It allowed us to identify at a glance the products formation, their shape, distribution and more importantly, it provided a way to identify different regions of interest for subsequent analysis by other means of characterization. Optical images have been acquired in a Zeiss microscope equipped with a digital camera "Axiocam 105 color" device, a tungsten halogen light source, and magnifications of 2.5×, 10× and 100×. Additional optical images were taken during Raman experiments with the help of the CDD camera coupled to the microscope that is used to perform the Raman confocal measurements.

3.2.2 Raman spectroscopy

Raman spectroscopy is a non-destructive technique which allows to extract information about the molecular vibrations, whose nature and existence is determined by the symmetry of the molecule. In this thesis confocal Raman spectroscopy has been

used to confirm the formation of new bonds upon polymerization reaction carried out at a liquid/liquid interface.

Working principle

Raman spectroscopy is based on the inelastic scattering of light by matter upon the exchange of energy between the incident photons and, for instance, the vibrational energy levels of a molecule. The interest of studying the vibrational energy levels is that they are unique for each molecule and readily susceptible to structural changes when these molecules are part of polymer and crystals. Also, detailed information about chemical structure and solid crystallinity can be obtained.[159–161]

Raman spectroscopy experiments are nowadays performed with (relatively) intense monochromatic photon sources (lasers). Most part of the light scattering from the sample is elastic (Rayleigh). A small portion of scattered light presents different wavelength (higher, Stokes, or lower, anti-Stokes) than the incident radiation (inelastic scattering), and this is the information that is relevant in Raman spectroscopy. In case of Stokes Raman scattering, an electron that is excited from the ground level interacts with a vibrational level and looses energy in this process, resulting in scattered light having lower energy than the incident one. In contrast, during anti-Stokes Raman scattering an electron transmitted interacts with a vibrational mode from which it receives energy, eventually yielding scattered light with more energy than the incident one. Both cases are shown in Figure 3.11.

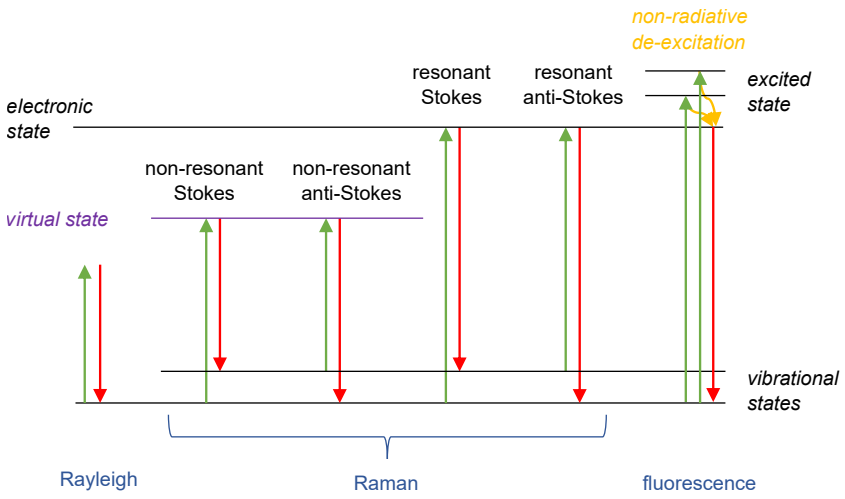

Figure 3.11: Electronic level diagram which depicts the scattering processes involved in Raman spectroscopy. The green and red arrows correspond to the incident and scattered light, respectively. Figure reproduced and adapted from reference 159.

In the same figure is also depicted the possible working modes of Raman. When the energy of incident radiation coincides with the energy difference between actual electronic levels in the system, the Raman scattering is resonant and more efficient, whereas if the energy does no correspond the difference between two energy levels, the Raman scattering is non-resonant.

One of the principal parasitic signal in Raman spectroscopy is the fluorescence. This phenomena occurs when the excitation light presents higher energy than one of the electronic states, being partially absorbed and re-emitted. The main difference with respect to the Raman scattering process is that the fluorescence works via non-radiative process. The most convenient and often-used method of fluorescence removal is 'photobleaching', that is, exposure of the sample to the laser beam until the fluorescence decays (during few minutes or for extreme cases, during several hours).

A Raman spectrum features a number of peaks, whose energy and bandwidth are analysed. Each peak corresponds to a specific molecular bond vibration, including individual bonds such as C-C, C=C, C=N, C-H, etc, and groups of bonds such, for instance, involved in the benzene ring breathing mode, polymer chain vibrations or lattice modes.

Experimental set-up

Raman spectroscopy was performed with a 532 nm Nd:YAG laser using a confocal WITEC spectrometer at room temperature under ambient conditions at Néel Institute. Also, 633 nm wavelength laser was tested to make sure that no specific resonance of some vibration mode of the polymer nanosheet would enhance their signal. A confocal Raman consists of a Raman spectrometer coupled to a microscope with sample illumination system and light collection optics, and a CCD. This combination allows the high magnification visualization of the sample and the Raman analysis at well-chosen locations. The confocal WITEC equipment that we have used for our Raman experiments is also equipped with a mechanical stage. The sample is placed on it and by the precise movement of piezoelectric elements, it is possible to move it in X, Y and Z directions. This allows to focus the laser beam and to perform high-precision Raman acquisitions over the sample. This microscope is also equipped with different magnification objectives 10×, 50× and 100×, which allow to get a spatial resolution in the order of 0.5-1 μm. Scattered light from the sample is collected by a large numerical aperture objective which is guided by a fiber to the spectrometer which further will be dispersed by the grating. In our setup there are 600 lines/mm grating with resolution of 3 cm^{-1} and 1800 lines/mm

grating with resolution of 0.5 cm^{-1}.

3.2.3 Electron microscopies

The electron microscopes employ an accelerated electron beam as a source of illumination. The wavelength of an electron beam accelerated into vacuum with voltages of hundreds of kilovolts is hundred times smaller than the wavelength of a light-optical microscope. This characteristic gives a higher resolving power. A brief summary of the main characteristics of scanning electron microscopy (SEM) and transmission electron microscopy (TEM) will be given in this section, employing the specialised book of the reference 162.

Transmission electron microscopy (TEM)

Transmission electron microscopy typically works with an electron beam accelerated between 50 to 300 kV. The shrinking of the wave function at these voltages allows the electrons to penetrate into a solid through few microns. However, to resolve the structure in the transmission geometry, the sample needs to be thinned down to the nanometer scale or less. In the case of a crystalline solid, the electrons can diffract with the atomic planes of the material generating an electron diffraction pattern by collecting the transmitted electrons. In the electron column, beam collimation is performed with electromagnetic lenses. As already mentioned the spatial resolution in a TEM is orders of magnitude better than in light-optical microscopy.

The TEM images and selected-area electron diffraction (SAED) pattern shown in this thesis were measured using a CM300 TEM microscope equipped with a LaB_6 thermionic emitter operated at 100 kV. These measurements were perfomed by Dr. Martien DEN-HERTOG at Néel Institute.

Scanning electron microscopy (SEM)

Scanning electron microscopes allow imaging thicker solids on their substrates, by collecting electrons emitted by the sample during irradiation. The incident electrons promote the emission of (secondary) electrons from the sample. Collecting these secondary electrons while the sample is scanned by an incident electron beam produces the SEM image. The typical SEM spatial resolution is between 1 to 10 nm.

The SEM images performed on polymer suspended nanosheets were recorded by using a Dual Beam SEM/FIB FEI Helios Nanolab 600i system and they were collected at the FEMTO-ST laboratory. In order to minimize the charge effects, a low

voltage of 2 kV and a low current of 43 pA were used. The secondary electrons were detected by the TLD (Through The Lens) detector and the scanning speed optimized to reach a compromise between the reduction of charge effects and the preserving of a good signal-to-noise ratio.

4 Stepwise oxidation, reorganisation, and bonding strength of a hexahydroxy-triphenylene on a copper surface

In this chapter an exhaustive microscopic and spectroscopic analysis on hexahydroxy-triphenylene molecules absorbed on Cu(111) is presented. A controlled stepwise oxidation (i.e. a dehydrogenation of the hydroxyl groups) of the molecule is achieved by thermal treatment, increasing its chemical reactivity. Density functional theoretical calculations shed light on the intermolecular and molecule-substrate interactions, confirming a strong acceptor character of the molecule in its fully dehydrogenated form. The chemical transformations of the molecules, concomitant to changes in the interaction with the substrate, are found to strongly influence their self-assembly. Some of our observations suggest that the dehydrogenated molecules coexist with close-by clusters of adatoms from the surface.

Contents

4.1 State of the art: hydroxy-triphenylene ligand

Since the synthesis for the first time of the triphenylene structure by the German chemist C. Mannich in 1907,[163] several chemical approach have been developed to functionalise it during the beginning of the last century. Considered as part of the important molecular organic group among polycyclic hydrocarbons, the emergence of the triphenylene family started with the synthesis of the methyl-triphenylene derivatives by Fieser *et al.*[164] and Bachman *et al.*[165] in 1939, and soon after by the synthesis of the oxygen-based derivatives by W. S. Rapson in 1941.[166] The development of more accurate chemical characterization techniques stimulated a more exhaustive analysis of these complex molecules in the following years. First calculations of proton chemical shifts and preliminary crystallographic data are reported from late 1970's.[167,168] Their planar configuration and electron-rich structure positioned triphenylene molecules as a good candidates for constructing organic self-assembled thin films and extended networks,[169] while their first morphological analysis was reported by Rabe *et al.* by means of scanning tunneling microscopy.[170]

Triphenylene derivatives, and in particular the 2,3,6,7,10,11 - hexahydroxytriphenylene (HHTP) molecule, have been attracting attention for above 20 years as possible building blocks for molecular (opto)electronics. Noteworthy, the HHTP molecule is a well-established building-block of so-called metal cathecolates, in which metal ions are coordinated by the pairs of oxygen atoms of the dihydrogenated HHTP molecule.[120] Ru(II)-hexahydroxytriphenylene based-complexes display a very strong and broad near-IR absorption, with absorption coefficients of 32000–74000 dm^3 $mol^{-1}cm^{-1}$, thanks to the ruthenium-to-ligand charge transfer.[171] Additionally, the possibility of reversible interconversion between cathecolate (or ortho-hydroxyl), semiquinone and quinone forms of the hydroxytriphenylene ligand allows tune the absorption energy of the Ru complex over a wide range. Compounds with high absorption in the near IR region of the spectrum are of considerable interest for optical data storage, where reading and writing are performed with the help of laser diodes, or for photodynamic therapy, taking advantage of the relative transparency of living tissue to NIR radiation.

Extended porous crystals, based on cathecolate ligands and highly conjugated molecules such as hexahydroxytriphenylene, in combination with transition metals (*e.g.* Fe, Co, Ni, Cu, Ti, V), have received a lot of interest.[120,172] These materials have demonstrated high chemical and thermal stability and porosity. An important consequence of the latter is the proton conductivity that these materials shown. Thanks to their permanent pores, the protons may become the main charge carriers and dominate the direct current. The most famous proton conductive polymer is the Nafion, which presents a proton conductivity of 0.070 S cm^{-1} at 100% of relative

humidity.[173] Fe-HHTP networks have shown a ultra high proton conductivity of 5.0 $\times$ 10^{-2} S cm^{-1} at 98% of relative humidity, which is comparable with several of the highest performing metal-organic frameworks. One of the major properties of two-dimensional cathecolate systems, and a reason why HHTP ligands have not ceased to be studied in recent years, is their inherent electrical conductivity. Single-crystal copper cathecolates has shown an electrical conductivity of 2.0 $\times$ 10^{-1} S cm^{-1} at room temperature, which is more than 1 order of magnitude higher than reported values for other iodine-loaded metal-organic frameworks.[120]

Electrical conductivity of extended porous crystals depends not only on the inherent crystal and electronic structure, but also on defects, crystal morphology, and the packing and orientation of crystal layers. In this context, new synthesis approaches have emerged for the control of crystal morphology of Cu-cathecolate films. Spray coating and layer-by-layer deposition of thin films, are for instance efficient already at room temperature and can be implemented onto a variety of substrates.[121,174] They have demonstrated to be good strategies for room temperature thin film growth, accompanied by the versatility of a wide variety of possible substrates (*e.g* glass, flexible polycarbonate foils, sapphire, quartz or Si/SiO_2). A texturation of the films, with laying parallel planes with respect to the surface, and good connexions between ligands and Cu(II) centres provide efficient pathways for charge carriers and thus, lead to high electrical conductivity. Moreover, the perpendicular-to-the-surface orientation of the pore channels makes them ideally accessible and allows for strong and fast responses. This is clearly advantageous for sensing applications. High sensitivity has been exhibited by Cu-cathecolate thin films ($<$ 100nm) towards the flammable, explosive and toxic ammonia gas. They act as a p-type sensor, where holes dominate the charge transport. When the ammonia comes in contact with the network, the recombination between holes and doped electron from analytes decreases the carrier concentration and increases the resistance of the sensor. Additional synthetic strategies, based on controlled on-surface growth of highly oriented and electroactive thin films has recently been reported.[114] The vapor-assisted conversion method proposed by Mahringer *et al.*, allows the growth of polycrystalline thin films, in which the crystalline grains orient favourably for charge carrier transport between electrodes in photovoltaic devices.

An additional and important application of highly conductive and high specific surface area metal-organic systems is energy storage or conversion. For energy storage purposes, the use of metal-organic frameworks in electrochemical capacitors, also called supercapacitors, has been extensively developed in recent years, due to their high power density and long cycle life.[127] Based on fast and reversible surface redox reactions developed by transition metals and conductive ligands, metal-cathelocate based materials have greatly contributed in this field. Highly oriented nanowires of conductive Cu-cathecolates exhibit a specific capacitance of 202 F g^{-1} at spe-

cific current of 0.5 A g^{-1},[128] which is beyond previously reported values for other metal-organic frameworks-based supercapacitors. In more recent works, hybrid materials based on Ni-cathecolates showed superior specific capacitance of 1877 F g^{-1} at specific current of 1.0 A g^{-1}.[175] The high accessibility of activated sites of metal-cathecolate nanoporus structures allows efficient mass transport, which is of great importance in the electrocatalysis oxygen reduction reaction.[76] The mass transport can be also improved in combination with commercial carbon black, thus, demonstrating the versatility of these materials as substitutive of the expensive and low abundance platinum group materials commonly used as cathodes.

In parallel to the development of metal-organic frameworks, covalent-organic frameworks, where organic ligands react to form strong covalent bonds, has attracted significant interest. Since the synthetic route proposed by Côté *et al.*[9] between HHTP and benzene boronic acid (BDBA) molecules, a new category of tunable porous, crystalline and covalent organic frameworks with high thermal stability has emerged. This strategy involves one-step condensation reactions of discrete molecules known to produce six– and five–membered rings that can suited for the synthesis of extended networks. The eclipsed arrangement of the layers, in which atoms of adjacent sheets lie directly over each other, and the formation of 1D hexagon mesopores with 27 Å of diameter was proven for the first time.[9] However, covalent organic networks are usually synthesised as insoluble and unprocessable powders. This motivated the search of new crystallizing methods, such as the simple solvothermal synthesis directly on single-layer graphene surfaces supported in turn onto more processable substrates (*e.g.* polycrystalline Cu foils, SiO_2 or SiC surfaces).[10] Transparent thin films of covalently linked HHTP and BDDA molecules forming a lattice with vertical alignment were obtained with such method. The photoluminiscence exhibited by the thin films suggests that they are good candidates for organic photovoltaics. The thermal fragility of some building blocks, though, calls for alternative methods able to produce long-range ordered single-layer two-dimensional covalent organic frameworks. Vapor-assisted conversion enabled the on-surface condensation reaction between BDBA and HHTP under very mild-conditions.[93] This method allows a precise control of the film thickness, preserving a smooth and homogeneous coating on a large sample areas and on different substrates.

The prospect for the use of ordered and extended materials as semiconducting nanostructures in electronic devices encouraged the development of surface covalent organic frameworks. Size and growth control, and the fact that on-surface materials are amenable to fine scrutiny with near-field microscopies, are the main strengths of this approach. Based on the boronate-chemistry already explored previously in solution, Zwaneveld *et al.* demonstrated near-complete monolayer nanoporous

structure grown on the Ag(111) surface.[53] Strong thermal stability, up to 750 K, was demonstrated, indicating the presence of strong, covalent linkage. A more exhaustive microscopic and spectroscopic study was carried out by Coratger *et al.* in the same system.[90] First polymerization steps analysis revealed a strong increase in the electron density of states on the organic components (*i.e.* HHTP and BDBA molecules), when they are part of the polymer structure, as well as their activation in some extent, after the loss of oxygen and/or hydrogen atoms. Moreover, the covalent bonding between molecules was confirmed. Parallel studies of supramolecular networks formed by HHTP molecules on Ag(111) surfaces followed this work.[176,177] They attempted an alternative strategy in the formation of stable molecular networks, thanks to the controlled oxidation of the HHTP components by several thermal treatments. These treatments increased their chemical reactivity, promoting both, intermolecular and molecule-substrate interactions.

Another exciting potential application of HHTP molecules is their use in metal-molecule or molecule-molecule heterojunctions, where they could act, for example, as strong electron acceptors, becoming alternatives to more established molecules such as perylenetetracarboxylic dianhydride,[63] tetracyanoquinodimethane,[42] or azine derivatives.[30] They hence may be used to facilitate charge injection from a metallic electrode into a molecular device via interface electrostatic dipoles, or to help spatial separation of charge carriers of opposite sign when combined with donor molecules – two functions opening the door to organic field effect transistors, light emitting diodes, or photovoltaics.

For all these applications, details about molecular orientation with respect to the surface, about the nature of molecule-metal and molecule-molecule interaction, are invaluable. When a molecule is evaporated onto a metallic surface, its morphology can suffer some modifications, which will derive in electrical changes too. After the molecular-surface interaction, the inherent surface dipole is altered as a result of the re-distribution of charges in the surface, which is accompanied by a re-alignment of molecular electronic levels. Additional contributions may come from the case of molecules which present inherent dipoles or strong electron donor/acceptor behaviour.[41] These details give a rationale to control and hopefully improve the performance of future devices, in terms of electric conduction through the molecular or cathecolate layer and of charge carrier injection at interfaces. To this respect, whether the HHTP molecule is dehydrogenated (oxidized) and to which extent is a key information. Indeed, the interaction with individual metal atoms in cathecolate structures, hence their degree of order, requires that the alcohol functions are fully oxidized;[120] the interaction with a metallic electrode, hence the existence/strength of an interface electrical dipole, is potentially dependent on the degree of oxidation, which should also influence the molecular self-assembly at the interface by authoriz-

ing the formation of hydrogen bonds.[42,176,178] The HHTP molecule has been widely used as part of covalent and metal organic networks synthesized either via in solution or on surface approaches. However, exhaustive microscopic and spectroscopic analysis on the self-organised network formed by HHTP molecules or in combination with other organic blocks on metallic surfaces, have been done exclusively on Ag(111)[53,176,177,179] and Au(111)[180]substrate.

Here, we explore the interaction of the HHTP molecule with copper (a typical electrode material and metal of choice in cathecolate systems), in a well-defined system – a Cu(111) surface, under ultrahigh vacuum. Using synchrotron X-ray photoelectron spectroscopy (XPS), near-edge X-ray absorption fine structure (NEXAFS), scanning tunneling microscopy (STM), and density functional theory (DFT) calculations, we are able to resolve the chemical, structural, and electronic transformations of the molecule as the temperature is increased, and the concomitant modification of their on-surface organization. We find that the molecules lay flat on the surface, and that beyond the interface layer the successive molecular layers are also laying flat. We find a stepwise oxidation of the alcohol functions (dehydrogenation) promoted by an increasing stabilisation from the metal surface, which forms strong bonds with the carbon atoms of the molecule and transfers as much as 1.9 electrons to each molecule (the molecule is hence a strong acceptor). This oxidation opens new possibilities for maximising the number of hydrogen bonds, which drives different forms of molecular organizations. We also find indication that copper adatoms tend to be coordinated by the oxygen atoms of the dehydrogenated molecules.

4.2 Chemical structure of HHTP molecules and its chemical synthesis

The 2,3,6,7,10,11-hexahydroxy-triphenylene molecule is an organic compound formed by 18 carbon atoms (grey balls), 6 oxygen atoms (red balls) and 12 hydrogen atoms (white balls) with the structure shown in Figure 4.1). The C atoms arrange forming four centrally fused benzene-like rings, with six hydroxyl chemical groups at the 2, 3, 6, 7, 10 and 11 positions. Its molecular size is 1 nm, taking into account the theoretical distances values for C=C, C-O and O-H bonds (1.4 Å, 1.43 Å, and 0.98 Å, respectively).

The 2,3,6,7,10,11-hexahydroxytriphenylene (HHTP) molecules were purchased from TCI-europe, (95% purity). Then, few purification steps (washing with organic solvents) were carried out until a sufficient molecular purity level of the desired product.

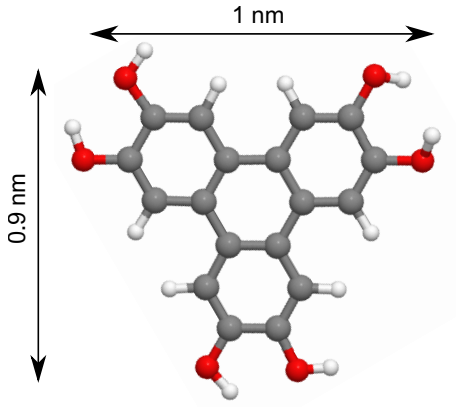

Figure 4.1: Schematic ball-and-stick representation of 2,3,6,7,10,11-hexahydroxy-triphenylene molecule employed during this thesis. The carbon, oxygen and hydrogen atoms correspond to the grey, red and white balls, respectively

4.3 HHTP molecules at room temperature on copper

4.3.1 X-ray photoelectron spectroscopy (XPS)

In a ultra-high vacuum system, HHTP molecules were deposited on an atomically clean Cu(111) surface held at room temperature. Both a multilayer and a sub-monolayer deposit were addressed by XPS and NEXAFS.

High-resolution *in situ* XPS was used to characterize the chemical state of the molecules and get hints on the reaction mechanism. The C 1s and O 1s XPS core-level spectra for a multilayer and a sub-monolayer molecular deposit are displayed in Figures 4.2a and 4.2b, respectively. The data were analysed using least-squares fits to the experimental spectra with Voigt functions describing the different components corresponding to chemically inequivalent states. The detail of the fits used to analyse the data are given in Table 4.1 and Table 4.2.

The multilayer phase features three components for the C 1s spectrum located at binding energies of 285.8 eV, 284.4 eV, and 284.1 eV (Figure 4.2a). These values are those expected for C atoms bond to O atoms, including the two possible connexions through C=O or C-OH (violet component labelled as "C-O") and sp^2 C from the triphenylene skeleton (blue and orange components labelled as "C_{ring}" and "C_{ring}-H", respectively).[181–183]

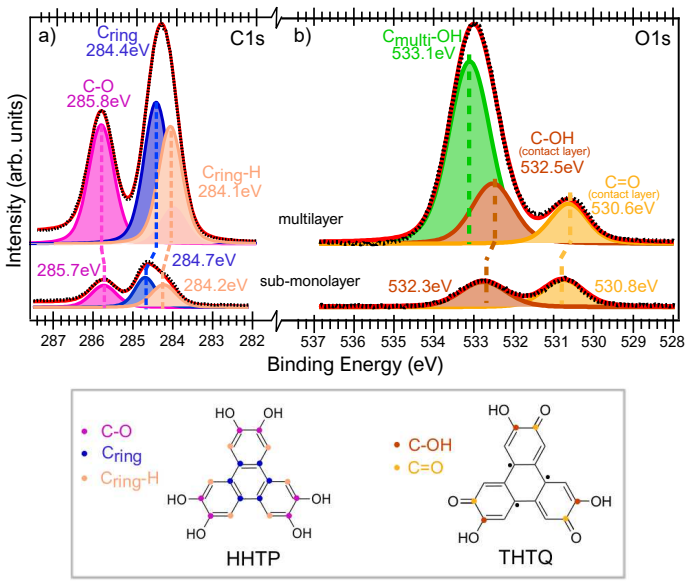

Figure 4.2: a) C 1s and b) O 1s core-level XPS spectra (full dots), after the subtraction of a Shirley background, for a multilayer and a sub-monolayer molecular deposit at room temperature, with a photon energy of 400 eV (C 1s) and 650 eV (O 1s). The spectra are fit (solid red curve) with different components (pink, blue, orange, green, brown and yellow-shaded curves) described by Voigt functions. The models are shown in the lower panel, where the different kinds of C atoms have been marked with colours matching those used for the core-level components displayed in *a* and *b* of intact/pristine HHTP and partially dehydrogenated (THTQ) molecules.

Species	Parameters	C1s/multilayer	C1s/sub-monolayer
C-O	BE(eV)	285.8	285.7
	Area	1.1	0.9
	FWHM	0.62	0.65
C-$_{ring}$	BE(eV)	284.4	284.7
	Area	1.2	1.1
	FWHM	0.69	0.47
C-$_{ring}$-H	BE(eV)	284.1	284.2
	Area	1.0	1.0
	FWHM	0.65	0.6

Table 4.1: Refined fit parameters used for the analysis of the XPS core level spectra for C 1s at 400 eV. The area ratios of all peaks are normalized with respect to "C_{ring}"-H peak.

Species	Parameters	O1s/multilayer	O1s/sub-monolayer
C-$_{multi}$-OH	BE(eV)	533.1	
	Area	2.1	
	FWHM	1.05	
C-OH	BE(eV)	532.5	532.8
	Area	1.6	1.0
	FWHM	1.1	1.2
C=O	BE(eV)	530.6	530.8
	Area	1.0	1.0
	FWHM	0.9	1.4

Table 4.2: Refined fit parameters used for the analysis of the XPS core level spectra for O 1s at a photon energy of 650 eV. The area ratios of all peaks are normalized with respect to "C=O" peak.

As discussed by Olivieri *et al.*,[184] discerning a contribution from fully and partially saturated sp^2 C atoms in the latter component is not always straightforward, and indeed here the "C_{ring}" and "C_{ring}-H" components are too broad and close in binding energy to be apparent at first sight in the experimental data. The 1:1:1 area ratio for the areas of the "C-O", "C_{ring}", and "C_{ring}-H" components nevertheless agrees well with our assignment for an intact HHTP molecule.

Turning to the XPS spectra of the sub-monolayer deposit, we now clearly observe the three components, with 285.7 eV ("C-O"), 284.7 eV ("C_{ring}"), and 284.2 eV ("C_{ring}-H") binding energies (Figure 4.2a). These values match those found for aromatic organic oxygen-containing molecules in contact with metallic surfaces such as Cu(111) and Ag(111).[75,91] The slightly differences notice in these binding energy values with respect the ones found for multilayer phase, can be explained by a charge redistribution within the molecule, as it has been already reported in an analogue system (hydroxycyanobeze on Au(110)).[184] The area ratio of the three components is here again 1:1:1, consistent with the fact that one third of the C atoms are linked to O atoms, and that the other two thirds are either fully saturated C atoms or C atoms bond to H atoms.

The chemical transformations appearing when contacting HHTP molecules with the Cu surface at RT become more evident when analysing the O 1s core-level spectra shown in Figure 4.2b. The multilayer phase displays two O 1s peaks located at binding energies of 533.1 eV and 530.6 eV. These values are very close to those obtained in a related system, tetrahydroxy-benzene molecules on Cu(111),

where the hydroxyl groups were transformed into ketone ones upon annealing of the surface up 440 K— with the ketone group corresponding to the highest binding energy peak.[179,181,185] In the multilayer phase, there are two categories of HHTP molecules; the ones which are in contact with the copper surface (referred in Figure 4.2 to as contact layer) and the ones that pile up on those ones (referred to as multi). The direct contact of the molecules with the substrate make them undergo to a spontaneous dehydrogenation, leading as in tetrahydroxy-benzene example, the transformation of these groups into ketone ones. This explains why in our system, the peak located at 530.6 eV corresponds to ketone groups ("C=O") and the third peak located at 532.5 eV reflects the presence of intact hydroxyl groups in the contact layer ("C-OH"). Finally, it only remains to assign the peak at 533.1 eV to the intact hydroxyl groups of the molecular layers above the contact one ("C_{multi}-OH"). The 1:2 area ratio of the "C=O" versus "C_{multi}-OH"+"C-OH" components indicates that most hydroxyl groups remain intact (fully hydrogenated).

Two main differences are observed compared to the O 1s core level spectrum of the sub-monolayer deposit (before thermal treatment): no "C_{multi}-OH" component is observed, and the ratio of the two remaining components is about 1:1. The binding energy difference of 0.6 eV between the "C_{multi}-OH" and "C-OH" components is small but significant, and it suggests a charge redistribution in the system due to the contact with the Cu(111) surface, just like we discussed previously in the case of the C 1s core level spectra. The 1:1 ratio shows that almost half of hydroxyl groups of the molecules which constitute the contact layer have been transformed into ketone groups upon dehydrogenation.

4.3.2 Near-edge X-ray absorption fine structure

Further insights about the presence of certain chemical functional groups and the nature of the carbon bonds can be obtained via an analysis of electronic transitions between occupied and unoccupied molecular orbitals. Such transitions have characteristic signatures in NEXAFS spectra, which we discuss now. Figure 4.3a shows two C 1s spectra, acquired for the multilayer deposit with a polarization of the electric field parallel (s-polarization) and perpendicular (p-polarization) to the surface. Each peak corresponds to a specific electronic transition, and the comparison of our data with measurements done with simpler compounds with carbon skeleton or chemical groups corresponding to those of the HHTP molecule (benzene and phenol) allows to assign them.[186–188]

The peaks at 284.9 eV and 288.9 eV (p-polarization) are also found in benzene, where they have been ascribed to transitions from the C 1s level to the first, sec-

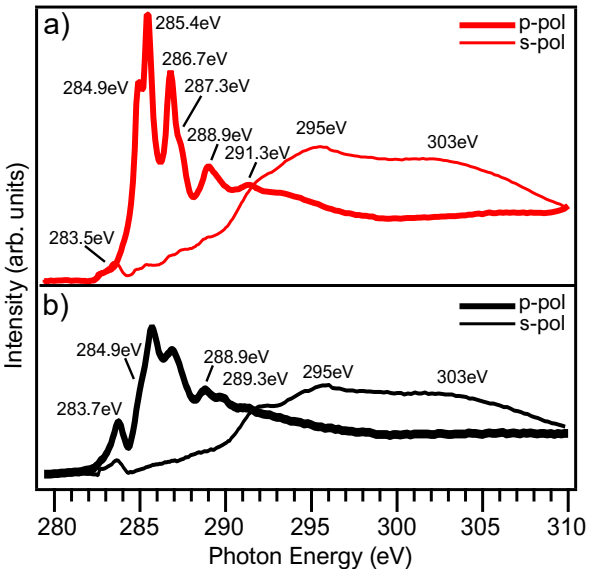

Figure 4.3: C 1s K-edge NEXAFS spectra, acquired with a p-polarization (electric field perpendicular to the surface) and s-polarization (electric field parallel to the surface) for a) multilayer and b) sub-monolayer (before thermal annealing).

ond, and third excited π^* states, as it is shown in Figure 4.4. It depicts a diagram of electronic states found for benzene molecule (on the left) and the one that one could qualitatively expect for HHTP molecules (on the right). Typical electronic transitions of benzene are expected to be found in the HHTP, since parts of its structure resembles to it. The full diagram includes the more likely electronic transitions of benzene (between C 1s ground state and first, second and third excited states - $\pi^*_{1,2}$ and π^*_3) and the splitting of the electronic states when more H, C=O and C-OH groups are present in the structure. Single dots between electronic levels in Figure 4.4 denote the possible existence of more intermediate electronic levels.

Four other peaks, which are not found for benzene, are observed in p-polarization at 285.4 eV, 286.7 eV, 287.3 eV, and 291.3 eV in Figure 4.3a. The HHTP molecule actually has three types of chemically inequivalent C atoms (those of the central rings, those at the peripheral rings bearing H atoms, and those at the peripheral rings bearing OH groups), and consequently it does not feature a unique C 1s level (consistent with the analysis of the XPS data) or a unique set of excited π^* states (see Figure 4.4). A possible assignment of the four above-mentioned peaks could hence invoke transitions from one of the C 1s levels to one or the other set of excited π^* states.

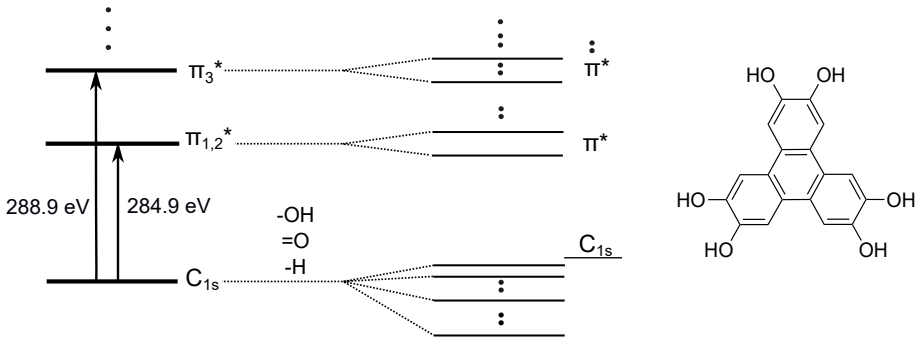

Figure 4.4: Diagram of electronic states of HHTP molecule. Reproduced and adapted from reference 186.

Measurements with a s-polarized light (Figure 4.3a) reveal broad peaks, whose energy (289.3 eV and 295-303 eV) is characteristic of electronic transitions to σ^* excited states, *i.e.* molecular orbitals with a strong planar character, for instance, associated to the carbon skeleton for instance. In deed, the peak at 289.3 eV corresponds to σ C-H bond of carbon skeleton transition, which energy can vary depending on the stretching of the bond.[189] The small peak appearing at 283.5 eV is a reminiscent contribution of the molecular contact layer, as occurred also in XPS experiments, which origin will be discussed below.

It is noteworthy that we observe separately the electronic transitions involving π^* and σ^* states with different light polarizations. This indicates that the molecules lay flat on the surface and grow layer by layer in the multilayer deposit.[30,190] Such an orientation could be promoted by π^*-π^* stacking or H bonds between the different layers. We will come back to it during the O 1s NEXAFS spectra analysis.

We now turn to the C 1s NEXAFS spectra acquired with p-polarization for the sub-monolayer deposit. Three main observations can be made: i) all peaks are now broader, ii) the peaks at 284.9 eV and 288.9 eV (those also found in benzene) have now a lower intensity, iii) and an additional peak is found at 283.7 eV (Figure 4.3b). All the three considerations are related to the re-hybridization that the molecules experience once they are in contact with the metallic substrate.[30] This contribution affects, in first instance, the width and intensity of the peaks corresponding to the π-transitions. Also, the peak located at 283.7 eV presumably originates from an internal charge re-distribution (already observed in XPS experiments), since it is reminiscent of the one observed in p-benzoquinone (two ketone groups in *para* position on a sp^2 hexagonal carbon ring), which was assigned as a transition to a

low-energy molecular C=C-C=O hybrid π^* orbital.[186] This points towards a (at least) partial dehydrogenation of the hydroxyl groups of the HHTP molecule upon contact with the Cu(111) surface, consistent with the XPS analysis. Finally, for s-polarized light, the NEXAFS spectra are starkly different, confirming that the molecules lay flat on the surface also in the sub-monolayer phase.

The O 1s NEXAFS spectra acquired with a p-polarization bring complementary information (see Figure 4.5). For the multilayer sample, we observe three main peaks at 532 eV, 535.0 eV, and 538.8 eV. In aminophenol molecules, the same peaks have been assigned to electronic transitions to, respectively, π^* hybrid orbitals between O and C atoms, σ^* hybrid orbitals between O and H atoms, and σ^* hybrid orbitals between O and C atoms. The second peak is thus a clear indication that the O-H bonds in the multilayer phase are not planar. A straightforward interpretation would be the presence of H-bond cross-links between the different layers of flat-laying HHTP molecules. This is, in a sense, reminiscent of the organization revealed in three-dimensional crystals made of HHTP molecules.[169,178,191] The first peak has a low intensity, such that it could actually correspond to the contact layer with the substrate.

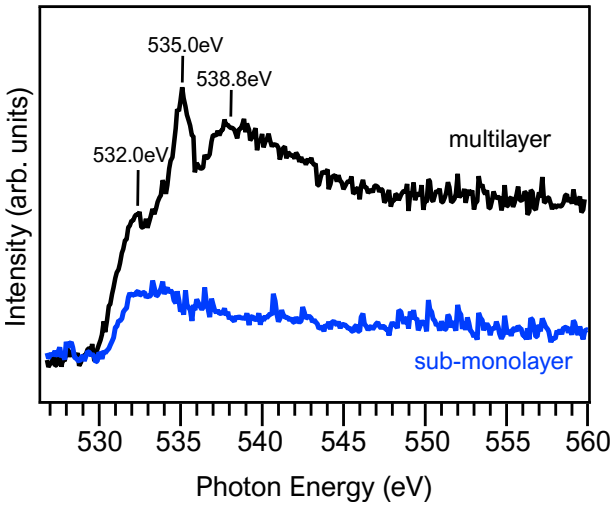

Figure 4.5: O 1s K-edge NEXAFS spectra acquired with a p-polarization (electric field perpendicular to the surface) for the multilayer deposit and the sub-monolayer deposits, before and after thermal annealing.

4.4 Thermally-induced dehydrogenation of the hydroxyl groups

4.4.1 Continuous temperature-dependent XPS study

As initial approach, a continuous temperature-dependent *in situ* study of the multilayer phase was carried out. This gives us a comprehensive overview of the system's evolution with the temperature for both, C 1s and O 1s core level spectra. O 1s core level spectra *versus* temperature map is shown in Figure 4.6. A first component is located at binding energy of around 532.5 eV, corresponding to the intact hydroxyl groups (C-OH) of the molecules. The second one is located at binding energy of 530.5 eV, corresponding to dehydrogenated hydroxyl groups. The intensity of this peak is increasing at the expense of the other component while increasing the temperature. At 590 K, the intensity of the peak starts decreasing indicating the decomposition of the molecules. It is noteworthy that the excess of HHTP molecules that compose the multilayer phase, are gradually desorbed from the surface leading to a HHTP monolayer on Cu(111) after the annealing process.

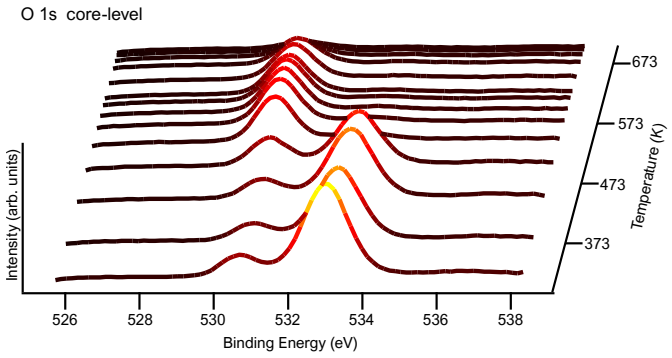

Figure 4.6: Map showing O 1s core-level spectra *versus* temperature starting from a multilayer of HHTP molecules deposited on Cu(111) at room temperature.

The C 1s core level spectra *versus* temperature map. As it is shown in Figure 4.7, two main components are observed already at room temperature. At higher binding energy values (285.8 eV), a less intense and narrower peak is attributed to the carbon atoms that are attached to oxygen ones (C-O), whereas the intense component at lower binding energies (284 eV) is related to the carbon skeleton of the HHTP molecules ("C_{ring}"). At around 590 K, the C-O component starts to disappear while the "C_{ring}" component is detected even at the highest tested temperature. This indicates that at such temperatures the triphenylene skeleton remains intact and no new covalent links are induced by the thermal treatment.

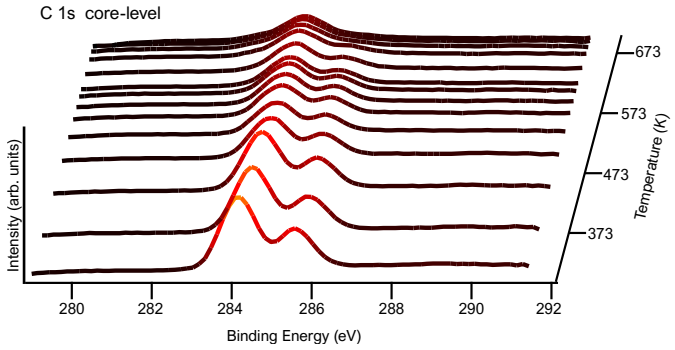

Figure 4.7: Maps showing C 1s core-level spectra *versus* temperature starting from a multilayer of HHTP molecules deposited on Cu(111) at room temperature.

4.4.2 XPS on thermally-induced sub-monolayer phase

The temperature-dependent XPS analysis revealed profound changes of the C 1s and O 1s core levels spectra above 500 K. Thus, we address in details samples obtained after a thermal treatment at 530 K in order to resolve the chemical transformation of the molecule, and to understand its effect on the molecule-molecule and molecule-surface interactions.

The main effect of annealing at 530 K the sub-monolayer molecular deposit is a shift of the entire XPS spectrum to lower binding energies. The "C-O", "C_{ring}", and "C_{ring}-H" components are shifted by 0.2 eV, 0.3 eV and 0.3 eV respectively (Figure 4.8). Shifts of comparable magnitude have been reported for quinoneazine systems and were ascribed to a charge donation from the copper substrate, thus increasing the electron charge population around C atoms.[30] The shifts are less strong than those observed alongside the Ullmann coupling reaction, where the formation of strong and highly-polarised C-Cu bonds in the intermediate reaction step yields a C 1s contribution centred at around 283 eV.[75] The detail of the fits used to analyse the data are given in Table 4.3 and Table 4.4.

Overall, the presence of three peaks on the C 1s core level spectra reveals three kinds of chemically-inequivalent C atoms in the molecules, and the observed shift between the corresponding binding energies before and after annealing suggests a charge transfer from the substrate to the molecule after a thermal annealing treatment. As we will now see, this effect is accompanied by a chemical transformation of the molecule.

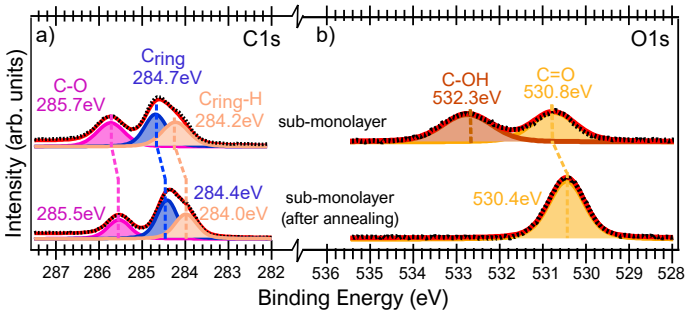

Figure 4.8: a) C 1s and b) O 1s core-level XPS spectra (full dots) after the subtraction of a Shirley background, for a sub-monolayer molecular deposit at room temperature and after annealing at 530 K. Measurements were carried out with a photon energy of 400 eV (C 1s) and 650 eV (O 1s). The spectra are fit (solid red curve) with different components (pink, blue, orange, green, brown and yellow-shaded curves) described by Voigt functions.

Species	Parameters	C1s/sub-monolayer	C1s/after annealing
C-$_{multi}$-OH	BE(eV)	285.7	285.7
	Area	0.9	0.8
	FWHM	0.6	0.5
C-OH	BE(eV)	284.7	284.4
	Area	1.1	1.4
	FWHM	0.5	0.4
C=O	BE(eV)	284.2	284.0
	Area	1.0	1.0
	FWHM	0.6	0.5

Table 4.3: Refined fit parameters used for the analysis of the XPS core level spectra for C 1s at a photon energy of 400 eV. The area ratios of all peaks are normalized with respect to "C=O" peak.

After the thermal annealing, the O 1s core level spectrum also changes. A single component is observed at a binding energy of 530.4 eV. This is an evidence that all hydroxyl groups have been dehydrogenated. This suggests a significant catalytic activity of the Cu(111) surface at 530 K. The corresponding product in the gas phase would have a sextu-radical form, or alternatively a hexaquinone form (product B in Scheme 4.1) — without considering the effect of the surface.

At this point we wish to mention that the analysis of the O 1s spectra of the sub-

Species	Parameters	O1s/sub-monolayer	O1s/after annealing
C-OH	BE(eV)	532.8	
	Area	1.0	
	FWHM	1.2	
C=O	BE(eV)	530.8	530.4
	Area	1.0	1.0
	FWHM	1.4	0.8

Table 4.4: Refined fit parameters used for the analysis of the XPS core level spectra for O 1s at a photon energy of 650 eV. The area ratios of all peaks are normalized with respect to "C=O" peak.

monolayer sample (before thermal annealing), shown in Figure 4.8b, does not feature a component between the "C-OH" and "C=O" components. This is at variance with the analysis made by Giovanelli *et al.* on a much related system, dehydrogenated HHTP molecules on Ag(111).[179] In our case, such an intermediate component is not needed to produce a good fit to the experimental data. This does not exclude that such a component exists, and since it was ascribed to H bonds between the molecules, we actually do expect it in principle (see discussion below). Equally good fits can actually be produced by introducing one or several (we expect different kinds of H bonds, see discussion below) intermediate components with low weight. It seems that nevertheless, if these components exist, they have relatively low weight. The difference with the case of a Ag(111) substrate might relate with strength of the H bonds between the C=O and H-O groups, which is possibly more limited in our case (Cu(111) substrate). The bowl-shape of the molecules on Cu(111) (we will come back to the morphological analysis of the molecules later) imposes that the C=O and H-O groups do not lay in the same plane, which is not optimal for strong H bonds.

Chemical pathway of thermally-induced dehydrogenation

On the basis of XPS and NEXAFS, we can conclude that the HHTP molecules are not stable on the Cu(111) surface. At room temperature, half of the hydroxyl groups have lost their hydrogen atoms. After thermal annealing at 530 K, all six hydroxyl groups have lost their hydrogen elements (see Scheme 1). Unlike what is reported by Giovanelli *et al.* where only a partial thermally-induced dehydrogenation (of only four of the six hydroxyl groups) accompanied by strong hydrogen bonds between dehydrogenated and still-hydrogenated hydroxyl groups is observed when HHTP molecules are deposited on Ag(111).[179] Imaging of the supramolecular self-assembly

before/after thermal treatment will give us further confirmation of the stepwise dehydrogenation of the HHTP molecules on Cu(111).

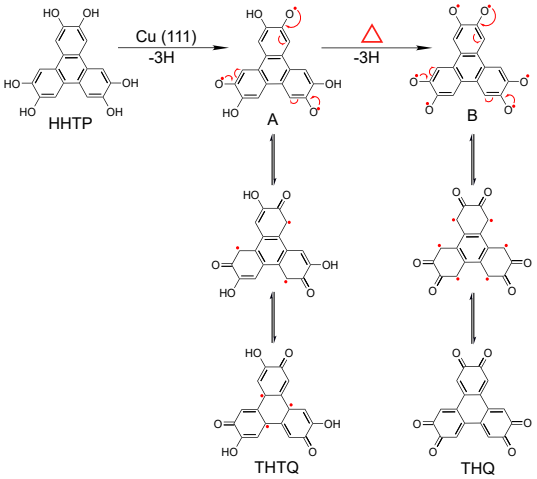

Scheme 4.1: Dehydrogenation of sub-monolayer of HHTP molecules on Cu(111) deposited at room temperature. Partial dehydrogenation produces A. Two other molecular forms are displayed, one of which, trihydoxy-triphenylene-quinone (THTQ), featuring a molecular resonance. Full dehydrogenation of the hydroxyl groups leads to product B. Two other molecular forms are displayed, one of which is a triphenylene-hexaquinone structure (THQ).

4.5 Effect of dehydrogenation on the assembly of HHTP on Cu(111)

In STM, the molecules appear as threefold-symmetry objects, equilateral triangles with a side-length of about 1.0 nm (Figure 4.9) matching the expected dimension of a flat-laying molecule (Scheme 4.1) on Cu(111). Before thermal annealing, the sub-molecular deposit forms domains of sizes of the order of a few tens of nm, as it is shown in Figure 4.10a. The molecular domains are delimited by dashed lines and they are well-oriented along $[1\,\bar{1}\,0]$ and $[0\,1\,\bar{1}]$ surface directions.

Different kinds of domains are found. An example of the first kind is shown in Figure 4.9a. The molecular lattice is triangular, and within the precision of our STM measurements, its unit cell seems to coincide with (5×5) unit cells of the Cu(111) surface (the crystallographic orientation of the substrate has been determined via electron diffraction), corresponding to a lattice constant of 1.1 ± 0.1 nm. The molecules are oriented with their mirror plane aligning a dense-packed row of the substrate ($[1\,1\,\bar{2}]$ direction, see Figure 4.9c). A second kind of domain is shown

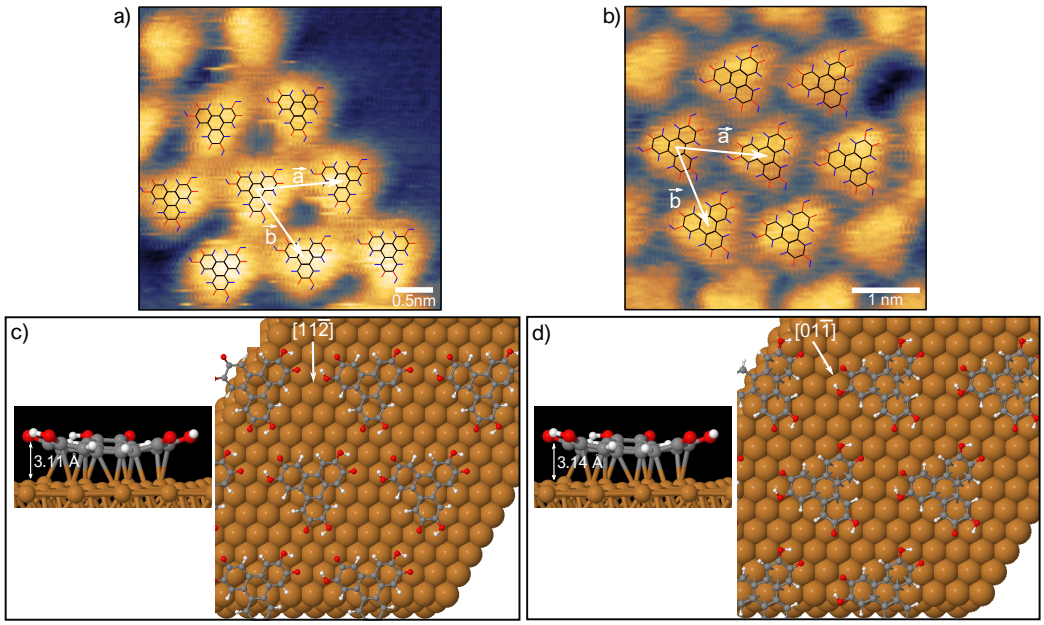

Figure 4.9: a,b) STM images, taken at constant current I = 0.1 nA and bias V = -0.8 V, of a sub-monolayer deposit, for two different kinds of supra-molecular networks (low and high density) coexisting on the surface. A few molecules are overlaid on the STM image and the unit cell's vectors are indicated. The molecules's structure is overlaid on the STM image (black sticks: C-C bonds, red sticks: C-O bonds, blue sticks: O-H and C-H bonds). c,d) Corresponding molecular models shown in top- and side-views, whose geometry has been optimized via DFT calculations.

in Figure 4.9b. The lattice is here also triangular, and seems to be commensurate to the substrate lattice too, once more with a (5×5) coincidence. In this unit cell, the molecules are organized differently, though. The lattice constant is the same as the other phase, naturally. The mirror plane of the molecules aligns to $[0\,1\,\bar{1}]$ direction of the substrate (Figure 4.9d). Both domains present a well-defined orientation along the three high-symmetry family $\langle\bar{1}\,0\,1\rangle$ directions with respect to the Cu(111) lattice as it is shown in Figure 4.10a.

Our STM images do not allow to directly determine the binding site of the molecules on the substrate. This information is nevertheless crucial to understand the relative importance of intermolecular and molecule-substrate interactions, which in turn is related to the chemical form of the molecules (fully hydrogenated or not). We remind that the joint XPS and NEXAFS analysis indicates that before thermal annealing, the HHTP molecule is partially dehydrogenated. According to DFT,

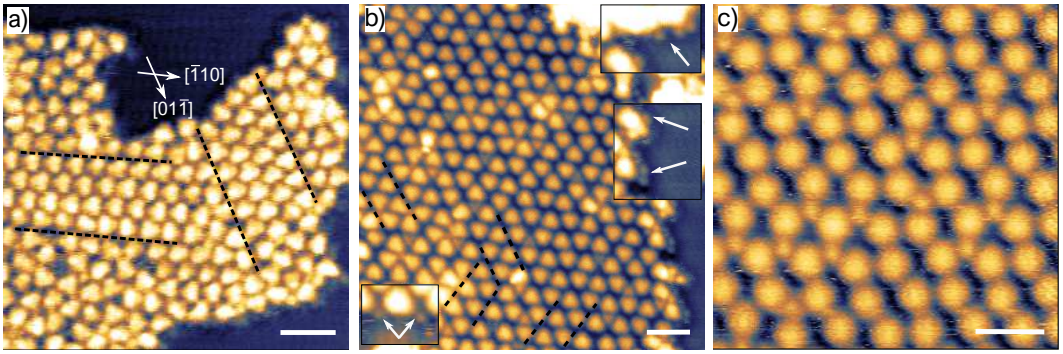

Figure 4.10: a) STM image of a sub-monolayer deposit on Cu(111) at room temperature, taken at constant current I = 0.1 nA, and V = -0.8 V (scale bar of 10 nm). b) STM image of a sub-monolayer deposit annealed at 530 K, taken at constant current I = 0.07 nA, with V = -0.8 V (scale bar of 2.5 nm). c) Close-view of a sub-monolayer of molecules deposited on Cu(111) held at 530 K. The STM image was taken at a constant current I = 0.1 nA, with V = +1.0 V (scale bar of 2 nm).

when it is far from other molecules, such a molecule on Cu(111) has a lowest-energy binding configuration with the C atoms of the central ring sitting almost exactly atop the hollow sites of the Cu(111) surface (Figure 4.11). In this case the molecule has a bowl shape, with a height of 3.14 Å.

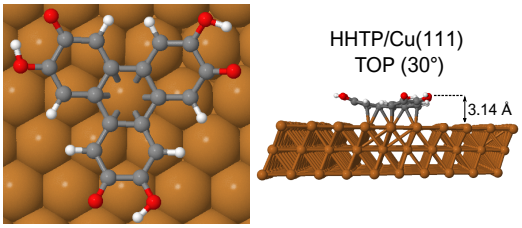

Preferential binding site position for HHTP (partially hydrogenated)	Adsorption energy (E_{ads})	Molecule-substrate height (Å)
TOP	0.00	3.14
FCC-HOLLOW	+0.11	3.14
HCP-HOLLOW	+0.12	3.14
BRIDGE	+0.17	3.14

Figure 4.11: Preferential binding site of a HHTP molecule on Cu(111) with the central ring laying on TOP sites of copper substrate. The table summarizes the adsorption energy values (E_{ads}) for the three possible sites (HOLLOW, TOP and BRIDGE) of the substrate, normalized to the most stable one (TOP) and the calculated heights for a HHTP molecule at each position.

The molecular arrangements discussed above are very similar to two local energy minima in the configuration landscape that we addressed with DFT. These minimum-energy configurations consist of the same coincidence lattices as those deduced from the STM observations. One of these configurations (5×5 with molecular orientation along $[1\,1\,\bar{2}]$ direction) features a molecular binding on the substrate with only two C atoms in the central ring sitting atop hollow sites of the substrate

(Figure 4.9c). This binding configuration is not the one found for the (quasi) isolated molecule (Figure 4.11), but it indeed has lower energy (i.e. the proximity of neighbour molecules modifies the hierarchy of the binding energy configurations). For the other configuration (5×5 with molecular orientation along [0 1 $\bar{1}$] direction), the molecular bonding resembles the case of far-appart molecules, with all C atoms of the central ring atop Cu(111) hollow sites (Figure 4.9d). Compared to the case of far-appart molecules (Figure 4.11), the molecules are rotated, which may be seen as a consequence of their mutual interaction. The shortest inter-molecular H-O bonds are 3.17 Å, which is typical of H-bonds.[5] The two configurations correspond to similar binding energies (4.21 *vs* 4.09 eV/molecule), and in both cases, the molecule has a bowl shape. Overall the molecular system is in a weak chemisorption regime following the Newns-Anderson model.[61]

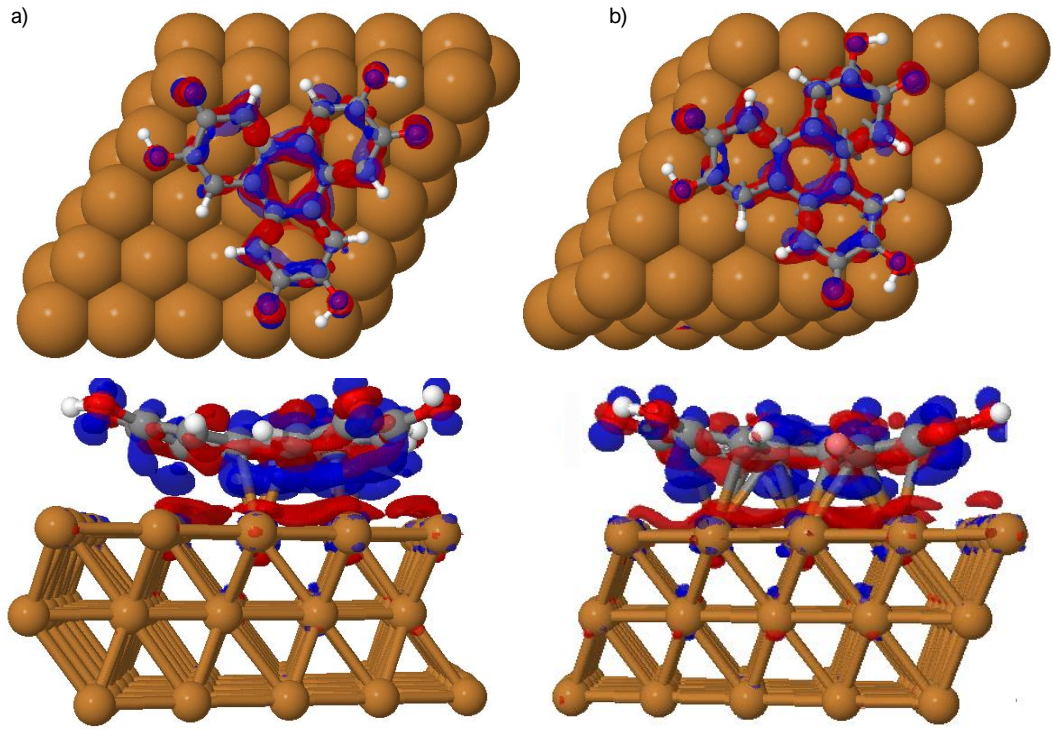

Figure 4.12: Isocontour of the charge distribution (top and side views) over an HHTP molecule partially dehydrogenated on Cu(111) for a) (5×5) configuration oriented along [1 1 $\bar{2}$] direction and b) (5×5) configuration oriented along [0 1 $\bar{1}$] direction. Blue and red colours represent accumulated and depletion charge areas, respectively. In both cases, an internal charge redistribution and a charge transfer from the substrate to the molecule take place.

In these minimum-energy configurations, all C bonds have the same length in the central ring, suggesting no alternating C-C and C=C bonds. This corresponds to the structure of THTQ molecule (Scheme 4.1). Our DFT calculation find strong charge transfers amounting 1.2 electrons per molecule from the Cu atoms to the C atoms (see Figure 4.12). This charge transfer is distributed unevenly across the molecules, with O atoms in the dehydrogenated OH groups having each an excess of 0.17-0.18 electrons, and the six C atoms bond to the central C ring having each an excess of 0.15-0.26 electrons.

For both molecular configurations (Figure 4.12a and b), important depletion charge areas (in red) are found on the copper surface, just below the molecule, confirming the direction of the charge transfer indicated previously (from the surface to the molecule). Also, all central C atoms and all O atoms are acceptor electrons (areas in blue) coming from either the surface or from inside the molecule itself, indicating a strong charge redistribution linked to the partial dehydrogenation of the molecule. This finding confirms the oxidized character of the dehydrogenated molecule, which acts as a good electron acceptor, and the loss of aromaticity in the central ring since due to an homogeneous distribution of charge over the six C atoms.

After annealing to 530 K (Figure 4.13a) or depositing at this temperature (Figure 4.10c), a different kind of supra-molecular network is observed. The domains are larger than in the case of molecules deposited at room temperature without annealing, but they comprise a large number of structural defects, that we will discuss later. For now, we focus on the ordered parts of the lattice. In these parts, the molecule's mirror axis aligns the $[1\,1\,\bar{2}]$ crystallographic direction of the substrate, and chains of molecules with a single orientation form. The parallel chains of molecules have alternating molecular orientation and bunch in sets of two closer chains. At least to a very good approximation, the molecular lattice coincides with (9×8) unit cells of the Cu(111) substrate (Figure 4.13c). It resembles the so-called zip phase reported by Coratger *et al.* for HHTP molecules on Ag(111).[90]

According to the XPS and NEXAFS analysis, the hydroxyl groups of the molecules are now expected to be fully dehydrogenated. We find that the distance between H atoms (which are bonded to C atoms of the triphenylene skeleton) and O atoms (which are bonded to C in the ketone group form) is between 1.75 and 3.0 Å, which is in range expected for H bonds in such a system: Parwin *et al.* reported 2.86 Å; with anthraquinon molecules.[192] One should keep in mind that the system features a certain degree of structural constraint imposed by the bonding to the substrate, which is sufficiently strong to lead to a commensurate molecular lattice. In the present case, the H bonds involve two H atoms and one O atom, and thereby should involve all the H atoms of the molecules. This maximized number of H bonds pre-

sumably is the reason why the molecular density is higher than in the previously discussed molecular lattices.

The molecular arrangement observed with STM is here also very similar to a minimum energy-configuration found with DFT for the same coincidence lattice. This configuration comprises three different kinds of molecular binding configurations (Figure 4.13c), one of which corresponding to the lowest-energy binding configuration in the case of far-appart molecules (all of the C atoms of the central ring fall atop in hollow sites, and O atoms lay over the top sites of the copper lattice, maximizing the contact with it).

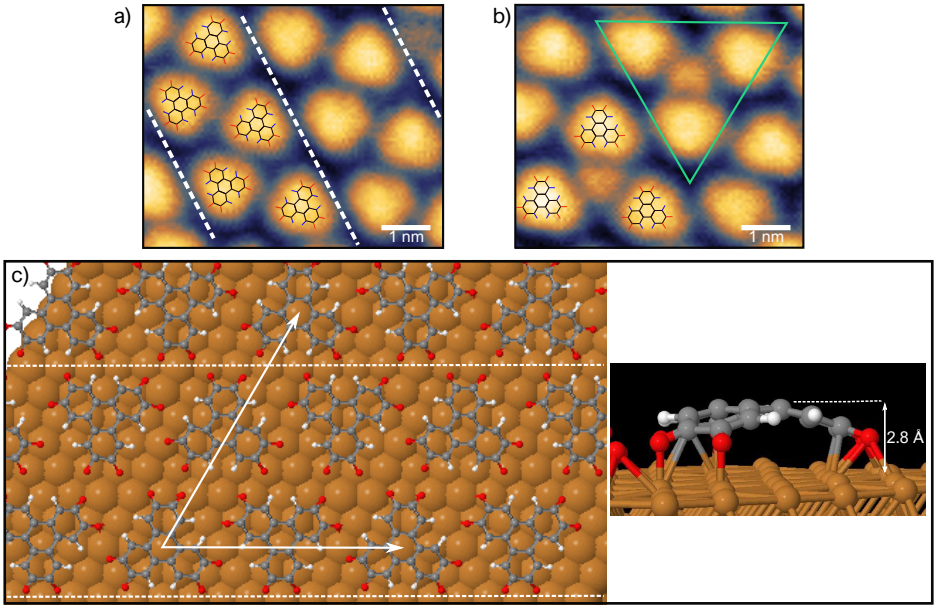

Figure 4.13: a,b) STM images, taken at constant current I = 0.07 nA and bias V = -0.8 V, of a sub-monolayer deposit after an annealing at 530 K. In a) ordered parts of the lattice are delimited by dashed lines. b) Shows the molecular trimers formed by three HHTP molecules with a trapped object at the hollow site at the center of the trimer. The structure of a few molecules is overlaid on the STM image (black sticks: C-C bonds, red sticks: C-O bonds, blue sticks: O-H and C-H bonds). c) Corresponding molecular models shown in top- and side-views, whose geometry has been optimized by DFT calculations.

Now, the molecules have a dome shape (Figure 4.13c) – and not a bowl shape as in the case of partially-dehydrogenated molecules. In the four C rings, the C bond length alternates from 1.38 Å to 1.45 Å, as expected for benzene rings. This form corresponds to the top-right structure shown in Scheme 4.1, where the O atoms

would be radicals if the molecule were in the gas phase. This is obviously not the case in the presence of Cu(111), but the DFT calculations do predict short Cu-O distances (consistent with the dome shape, Figure 4.13c) and strong electron transfers from Cu to O atoms. In total, 1.9 electrons are transferred from the substrate to the dehydrogenated molecule. This charge transfer is especially strong, beyond the values obtained with molecules such as perylenetetracarboxylic dianhydride, tetracyanoquinodimethane, and azine derivatives that are acknowledgedly strong electron acceptors.[30,42,63]

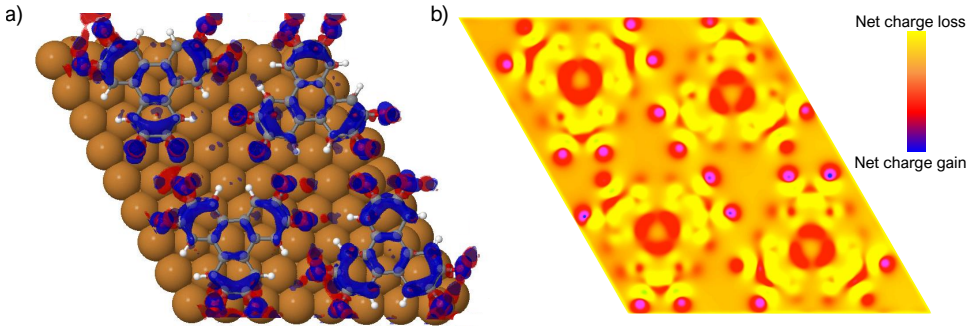

Figure 4.14: a) Isocontour of the charge distribution over fully dehydrogenated HHTP molecules on Cu(111) for (9×8) configuration, obtained after annealing at 530 K. Blue and red colours represent accumulated and depletion charge areas, respectively. In both cases, an internal charge redistribution and a charge transfer from the substrate to the molecule take place. b) Net charge loss and gain calculated in a plane comprising the lowest-laying C atoms of the molecule.

Singular charge distribution can be observed in Figure 4.14a. Depletion charge areas are found at specific places on the copper surface (below the oxygen atoms are linked to it) whereas charge accumulation occurs on C and O atoms. Compared to the partially dehydrogenated molecules, the six C atoms bond to the central C ring have less excess electrons (0.11-0.17), while all O atoms now have an excess of 0.16-0.18 electrons. As pointed out previously with the C-C distances of the central ring, the aromaticity seems to be recovered since now, alternate charge accumulation areas are displayed in this part of the molecules. Also, important charge accumulation is clearly found at the O atoms that are linked to the copper surface, when the charge loss/gain at lower C plane is drawn (Figure 4.14).

4.5.1 Defects in the lattice of dehydrogenated molecules

The molecular phase we just described contains a significant density of defects. These defects occur whenever along a molecular chain, a molecular stacking fault

(*i.e.* a molecule rotated by 180° with respect to the others along the chain) is found. Overall, the defect can be described as a trimer of molecules all of them pointing in the same direction (delimited by a green triangle Figure 4.13b), with the distance between the molecules' center of around 2.4 ± 0.1 nm. At the center of this trimer, an object is systemically found, whose (apparent) height is intermediate between that of the pristine Cu(111) surface and that of the molecule (Figure 4.13b), and whose lateral size is significantly smaller than that of a molecule. Careful inspection at the edges of the molecular domains reveals even smaller objects with similar height. This is highlighted in inset images of Figure 4.10b, which correspond to zooms at the island edges, where white arrows point to what we assign to Cu adatoms. The size of these objects overall seems incompatible with a molecular origin, suggesting that they could be individual atoms or small clusters of atoms. Figure 4.15 shows the corresponding apparent heigh profiles for (presumably) Cu adatoms found either the border of the molecular islands or inside trimers of HHTP molecules oriented in the same direction, created after annealing. The apparent heigh values found for both species are 0.25 Å, suggesting that the small fragments created inside of the trimers and the laterally smaller features at the molecular islands' edges are of the same nature (individual or clustered Cu adatoms).

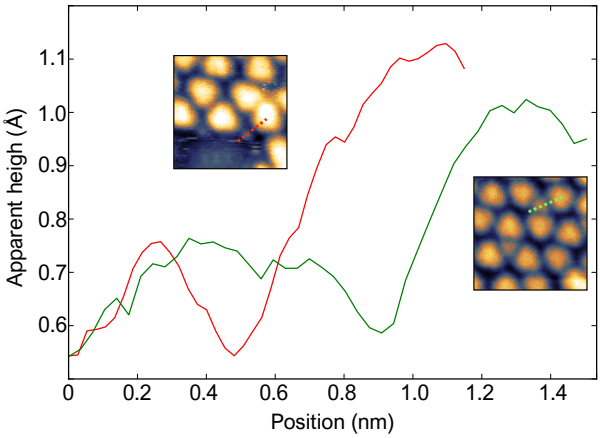

Figure 4.15: Apparent heigh profiles of individual or clustered Cu adatoms and HHTP molecules after annealing. The red profile corresponds to a Cu adatom found in the border of the molecular island whereas the green profile corresponds to the Cu cluster created alongside the formation of triangular defects in the supramolecular lattice. Inset STM images and coloured dash lines show the place where the profiles were taken.

The Cu(111) surface is actually known to be in equilibrium with individual Cu adatoms, specially so when the temperature is increased above room temperature like in our experiments.[193] These adatoms were reported to be involved in the

formation of metal-organic systems, via linkage with oxygen,[30,71,181,185,194] nitrogen,[91,92,195] or sulphur atoms.[196] The smallest of the objects we find at the edges of the molecular islands have a size compatible (keeping in mind the convolution with the shape of the scanning STM tip) with the lateral extension of a molecule imaged on a surface, (see inset of Figure 4.15) we note that some of these objects are located at the corners of the molecules, in the immediate vicinity of the dehydrogenated OH groups (O atoms, hence) which are expected to readily coordinate with Cu atoms (forming Cu-O-C bonds).

Arguments supporting this view are found in DFT calculations performed with trimers of dehydrogenated molecules, with and without a few-atom Cu cluster trapped in the region delimited by the molecular trimer. Figure 4.16 shows most relevant trimer configurations with their corresponding absorption energy values per molecule. As previously noted, the dehydrogenated HHTP molecules which conform a trimer structure are oriented in the same direction.

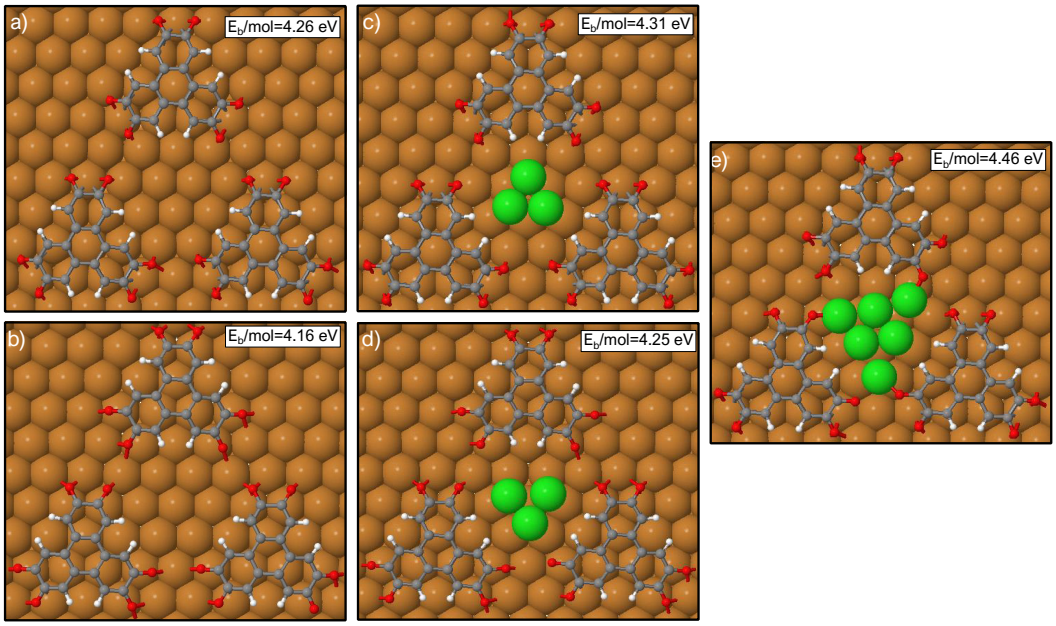

Figure 4.16: Molecular models shown in top-views for trimers generated after annealing of the sample at 530 K, whose geometry has been optimized by DFT calculations. Each configuration is displayed with by its associated binding energy per molecule (E_b/mol). The green balls represent Cu adatoms trapped in the centre of the trimer structure.

A trimer structure without small fragment in its centre is more stable if all C atoms of the central ring lay at atop hollow sites, giving an absorption energy of 4.26 eV (Figure 4.16a). This agrees with what was pointed out in previous section,

since in this configuration the O atoms that are linked to the surface do so through top copper sites. The inclusion of three Cu atoms at the center of the trimer (represented by green balls in Figure 4.16c) leads to a stabilization of the molecule (with respect to the situation without the Cu cluster), as witnessed by a binding energy larger by about 50 meV. Whether the stabilization is direct, via a tendency to bonding between O or H atoms to Cu adatoms, or indirect, via the substrate, remains an open question. The Cu adatoms binding more favourably on the hollow site of the substrate. To confirm our analysis, we also considered another stable binding configuration for the three dehydrogenated HHTP molecules, where only half the C atoms in the central ring lay on hollow sites of the Cu substrate (Figure 4.16b). In this case too, the inclusion of the Cu cluster in the center of the molecular trimer leads to an increased binding energy for the molecule, this time by 90 meV (Figure 4.16d). Finally, if instead of three Cu atoms, we consider six Cu atoms, we also find that the molecular binding energy is increased, by 200 meV. Now, some of the Cu atoms are very close to O atoms, suggesting that Cu-O-C bonds could form.

4.6 Conclusions

In this chapter the chemical structure, morphology and interaction of HHTP molecules adsorbed on Cu(111) at room temperature and after annealing at 530 K have been studied by means of XPS, NEXAFS, STM and DFT calculations.

By high-resolution XPS analysis, two inequivalent oxygen atoms with 1:1 area ratio have been identified upon deposition at room temperature, indicating the partial dehydrogenation of the molecules catalyzed by the substrate. The binding energy values shifs observed in C 1s and O 1s regions for multilayer and sub-monolayer phases, indicate a charge-redistribution within the molecular structure due to the chemical transformation. By in-situ NEXAFS measurements, these conclusions have been confirmed, since important changes on the spectra (broader and less intense peaks and the presence of a new peak at low photon energy) have been observed as a result of a re-hybridization and chemical transformation upon deposition. Additionally, the observation of signatures for electronic transitions involving π^* and σ^* states with different light polarization, we deduce that the molecules lay parallel to the surface in the three studied phases.

In order to confirm the stepwise oxidation of the triphenylene derivative on Cu(111), a complementary microscopic analysis was carried out on the supramolecular self-assembly formed upon absorption at room temperature. The most important effect on the molecular organization due to the partial dehydrogenation of the

molecule is the formation of triangular domains homogeneously distributed on the surface. Two possible orientations of the molecules within these domains have been observed (along $(1\,1\,\bar{2})$ and $(0\,1\,\bar{1})$ directions) with a unit cell that coincides with (5×5) unit cells of the Cu(111) surface. DFT calculations of this phase revealed the bowl shape of the molecules with an important interaction with the substrate, mainly through the carbons of the central ring. The (at least) partial loss of molecular aromaticity is confirmed by the homogeneous C-C bond length in the central ring derived at this step. Also, the formation of H-bond between adjacent molecules is plausible, with an average distance of 3.17 Å. A charge transfer of 1.2 electrons per molecule from the substrate to the molecules has been calculated and a charge distribution maps over the system confirms: i) the electron donor character of the substrate ii) the electron acceptor behaviour of the molecule and iii) the charge re-distribution that was suggested by the spectroscopic analysis.

Additional spectroscopic characterizations have been carried out on the resulting phase upon annealing at 530 K. The enhanced catalytic effect of the surface by the temperature is confirmed after the XPS analysis of the O 1s region, since only one peak reported at similar values in the literature for of ketone groups is found, indicating the full dehydrogenation of the molecules. This dramatic chemical transformation is again followed by a large binding energy shift towards lower values for C 1s and O1s peaks, suggesting an important charge transfer from the substrate to the molecule. By STM analysis, a different kind of supra-molecular network is observed, that complies (by forming additional bonds) with the the chemical transformation of the molecule. Now, parallel chains of molecules have alternating molecular orientation and bunch in set of two closer chains. The molecular lattice coincides with (9×8) unit cells of the Cu(111) substrate. Here also, the molecular interaction with the substrate and between the molecules was studied by DFT calculations. The molecules present a dome shape with direct linking between the oxygen atoms and the copper surface, and seem to recover aromaticity over all four carbon rings. In this sense the molecules resemble the (hypothetical) case of fully dehydrogenated HHTP molecules in the gas phase with six O atoms as radicals. H-bond, with length between 1.7 and 3.0 Å, seem to play a more importance in the cohesion of the supra-molecular assembly in this case. Most importantly is that in this phase a strong charge transfer of 1.9 electrons per molecule from the substrate to the molecule occurs.This is higher than the values obtained with molecules that are acknowledgedly strong acceptor species.[30,42,63]

Within this phase, an important amount of defects has been observed with STM, which are constituted by three HHTP molecules oriented in the same direction with an unknown species at their centre. The characteristic height and size of these objects suggests that they could consist of few Cu adatoms released from the surface,

and trapped in between molecules. The characteristic height and size of these objects suggests that they could consist of few Cu adatoms released from the surface, and trapped in between molecules. DFT further suggests the possible formation of Cu-O-C bonds between the Cu clusters and the dehydrogenated molecules.

5 Synthesis of polymeric arene(ruthenium) nano-sheets via imine chemistry at a liquid/liquid interface

In this chapter we show the results derived from a polymeric synthesis carried out at a liquid/liquid interface. The presented strategy is based on a Schiff condensations scheme which involves a commercial diamine precursor and an organometallic complex ended by trialdehyde groups, specifically designed for this purpose. Spectroscopic characterization techniques have been employed to demonstrate the formation of the new (C=N) bonds, and a combination of microscopic and diffraction techniques have proven the formation of ultrathin organometallic polymeric sheets, that can be suspended across the holes of membranes.

Contents

5.1 State of the art

Polymerization reactions offer various paths to the formation of extended ultra-thin or even two-dimensional (2D) materials under mild and low-cost conditions.[11] Benefiting from the abundance of a wide variety of building blocks, these new kinds of materials are expected to host a great diversity of physical and chemical properties. In contrast, the synthesis of inorganic 2D materials like graphene, boron nitride, or transition metal dichalcogenides, is more demanding, requiring *e.g.* (ultra) high vacuum and high temperatures found in molecular beam epitaxy or chemical/physical vapour deposition reactors.[197,198]

Organometallic polymeric sheets stand out owing to a superior electronic conduction down to the 2D limit.[106] Organic π-conjugated two dimensional materials can be prepared by a favourable combination between metal ions and chelating π-conjugated lingands, forming a framework that can host hybrid orbitals, starting from the d orbitals of the transition metal centers and the frontier orbitals of the conjugated carbon units. Huang *et al.* have shown the formation, via an interfacial reaction, of a highly crystalline thin film of a novel copper coordination polymer, Cu(BHT) (BHT=benzenehexathiol), with planar 2D lattice. It presents a high electrical conductivity (1580 S cm^{-1} at room temperature), and this, together with its good transmittance in the visible region, highlights its potential to serve as a transparent electrode. These organometallic nanosheets have been also in the spotlight of the scientific community in the last years as potential practical realizations of quantum phases deriving from the spin-orbit interaction or magnetism associated with the metal centers.[199–201] The first experimental example of a two dimensional organometallic polymer synthesised by interfacial reaction which could exhibit topologically non-trivial electronic states was the Ni(BHT) complex.[103,202] It adopts a kagomé lattice, showing a flat band above two Dirac bands in its calculated band structure. The presence of the metallic centers in the polymer, induce spin-orbit coupling effects, which lift the degeneracy at the the Dirac point close to the Fermi level. Small band gaps between these three kagomé bands were predicted based on first-principle calculations. Additionally, calculations predict that in the absence of SOC, the band gaps vanish. Electronic edge states, at the border of crystalline grain, were predicted to be robust against (reasonable) introduction of disorder, protected by the topology of the electronic band structure.

Most organometallic polymeric sheets are obtained via reactions where each metallic center is at the center of a coordination complex, being either linkers[75,103,118,196,201] or reticulation nodes.[106,185,203] In these systems, electronic delocalisation involves both π and d orbitals and since the metal-coordination bonds are reversible, the preparation of long-range ordered networks become feasible. A recent example

of metal-organic frameworks with topologically-protected electronic properties was proposed by Kumar *et al.*.[203] A controlled synthesis of a high quality honeycomb metal-organic framework on epitaxial graphene allowed to electronically decouple the organic linkers from the metallic substrate. By means of scanning tunneling spectroscopy, the authors claimed the formation of a stable Co-dycianoanthracene network with significant in-plane hybridization between the Co atoms and the organic blocks, confirming the formation of an extended electron system. Alternative routes to polymers featuring electronic delocalisation are chemical reactions forming covalent bonds that extend π conjugation throughout the polymer.[9,75,95] Grill *et al.* demonstrated that by using predefined connections points in the organic units which will take part in the polymeric reaction, a precise control on the lattice symmetry and motif of the final product can be addressed.[39] In this work, the new covalent bonds formed between porphyrin molecules ensured the stability of the final network as well as a collective charge transport. However, the strength of the covalent bonds is often a kinetic hinderance to the healing of defects that stochastically form during synthesis. As a possible workaround to this issue, self-correcting reactions have been used recently, in particular dynamic imine chemistry.[110] This approach allowed to synthesize fully-organic[111] and metalorganic[112] 2D polymers. In the former case, illustrated by Dai *et al.*, a two-dimensional covalent organic framework was synthesised from simple aromatic triamine and dialdehyde molecules at the air/water interface. Spectroscopic characterization of the resulting monolayer, demonstrates the imine-bond formation during the Schiff base condensation reaction. The air/water synthesis approach released a smooth, coherent, large and free-standing polyimine monolayer, representing a step towards conjugated polymers for electronic or optoelectronic applications. The work of Sahabudeen *et al.*, that are most relevant to ours, gave a demonstration that metallic centers can be introduced in the polymer without involving them in the polymerization reaction. In that case, the organic building blocks that are involved in the reaction correspond to Co(II)-porphyrin derivatives and terephthalaldehyde. Separating the two problems (polymerization and functionalization) is obviously desirable for versatile design organometallic polymers at will.

We propose a new synthesis scheme also based on dynamic imine chemistry, at a liquid/liquid interface, allowing versatile transfer of the polymeric sheets to virtually any kind of support via a Langmuir-Blodgett or Langmuir-Schaefer methods (or derivatives).[100,103,106,111,204] The chosen reaction is a Schiff-base condensation, between a diamine (*p*-phenylenediamine, monomer 2) acting as a linker and a trialdehyde (Ru[η^6(hexamethyl-benzene)]-biphenyl-aldehyde, monomer 1) acting as a reticulation node, which provides a new illustration of a reticulation process that does not involve the metallic centers. Like with the other known dynamic imine chemistry polymerization scheme liable to yield organometallic systems, with the

metallic center hosted by a porphiryn,[112] here the hosting by a sulfur-linked arene[205] (label 3) yields a +II oxidation number.

In this chapter we show UV-visible and Raman spectroscopy analysis done to characterize the formation of the imine bonds. Together with optical, scanning and transmission electron microscopies (SEM, TEM) and selected-area electron diffraction (SAED), this allows us to demonstrate the formation of ultrathin (< 20 nm) organometallic polymeric sheets that can be transfered to virtually any kind of substrate, *e.g.* the oxidized surface of silicon wafers, Si_3N_4 TEM grids, quartz plates.

5.2 Starting materials

All molecular products employed for the synthesis of the polymeric Ru-imine nanosheet were synthesised and supplied by Frédéric Chérioux at FEMTO-ST laboratory, in Besançon (FRANCE).

All reactions were carried out under nitrogen, by using standard Schlenk techniques. Solvents were degassed prior to use. The dinuclear dichloro complexes $[Ru(C_6Me_6)Cl_2]_2$, with label (A) in Scheme 5.1 and $[Ru_2(C_6Me_6)_2(p\text{-}S\text{-}C_6H_4\text{-}Br)_3]Cl$, with label (B) in the same scheme, were synthesised by previously described methods.[206–210]

5.2.1 Chemical synthesis of the Ru trialdehyde monomer

The Ru-trialdehyde monomer, with chemical formula of $[Ru_2(C_6Me_6)_2(p\text{-}SC_6H_4\text{-}C_6H_4\text{-}CHO)_3]Cl$, compound 1 in Scheme 5.1, is a dinuclear ruthenium (II) complex with bypiramidal triangular shape. Each Ru centre coordinates to one methylbenzene (HMB) ligand and three sulphur atom bridges. These three S atoms are themselves linked each to a biphenylaldehyde (biPh-aldehyde), giving the triangular geometry of this monomer. Its chemical synthesis is shown in Scheme 5.1.

The trisbromodinuclear complex (C), $[Ru_2(C_6Me_6)_2(p\text{-}S\text{-}C_6H_4\text{-}Br)_3]Cl$ (0.1 mmol) and pinacol ester derivatives $(CHO\text{-}C_6H_5\text{-}B(OR))_2$; 0.33 mmol), were dissolved in tetrahydrofuran. Then, an aqueous solution of Cs_2CO_3 (1 mL), and $Pd(PPh_3)_4$ catalyst (0.01 mmol, 11 mg) was added. The resulting mixture was refluxed in ethanol for 48 hours. After cooling to 293 K, the red solution was filtered through Celite and the solvent was removed under reduced pressure. The oil obtained was purified by column chromatography (silica gel, dichloromethane/ethanol 10:1; rf close to 0.8). $[Ru_2(C_6Me_6)_2(p\text{-}S\text{-}C_6H_4\text{-}C_6H_4\text{-}CHO)_3]Cl$, compound 1 in Scheme 5.1, was isolated

after evaporation of the solvent, as red-orange powder.

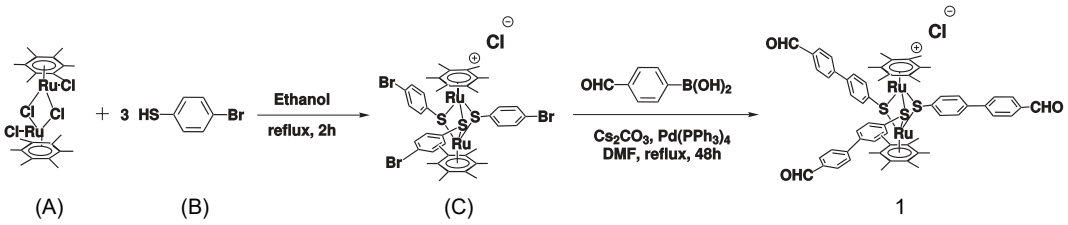

Scheme 5.1: Synthesis protocol of the Ru trialdehyde monomer, label 1. The compounds (A) and (B) were synthesised by previously described methods.[206–210]

The $[Ru_2(C_6Me_6)_2(p\text{-}S\text{-}C_6H_4\text{-}C_6H_4\text{-}CHO)_3]Cl$ compound was characterize by nuclear magnetic resonance technique, showing the following chemical shifts:

^1H NMR (300 MHz, $CDCl_3$, 21°C): δ = 1.58 (s, 36H, CH_3-Ar), 7.81 (d, $^3J_{H,H}$ = 8.2 Hz, 6H, CH–Ar), 7.82 (d, $^3J_{H,H}$ = 8.2 Hz, 6H, CH –Ar), 7.96 (d, $^3J_{H,H}$ = 8.2 Hz, 6H, CH –Ar), 7.98 (d, $^3J_{H,H}$ = 8.2 Hz, 6H, CH –Ar), 10.02 (s, 3H, -CHO). ^{13}C NMR (50 MHz, $CDCl_3$, 21°C): δ = 15 (CH_3-Ar), 95 (Ru-C-Ar), 127 (C-Ar), 130 (C-Ar), 135 (C-Ar), 140 (C-Ar), 201 (C-Ar), 135.48 (C=O).

5.2.2 Chemical synthesis of the Ru-imine-compound as molecular reference

To characterise the formation of the imine bonds, we will compare the spectroscopy of the polymer (compound 3 of Figure 5.1) with that of a reference (simpler) compound (label 4 in Scheme 5.2), since it presents the main chemical groups expected in the polymer. It is obtained by reacting monomer 1 with aniline as it is shown in Scheme 5.2.

The trisbromodinuclear complex $[Ru_2(C_6Me_6)_2(p\text{-}S\text{-}C_6H_4\text{-}C_6H_4\text{-}CHO)_3]Cl$, compound 1 (0.1 mmol) and 4-cyanoaniline (NH_2-C_6H_4-CN; 100 mmol), were dissolved in ethanol. The resulting mixture was refluxed overnight. After cooling to 293 K, the red solution was filtered through Celite and the solvent was removed under reduced pressure. The oil obtained was washed with diethylether (3×50 ml). The obtained red powder was purified by column chromatography (silica gel, dichloromethane/ethanol 10:1; rf close to 0.8). The $[Ru_2(C_6Me_6)_2(p\text{-}S\text{-}C_6H_4\text{-}C_6H_4\text{-}CH{=}N\text{-}C_6H_4\text{-}CN)_3]Cl$ compound was isolated after evaporation of the solvent, as red-orange powder.

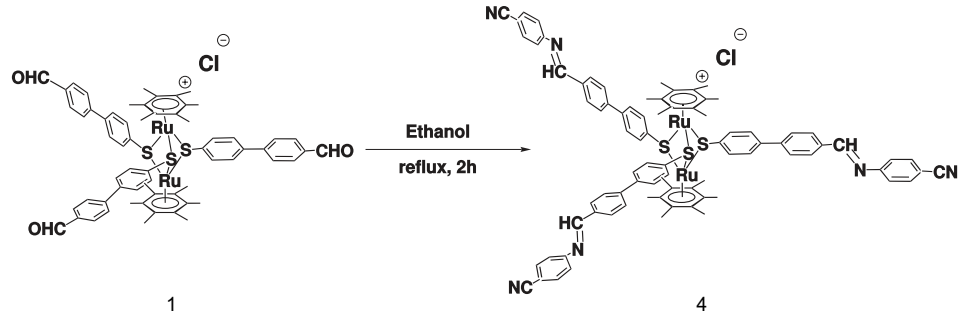

Scheme 5.2: Synthesis protocol of the Ru-imine-compound, label 4.

The $[Ru_2(C_6Me_6)_2(p\text{-}S\text{-}C_6H_4\text{-}C_6H_4\text{-}CH{=}N\text{-}C_6H_4\text{-}CN)_3]Cl$ compound was characterize by nuclear magnetic resonance technique, showing the following chemical shifts:

^{1}H NMR (300 MHz, DMSO-d$_6$, 21°C): δ = 1.58 (s, 36H, CH$_3$-Ar), 7.81 (d, $^3J_{H,H}$ = 8.2 Hz, 6H, CH –Ar), 7.82 (d, $^3J_{H,H}$ = 8.2 Hz, 6H, CH –Ar), 7.90-8.00 (m, 18H, CH –Ar), 8.06 (s, 3H, -CH=N-), 8.18 (d, $^3J_{H,H}$ =8.2 Hz, 6H, CH –Ar).

5.2.3 *p*-phenylenediamine

The *p*-phenylenediamine molecule, monomer 2 in the chemical reaction scheme of Figure 5.1, is the second component employed in the imine-polymerization reaction. Its structure is shown in Figure 5.1b and it was purchased in SigmaAldrich and used as received. It presents a melting point of 411-416 K and a vapor pressure of 1.08 mmHg (473 K).

5.3 Synthesis at liquid/liquid interface

The polymerization of monomers 1 and 2 is expected to extend via the formation of imine (C=N) bonds, by a Schiff-base condensation between the aldhehyde and amine groups, as it is detailed in the chemical reaction Scheme of Figure 5.1b.

To perform the polymerization reaction we dissolved monomers 1 and 2 in a mixture of chloroform/ethyl acetate (top organic phase) and in water (bottom aqueous phase), respectively (Figure 5.1a). Given its lower density, the aqueous phase was the first introduced in the beaker. The organic phase was then carefully introduced on top with the help of a pipette along the walls of the beaker, avoiding as much as possible to disturb the interface between the two phases. Before introducing the two phases, the host substrate for the polymer was placed at the bottom of the beaker. After overnight reaction, a solid orange sheet forming at the liquid/liquid

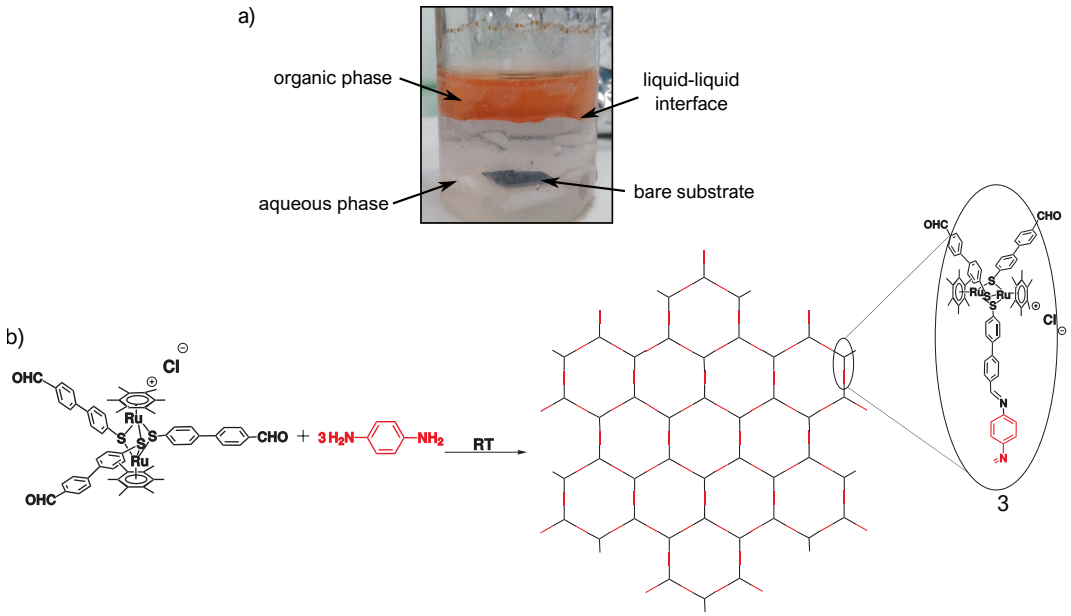

Figure 5.1: a) Photograph of the reaction beaker highlighting the liquid/liquid chloroform-ethyl acetate/water interface and involved phases. b) Reaction synthesis of Ru-imine polymer 3 from Ru-trialdehyde 1 and *p*-phenylenediamine 2 monomers.

interface is observed. Then, the aqueous phase was drained again with the help of a pipette until the interface touched the surface of the substrate. We consider that the observation of a meniscus at the surface of the substrate marks the moment when the polymer comes in contact with the substrate. We then drain completely the aqueous phase and finally remove the substrate from the bottom of the beaker. This approach can be viewed as a variant of the Langmuir-Schaefer method (Figure 5.2).

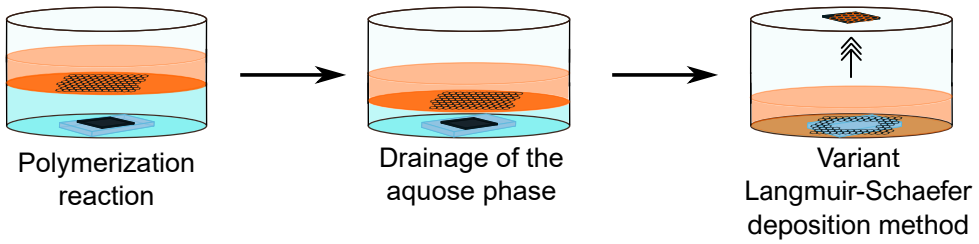

Figure 5.2: Schematic depiction of the nano-sheet transfer onto a bare substrate

Precursor quantities and volumes employed for the synthesis of imine-nanosheets are summarized in Table 5.1. Different concentrations were used depending on the investigated host substrate. A thinner imine-polymer was synthesised when deposited on TEM grids substrates, which are in deed the samples on which we will focus our discussion along this chapter.

		For SiO_2/Si substrate	For TEM grids
Product	M.W (g/mol)	Quantity	Quantity
Monomer 1	1377,45	0.5mg	0.2mg
Monomer 2	108,14	58μg	23μg
H_2O		At substrate level	At substrate level
$CHCl_3$		2mL	2mL
AcOEt		18mL	18mL

Table 5.1: Summary of precursor quantities used for synthesis of Ru-imine polymer, depending on the host substrate employed.

5.4 Evidence for polymerization via UV-Vis spectroscopy

UV-visible spectra were collected using an UV-Vis Spectrophotometer Lamba 900 (PerkinElmer) apparatus. A series of UV-visible absorption spectra were measured as a function of reaction time (0, 1, 3, 5, 22 hours) after monomers 1 and 2 have been introduced in their respective phases. As shown in Figure 5.3, already after 1 h of reaction, two broad bands are observed, one centered in the UV range (beyond the explored range) and the other centered at 480 nm. As it was already reported, these two bands correspond to π/π^* electronic transitions of hexamethyl-benzene ligand and metal-ligand charge transfer, respectively.[205,211] However, the absorption value of the latter, is red-shifted with the ones found in the bibliography. Our theory is that the presence of an extended network by result of the reaction of monomers 1 and 2 may alter the metal-ligand charge transfer process, producing its red-shift value.

Moreover, the intensity of these bands grow with the reaction time, confirming that the polymerization reaction develops successfully.

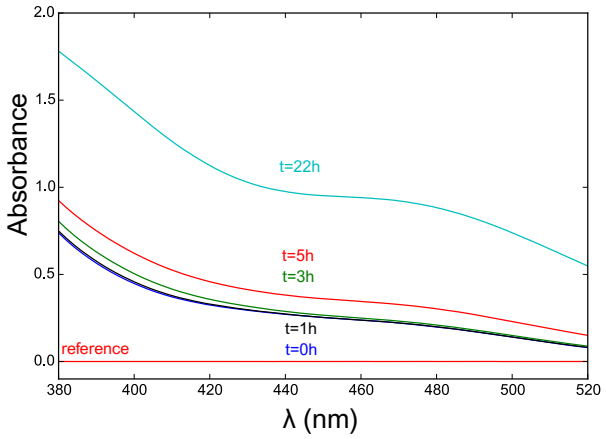

Figure 5.3: Time-dependent absorption spectra of polymerisation reaction on quartz substrate.

5.5 Suspended nano-sheets

As summarized in Table 5.1, different precursor quantities were used for the synthesis of the imine-polymer, depending the host substrate. A thick film was prepared and deposited on 300nm SiO_2/Si substrate whereas a thinner film was targeted for the case of the suspended polymer on the Si_3N_4 TEM grids. In the latter case we planned cross-characterization with various techniques performed on the very same region of the suspended polymer. We planned transmission electron microscopy experiments, for which the thinnest possible films are preferred. We also planed Raman spectroscopy experiments. For these ones, a several 100 nm wide laser beam was used. This beam "sensing" the surrounding TEM membrane (whose holes are 500 nm in diameter). Hence the membrane yields a spurious background signal. This lead us to address no too-thin films liable to produce a Raman signal above this background.

5.5.1 Validation of Langmuir-Schaefer deposition method

Once the success of the reaction was confirmed by UV-Vis spectroscopy, the next step was to transfer the samples from the interface to the desired substrates. We used a variant of the Langmuir Schaefer method, which is described in section 5.3. For this purpose, a first look onto the samples was taken by means of optical microcopy.

Optical microscopy informs about the shape, quantity and distribution of the

final products generated by the reaction and the residuals from the starting reactants. Importantly as well, this technique is indispensable to localise surface features (products, residuals) that will be analysed afterwards with other characterization techniques. Optical images have been acquired in a Zeiss microscope equipped with a digital camera "axiocam 105 color" device, a tungsten halogen light source, and magnifications of 2.5×, 10× and 100×. Additional optical images were taken during Raman experiments with the help of the CDD camera coupled to the microscope that is used to perform the Raman confocal measurements.

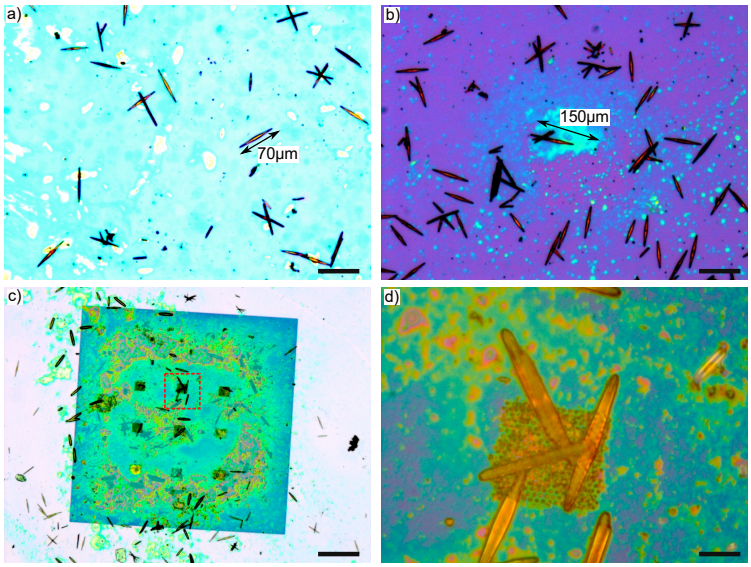

Figure 5.4: a) and b) Set of optical microscopy images taken on the polymer deposited on a Si sample covered with 300 nm SiO_2. c) and d) Set of optical microscopy images taken on polymer deposited on a Si_3N_4 TEM grid. Scale bar of 100 μm a), b) and c); scale bar of 10 μm d).

As it is observed in Figure 5.4a and b, several types of features were found on the surface: flakes with different degree of density and solid objects with needle shape mainly. The needles are found across the surface and they exhibit a characteristic length of the order of 70 μm. The flakes have variable sizes from, 30 to 150 μm. They do not have a well-define optical contrast, suggesting that they are not homogeneous in thickness, density or composition. Similar observations are made when the polymer was deposited on TEM grids, as observed in Figure 5.4c and d. Close inspection shows that this sheet can cover the 500 nm-diameter holes of the TEM grid.

A better spatial resolution is obtained with scanning and transmission electron microscopies as it is shown in Figure 5.5. A large scale SEM image (Figure 5.5a)

shows the aspect of a freshly prepared sample, where it is possible to find covered (pointed out by white circles and arrows) and uncovered holes by the polymer nanosheet after the deposition by Langmuir Schaefer method. In Figure 5.5b, the covered area with thicker polymer nanosheet corresponds to the fainter holes. By means of SEM analysis, the average polymer thickness is determined to be $<$20 nm.

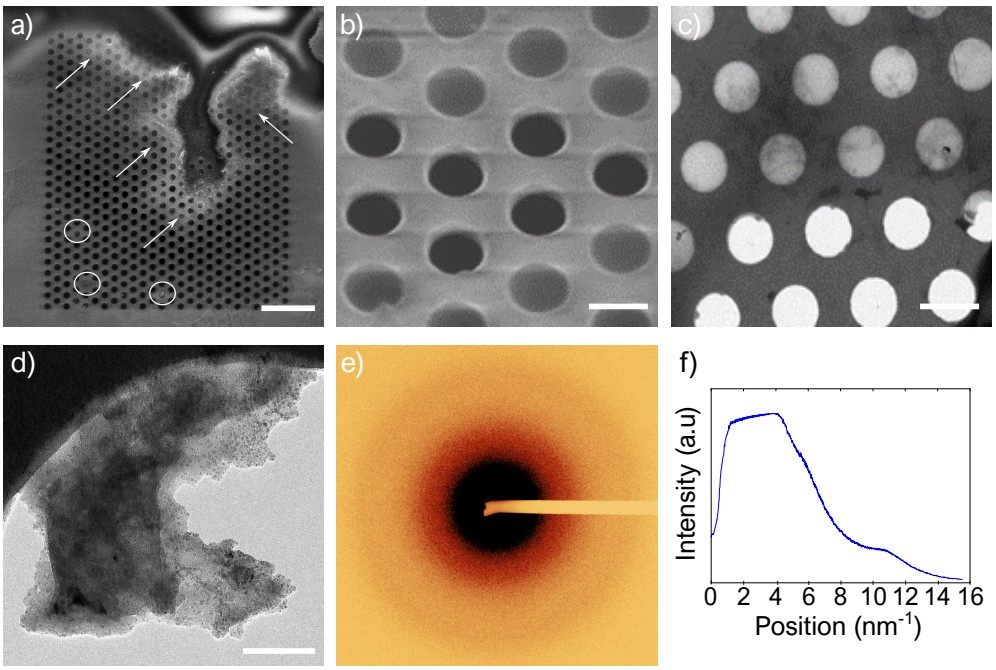

Figure 5.5: a) Large-scale and b) close-view SEM images of the polymer deposited on a TEM grid. White circles and arrows indicate the covered areas. Series of TEM images with increasing magnification, c) taken on the polymer suspended on a TEM-grid after irradiation by an intense laser spot. d) High-resolution TEM image. e) SAED pattern taken on the polymer suspended and f) its intensity profile. Scale bar of 5 μm, a); Scale bar of 500 nm, b); Scale bar of 500 nm, c); Scale bar of 150 nm, d).

Similar observations were done by TEM on the same samples as those studied with Raman spectroscopy. Figure 5.5c, is centered in a zone where it is possible to find both the suspended polymer(darker holes) and uncovered membrane holes. The latter were actually initially covered with the polymer, but the use of a too high laser power during Raman spectroscopy measurements burnt the polymer. The beam was also focused onto a needle, which was also burnt together with the suspended polymer around/below it, on the membrane. After the irradiation by the intense laser beam (0.3 mW/μm^2), a small flake remains at the side of the membrane hole and crystalline nanoparticles were observed (Figure 5.5d). These particles are

presumably a product of the thermal degradation of the polymer, since we do not observe them without laser irradiation or after irradiation with a less intense laser beam. We are not able to tell if the nanoparticles are embedded in the flake, or simply located on top or below it. The polymer hence forms a sensitive sheet that is self-supported, at least at the 500 nm scale investigated here.

The SAED pattern measured on a suspended sheet consists of a ring with uniform intensity (Figure 5.5e). This shows that at the scale of the electron beam (few hundred nanometres), the sheet is composed of randomly in-plane oriented grains (strong disorder on the system within the electron beam size). The radial scattered intensity distribution extracted from the SAED pattern (Figure 5.5f) exhibits a peak centered at 11 nm^{-1}, corresponding to a real space distance of 0.114 nm. This distance is precisely the one that we measured for a lacey carbon TEM grid, and can hence be ascribed to the C-C bonds we expect in the polymer.

5.5.2 Imine bond formation in the polymer nano-sheet

Raman spectroscopy was used to search for signatures of the bond's formation following the polymerisation reaction. We expect to detect low-energy vibration modes related to the polymeric framework, as well as modes related to the imine group, that should differ from those of the aldehyde groups in the precursor.

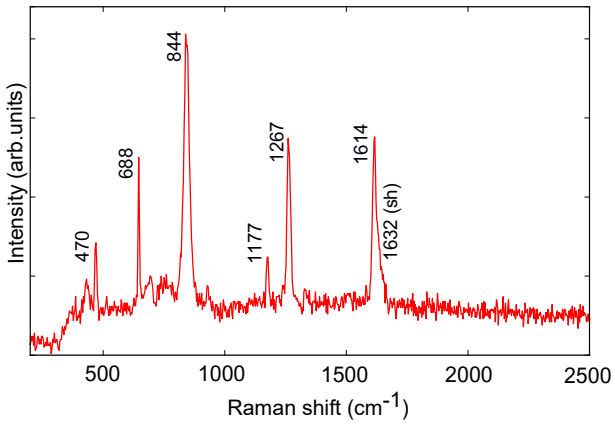

Figure 5.6: Raman spectra acquired on monomer 2 (diamine molecule) in powder, taken with a laser wavelenght of 633 nm laser, a power of 1.8 $mW/\mu m^2$ and 500 s acquisition time.

Powders of compounds 1, 2, and 4 were analysed, in order to have a reference spectra before the reaction. In the case of monomer 2, we observe a strong background with a 532 nm wavelength, which we ascribe to fluoresecence. The Raman

spectra of this compound is clearer with a 633 nm wavelength for which fluorescence is suppressed (Figure 5.6). The observed vibrational modes are summarized in Table 5.2, together with their assignment, and the experimental and calculated vibrational modes for diamine in solution found in the bibliography.[212]

Observed	Bibliography (Experimental)	Bibliography (Calculated)	Assignment
367	367	352	ring deformation ω (C-C) or ring wag.
470	466	475	δ (C-C) or ring bend.
648	648	662	δ (C-C-C) or ring bend. def. ν (C-C-C) or ring str. def
844	844	857	ring breathing δ (C-C-C) or ring bend. def.
1177	1178	1157	ν (C-C-C) or ring str. Def
1267	1265	1299	ν (C-N) or C-N str. ring breathing ν (ring-N) or ring-N str.
1614	1615	1628	ν (C-C-C) or ring str. Def
1632(sh)	1640	1661	δ (NH2) or NH2 scissor(bending)

Table 5.2: Observed and bibliographic (experimental and calculated) vibrational modes of diamine molecule. Observed spectrum of diamine molecule in powder was taken with a laser wavelength of 633 nm laser, a power of 1.8 mW/μm^2 and 500 s of acquisition time. The experimental spectrum of diamine molecule published in the literature was taken in chloroform and water solution,[212] while the calculated values were optimized at the B3LYP/6-311G**level of theory.[212]

We find a very good agreement between the Raman shifts of the different bands we measure for a powder of monomer 2 and those reported previously for the compound in solution.[212] We find deviations amount at most a few 1 cm^{-1}. The laser wavelength used in reference 212 is unknown, hence we cannot exclude that some of the vibration modes are dispersive. The calculations provide a good qualitative account of the observations, and allow to assign the different bands. The bands at 376 cm^{-1}, 470 cm^{-1}, 648 cm^{-1}, 844 cm^{-1}, 1177 cm^{-1}, and 1614 cm^{-1}, all correspond to vibrations involving C-C bonds. The band at 1267 cm^{-1} and the shoulder at 1632 cm^{-1} involve N atoms. The latter shoulder is a clear cut evidence of the presence of the amine function. Its absence, *e.g.* in the final polymer, is thus in principle a proof that all amine bonds have been transformed. Unfortunately, its intensity is in general too low to make definitive statements based on this argument only. We will rather track the presence or absence of the band at 1267 cm^{-1} for this purpose.

Raman spectra of monomer 1 and compound 4 were measured with a 532 nm laser

wavelength. In an extended range of wavenumbers (100-900 cm^1, 1000-1750 cm^1, 2650-3300 cm^1), the two Raman spectra share many similar or identical bands, and also show a few important differences that will help us to unambiguously confirm the formation of the imine bond (Figure 5.7). Bands at 438 cm^1 and 666 cm^1 (skeletal vibration related to the presence of C≡N groups), and 1202 cm^1 (C-C bonds of the aromatic rings) are only found for compound 4, while bands at 710 cm^1 (which unknown origin), 1171, 1193 cm^1 (C-C bonds of the aromatic rings) and $\sim$ 2900 cm^1 (C-H stretching mode of aldehyde groups) are absent for this compound. In the following we will track the presence/absence of the doublet at 1171, 1193 cm^1, which is transformed into a single peak in compound 4 presumably due to the replacement of the carboxylic acid function grafted on the aromatic rings by the imine groups.

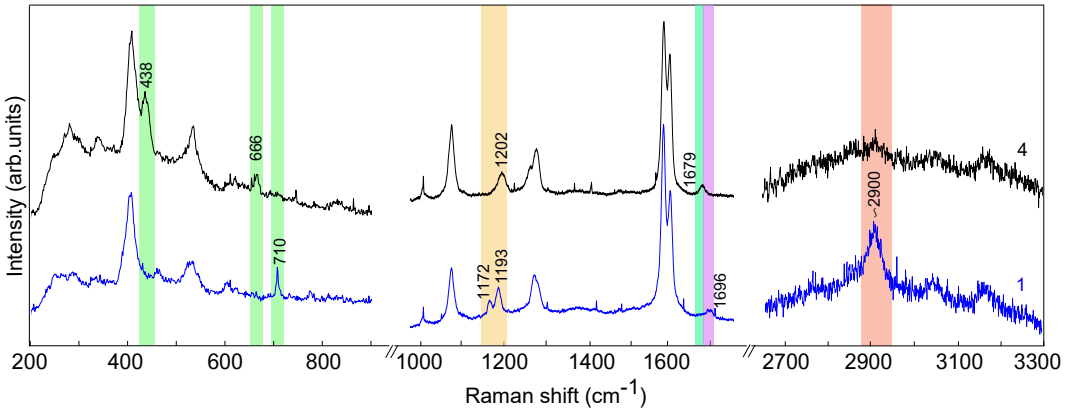

Figure 5.7: Raman spectra acquired on monomer 1 and compound 4 in powder from 200-900 cm^{-1}, from 1000-1750 cm^{-1} and from 2650-3300 cm^{-1}, taken at laser power of 1.7 mW/μm^2 and 300 s of acquisition time.

Then, the polymer suspended on Si_3N_4 TEM grids were analysed on the intermediate range of Raman shift (from 1000 to 1800 cm^{-1}), for which the acquisition conditions were more favourable and simple for compound 3. The laser spot size was $\sim$ 1 μm and the focal point of the optical setup was adjusted to maximise the signal from the polymer. The signal was collected through a 50× objective with a numerical aperture of 0.75. For the Raman spectra, the power was varied between 0.02 and 2.0 mW/μm^2, in order to test the degradation of the samples under the laser spot and optimise counting times. The effect of an excessive laser power can be seen in Figure 5.9 (inset), where a needle and its surroundings are completely burnt after the Raman experiment. The acquisition time was varied to increase the signal-to-noise ratio, and to allow the detection of the weak signal corresponding to some vibration modes; typically 300 s are needed to measure a "good" spectrum for powder samples and 1000 s for a suspended sample. Then a 1800 lines/mm grating

were used in the spectrometer to high resolution spectrum.

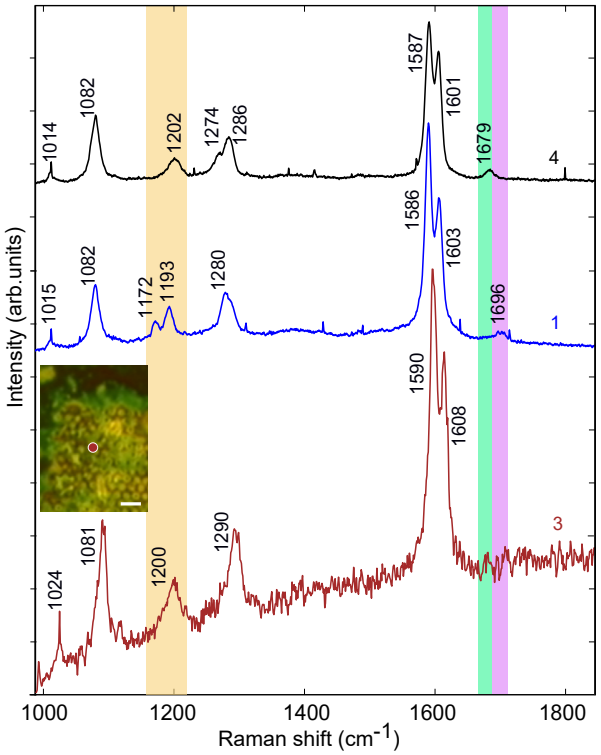

Figure 5.8: Raman spectra acquired on monomer 1 (label '1') and compound 4 (label '4') in powder, taken with a laser wavelenght of 532 nm laser, a power of 1.7 mW/μm^2 and 300 s acquisition time. Raman spectrum of the polymer suspended on a Si_3N_4 TEM grid (label '3'), taken with a laser wavelenght of 532 nm, a power of 0.17 mW/μm^2 and an acquisition time of 1000 s. Inset image shows the exact position where the Raman was taken (burgundy spot). Scale bar of 2 μm.

We now focus on the local vibrational analysis of a suspended sheet. The background level is rather high whatever the incident light power compared to the case of the spectra acquired on the powders of monomers 1 and of compound 4 (Figure 5.8), presumably because of the measurement configuration: we expect a non-negligible contribution from the material of the TEM membrane that is illuminated by the tails of the laser beam (focused on a few 100 nm spot). Table 5.3 lists the different bands observed in Figure 5.8 for the monomer 1 and both, compounds 3 (polymer) and 4, and a tentative assignment of these bands.[160,161]

For the polymer (compound 3), we observe a number of bands above background level, at 1024 cm^{-1}, 1081 cm^{-1}, 1200 cm^{-1}, 1290 cm^{-1}, 1590 cm^{-1} and 1608 cm^{-1}.

	Raman mode wavenumbers		
Vibration model	Monomer 1 (cm-1)	Compound 4 (cm-1)	Compound 3 (cm-1)
	1015	1014	1024
β(C-H)	1082	1082	1081
ν(C-C)$_{arom}$	Doublet 1172 / 1193	1202	1200
ν(C-C)$_{arom}$	1280	Doublet 1274/1286	1290
ν(C=N)$_{arom}$	1586	1587	1590
ν(C=C)$_{arom}$	1603	1601	1608
ν(C=O)	1696	-	-
ν(C=N)	-	1679	-

Table 5.3: Experimental vibration modes for monomer 1 and both, compound 3 (polymer) and 4, and their assignment based on refereces 111, 160, 161, 205.

These bands correspond to the C-C vibrations expected from the diphenyl branches (1015 cm^{-1}, 1080 cm^{-1}, 1204 cm^{-1}, 1285 cm^{-1}, 1587 cm^{-1} and 1605 cm^{-1}),[205] and to the C=N vibration of imine bonds (1586 cm^{-1}).[111] Conversely, the characteristic band corresponding to the C=O vibration (aldehyde, 1690 cm^{-1}) is not detected, and no clear double band is observed slightly below 1200 cm^{-1}, unlike in the spectra of monomer 1. In deed, the value of 1200 cm^{-1} is closer to the single peak in compound 4 (1202 cm^{-1}). Note also that the comparison between Raman spectra for monomer 1 and compound 4 reveals the signature of the imine bonds (C=N) at 1679 cm^{-1}. The corresponding band has low intensity, and given the rather important background level in the Raman spectra measured for the suspended polymeric sheet, it is not surprising that this characteristic band could not be detected unambiguously.

It is important to keep in mind that the spectrum measured from the compound 4 will not necessarily be the same as that of the final polymer. Indeed, since the polymer is not simply a (rather) small isolated molecule, additional vibrational modes could exist, some other modes could become silent, and existing modes could have slightly different energy or bandwidth. Raman spectroscopy hence overall supports the claim that indeed a self-supporting polymeric sheet has been obtained.

As it was shown in Figure 5.4d, the polymeric sheet is accompanied with needles distributed at random. Raman spectra recorded on a needle is shown in Figure 5.9. As explained before, the presence of the doublet around 1200 cm^{-1} and the small band closer to 1700 cm^{-1} rather than to 1650 cm^{-1}, reveals that the needles cor-

respond to unreacted monomer 1. This fact indicates that an excess of monomer 1 was employed for the synthesis of thin polymer nano-sheets and a readjust of the reaction conditions is needed.

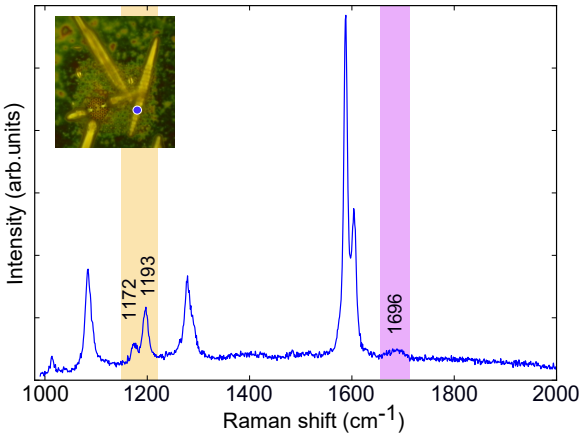

Figure 5.9: Raman spectra acquired on a needle, at the location marked with a blue spot in the optical micrograph (inset). Measurement settings: laser power of 0.13 mW/μm^2 and 100 s acquisition time.

5.6 Conclusions

A new synthesis scheme based on dynamic imine chemistry at a liquid/liquid interface has been proposed. The chosen reaction is a Schiff base condensation between *p*-phenylenediamine, which acts as a linker, and a trialdehyde (Ru[η^6(hexamethylbenzene)]-biphenyl-aldehyde, which acts as a reticulation node. We report the formation of a ultrathin organometallic polymeric sheets by means of optical, scanning and transmission electron microscopies (SEM, TEM) and selected-area electron diffraction (SAED). The synthesis strategy leads to a reticulation process which does not invole the metallic centers and where the polymerization and functionalization stages are performed in a single step.

The sheets are readily transferred to various kinds of substrates via Langmuir-Schaefer method and can be self-suspended on top of membranes. The formation of the imine bonds has been demonstrated by UV-Vis and Raman spectroscopy. It is expected that this covalent bond allows the extension of the π-conjugation over the whole system, yielding a polymeric nanosheet that could serve as a flexible electronic conductor, or thermoelectric material, where the presence of high-atomic-number metallic centers is crucial.

6 Conclusions and perspectives

In this thesis, we have attempted the synthesis and the characterization of organometallic molecular architectures via interface chemistry. Two systems have been studied: i) molecular self-assemblies of triphenylene derivatives, hexahydroxyl- triphenylene (HHTP) molecules which are important constituents in molecular electronic systems, that were deposited at the vacuum/solid interface, on Cu(111) and ii) polymeric organometallic nanosheets at a liquid/liquid interface. These systems present desirable features in the prospect of low-dimensionality organo-metallic materials. As we will explain below, self-assembly networks of HHTP molecules exhibit interesting electron-acceptor properties and the polymerization of arene(ruthenium) polymeric nanosheets, organo-metallic in nature, has been demonstrated via dynamic imine chemistry and they could be suspended across the holes of membranes.

The analysis of the literature (chapter 2) was focused on the development of molecular systems, with the final goal to achieve ultrathin sheets, with or without internal covalent bonds, that could serve in future molecular electronic devices. Given the two research directions we have investigated during the PhD thesis works, we have reviewed to synthesis strategies and properties of two classes of systems, one prepared at the interface between two fluids, and the other at well-defined surface, under ultrahigh vacuum.

The next chapter presented the tools and methods that we used in three laboratories and at a synchrotron faculty. It is probably interesting to note that at the time our work started, molecular systems had not been studied in the research group I belonged to, at least not with the surface science probes available in the group. The PhD works held them a strong explorative aspect, not only regarding the scientific questions that we addressed, but also regarding instrumentation.

As it has been presented in chapter 4, the stepwise oxidation of the HHTP molecule on Cu(111) spontaneously occurs at room temperature upon its absorption on the surface and then, by an additional thermal treatment. By this procedure, the dehydrogenation (oxidation of the alcohol functions) strongly alters the chemical reactivity with other molecules and the substrate, and the molecular structure/morphology, compared to the parent molecule. These effects are analysed with high resolution XPS, NEXAFS, and STM. While in a much related system, HHTP

molecules on a Ag(111) surface, self-assembled molecular lattices form with partially dehydrogenated molecules, in the case of a Cu(111) substrate that we studied, a full dehydrogenation occurs. According to DFT calculations, we find that from a partially dehydrogenated to a fully dehydrogenated molecule, a qualitative morphological modification occurs, from a bowl shape before annealing, when the molecule is partially dehydrogenated, to a dome shape after the thermal treatment, when the molecule is completely oxidized. Not only the shape is affected by the chemical transformation. The interaction with the substrate is dramatically affected, corresponding to a weak chemisorption regime through the C atoms of the central ring, after deposition, and mainly through the O atoms, upon the full dehydrogenation. Moreover, these two different absorption configurations carry distinct charge transfer values (always from the substrate to the molecule). When the molecule is attached to the surface through the C atoms (partially dehydrogenated), the charge transfer is lower (1.2 electrons per molecule) than in the case of the linking to the surface through the oxygen atoms (full dehydrogenation with 1.9 electrons per molecule). This is consistent with the higher electronegativity of the O atoms, with respect to the C, enhancing the electron-acceptor character of the molecule. Interestingly, bonding via the O atoms seems to restore the aromaticity of the carbon skeleton of the molecules.

Within the dehydrogenated system, we find possible signs of the fomation of organo-metallic structures. They noticeably involve trimers of molecules all of them pointing in the same direction presumably enclosing a small cluster of copper atoms in the centre. The elucidation of the nature of the cluster have been suggested by STM analysis (through comparison of the apparent height with similar objects accumulated in the border of the molecular networks) and DFT calculations. The latter indicate that the presence of a Cu clusters enhances the binding of the molecules on the surface, and that Cu-O-C bonds may form depending on the nature of the cluster. All these observations turn to be crucial for further investigations based on the combination of the HHTP ligand with other organic molecules or other metallic centres, with the prospect of hopefully long-range ordered systems with high electron transfer from the copper surface. In this regard, preliminary experiments focused on the analysis of hexabromo-methyl-benzene (HBMB) molecule on Cu(111) as a potential molecular candidate have been carried out by means of STM. With this prior analysis, the molecular debromination starts upon deposition at room temperature and it could be controlled by further thermal treatments. With this stepwise molecular activation, the reaction between HBMB and HHTP ligands is expected on Cu(111), leading to a 2D network.

Chapter 5 was devoted to another class of system based on polymeric nanosheets grown at a liquid/liquid interface. A new synthesis reaction has been presented

based on dynamic imine chemistry. By means of this strategy, self-correction processes can take place during the reaction process, in principle allowing the synthesis of defect-free and long range ordered two-dimensional networks (even though we eventually did not manage to obtain evidences of good order). New imine (C=N) bonds have been formed between diamine and arene(ruthenium)-byphenyl-trialdehyde monomers (through a Schiff-base condensation reaction). In our work, including ruthenium centres in the monomer was motivated by the prospect of interesting quantum phases properties that may derived from the spin-orbit interaction or magnetism associated with the inclusion of metallic centres in the polymer structure (this long-standing goal was actually the scope of the national project involving Institut Néel, Institut FEMTO-ST, and IPCMS). The literature is full of examples where the metallic elements constitute the linkages of the network, but few works gave a demonstration that they can be introduced in the polymer without involving them in the polymerization reaction. Here, we attempt this synthesis at a liquid/liquid interface, which is a configuration known to favour the development of smooth, large area polymers. UV-Vis and Raman spectroscopy confirmed the formation of the imine bonds in the structure, suggesting the extension of the π-conjugation over the whole system. Together with SEM and TEM an ultrathin ($<$ 20 nm) organometallic polymeric nano-sheet was observed and SAED analysis on a suspended sample revealed structural disorder at least at the scale of the electron beam. Future investigations could be oriented to improve the crystallinity of the polymeric nanosheets by a systematic study of the synthetic conditions (temperature, concentration type of precursors) and by addition of chemical substances that could help the monomers to better order at the interface, as it has been recently reported by Fang *et al.*[213] This would open the way to finer structural investigations, for instance with scanning probe techniques or electron microscopy. In order to facilitate the characterization process of the imine bond formation, efforts should also be focused on the development of suspending membrane yielding low background level in the spectroscopy measurements, which we believe would be optimal in the case of larger holes and silicon-based membranes. This will jointly require to control the transfer process so that extended suspension of the rather fragile polymer nanosheets is effective without disrupting them. Finally, thanks to these improvements on the polymer quality, electronic transport measurements on the nano-sheets deposited on SiO_2/Si substrates can be envisaged.

Bibliography

[1] R. Feynman, "There's plenty of room at the bottom," *Eng. Sci.*, vol. 23, no. 5, pp. 22–36, 1960.

[2] T. R. Society and T. R. A. of Engineering, eds., *Nanoscience and nanotechnologies: opportunities and uncertainties*. Latimer Trend Ltd, Plymouth, UK: Royal Society, 2004.

[3] C. Bréchignac, P. Houdy, and M. Lahmani, eds., *Nanomaterials an Nanotechnology*. Verlag Berlin Heidelberg, New York: Springer, 2007.

[4] R. M. J. Cotterill, ed., *Biophsics: An introduction*. Baffins Lane, Chichester, West Sussex PO19 1UD, England: John Wiley & Sons Ltd, 2002.

[5] T. Steiner, "The hydrogen bond in the solid state," *Angew. Chem. Int. Ed.*, vol. 41, no. 1, pp. 48–76, 2002.

[6] G. C. Pimentel and A. L. McClellan, eds., *The hydrogen bond*. San Francisco: Freeman, 1960.

[7] O. M. Yaghi, M. O'Keeffe, N. W. Ockwig, H. K. Chae, M. Eddaoudi, and J. Kim, "Reticular synthesis and the design of new materials," *Nature*, vol. 423, pp. 705–714, 2003.

[8] C. S. Diercks and O. M. Yaghi, "The atom, the molecule and the covalent organic framework," *Science*, vol. 355, 2017.

[9] A. P. Côté, A. I. Benin, N. W. Ockwig, O. Michael, A. J. Matzger, and O. M. Yaghi, "Porous, crystalline, covalent organic frameworks," *Science*, vol. 310, no. 5751, pp. 1166–1170, 2005.

[10] J. W. Colson, A. R. Woll, A. Mukherjee, M. P. Levendorf, E. L. Spitler, V. B. Shields, M. G. Spencer, J. Park, and W. R. Ditchel, "Oriented 2d covalent organic framework thin films on single-layer graphene," *Science*, vol. 332, no. 6026, pp. 228–231, 2011.

[11] W. Wang and A. Schlüter, "Synthetic 2D polymers: A critical perspective and a look into the future," *Macromol. Rapid Commun.*, vol. 40, no. 1, p. 1800719, 2018.

[12] P. Payamyar, B. T. King, H. C. öttinger, and A. D. Schlüter, "Two-dimensional polymers: concepts and perspectives," *Chem. Commun.*, vol. 52, no. 1, pp. 18–34, 2016.

[13] J. Sakamoto, J. van Heijst, O. Lukin, and A. D. Schlüter, "Two-dimensional polymers: Just a dream of synthetic chemists?," *Angew. Chem. Int. Ed.*, vol. 48, pp. 1030–1069, 2009.

[14] S. Leininger, B. Olenyuk, and P. J. Stang, "Self-assembly of discrete cyclic nanostructures mediated by transition metals," *Chem. Rev.*, vol. 100, no. 3, pp. 853–908, 2000.

[15] R. Sakamoto, K. Hoshiko, K. Q. Liu, T. Yagi, T. Nagayama, S. Kusaka, M. Tsuchiya, Y. Kitagawa, W. Y. Wong, and H. Nishihara, "A photofunctional bottom-up bis(dipyrrinato)zinc(II) complex nanosheet," *Nat. Commun.*, vol. 6, p. 6713, 2015.

[16] P. M. Stricklen, E. J. Volcko, and J. G. Verkade, "Novel homo- and heterometallic coordination macrocycles," *J. Am. Chem. Soc.*, vol. 105, no. 8, pp. 2494–2495, 1983.

[17] J. M. Lehn, A. Rigault, J. Siegel, J. Harrowfield, B. Chevrier, and D. Moras, "Spontaneous assembly of double-stranded helicates from oligobipyridine ligands and copper(I) cations: Structure of an inorganic double helix," *Proc. Natl. Acad. Sci. USA*, vol. 84, no. 9, pp. 2265–2269, 1987.

[18] B. F. Hoskins and R. Robson, "Infinite polymeric frameworks consisting of three dimensionally linked rod-like segments," *J. Am. Chem. Soc.*, vol. 111, no. 15, pp. 5962–5964, 1989.

[19] A. M. Garcia, F. J. Romero-Salguero, D. M. Bassani, J.-M. Lehn, G. Baum, and D. Fenske, "Self-assembly and characterization of multimetallic grid-type lead(II) complexes," *Chem. Eur. J.*, vol. 5, p. 6, 1999.

[20] P. N. W. Baxter, J.-M. Lehn, J. Fischer, and M.-T. Youinou, "Self-assembly and structure of a 3×3 inorganic grid from nine silver ions and six ligand components," *Angew. Chem. Int. Ed.*, vol. 33, no. 22, pp. 2284–2287, 1994.

[21] M. Yoshizawa, J. K. Klosterman, and M. Fujita, "Functional molecular flasks: new properties and reactions within discrete, self-assembled hosts," *Angew. Chem. Int. Ed.*, vol. 48, no. 19, pp. 3418–3438, 2009.

[22] "2012 metal-organic frameworks issue," *Chem. Rev.*, vol. 112, no. 2, pp. 673–1268, 2012.

[23] H. Li, M. Eddaoudi, M. O'Keeffe, and O. M. Yaghi, "Design and synthesis of an exceptionally stable and highly porous metal-organic framework," *Nature*, vol. 402, pp. 276–279, 1999.

[24] J. R. Hunt, C. J. Doonan, J. D. LeVangie, A. Côté, and O. M. Yaghi, "Reticular synthesis of covalent organic borosilicate frameworks," *J. Am. Chem. Soc.*, vol. 130, pp. 11872–11873, 2008.

[25] F. J. Uribe-Romo, J. R. Hunt, H. Furukawa, C. Klöck, M. O'Keeffe, and O. M. Yaghi, "A crystalline imine-linked 3-d porous covalent organic framework," *J. Am. Chem. Soc.*, vol. 131, no. 13, pp. 4570–4571, 2009.

[26] P. Kuhn, M. Antonietti, and A. Thomas, "Porous, covalent triazine-based frameworks prepared by ionothermal synthesis," *Ang. Chem. Int. Ed*, vol. 47, no. 18, pp. 3450–3453, 2008.

[27] X. Zhuang, W. Zhao, F. Zhang, Y. Cao, F. Liu, S. Bia, and X. Feng, "A two-dimensional conjugated polymer framework with fully sp^2-bonded carbon skeleton," *Polym. Chem.*, vol. 7, no. 25, pp. 4176–4181, 2016.

[28] Q. Fang, Z. Zhuang, S. Gu, R. B. Kaspar, J. Zheng, J. Wang, S. Qiu, and Y. Yan, "Designed synthesis of large-pore crystalline polyimide covalent organic frameworks," *Nat. Commun.*, vol. 23, no. 5, p. 4503, 2014.

[29] K. T. Jackson, T. E. Reicha, and H. M. El-Kaderi, "Targeted synthesis of a porous borazine-linked covalent organic framework," *Chem. Commun.*, vol. 48, no. 70, pp. 8823–8825, 2012.

[30] N. Ruiz-del Árbol, I. Palacio, G. Otero-Irurueta, J. I. Martínez, P. L. de Andrés, O. Stetsovych, M. Moro-Lagares, P. Mutombo, M. Svec, P. Jelínek, A. Cossaro, L. Floreano, G. J. Ellis, M. F. López, and J. A. Martín-Gago, "On-surface bottom-up synthesis of azine derivatives displaying strong acceptor behavior," *Angew. Chem. Int. Ed.*, vol. 57, no. 28, pp. 8582–8586, 2018.

[31] S. S. Han, H. Furukawa, Y. O. M., and W. A. Goddard, "Covalent organic frameworks as exceptional hydrogen storage materials," *J. Am. Chem. Soc.*, vol. 130, no. 35, pp. 11580–11581, 2008.

[32] H. Furukawa and O. M. Yaghi, "Storage of hydrogen, methane, and carbon dioxide in highly porous covalent organic frameworks for clean energy applications," *J. Am. Chem. Soc.*, vol. 131, no. 25, pp. 8875–8883, 2009.

[33] S.-Y. Ding, J. Gao, Q. Wang, Y. Zhang, W.-G. Song, C.-Y. Su, and W. Wang, "Construction of covalent organic framework for catalysis: Pd/COF-LZU1 in

Suzuki-Miyaura coupling reaction," *J. Am. Chem. Soc.*, vol. 133, no. 49, pp. 19816–19822, 2011.

[34] C. Tan, X. Cao, X.-J. Wu, Q. He, J. Yang, X. Zhang, J. Chen, W. Zhao, S. Han, G.-H. Nam, M. Sindoro, and H. Zhang, "Recent advances in ultrathin two-dimensional nanomaterials," *Chem. Rev.*, vol. 117, no. 9, pp. 6225–6331, 2017.

[35] G. E. Moore, "Cramming more components onto integrated circuits," *Electronics*, vol. 38, no. 8, 1965.

[36] M. A. Reed, "Molecular-scale electronics," *IEEE*, vol. 87, no. 4, pp. 652–658, 1999.

[37] A. Aviram and M. A. Ratner, "Molecular rectifiers," *Chem. Phys. Lett.*, vol. 29, no. 2, pp. 277–283, 1974.

[38] D. L. Pearson and J. M. Tour, "Rapid syntheses of oligo(2,5-thiophene-ethynylene)s with thioester termini: potential molecular scale wires with alligator clips," *J. Org. Chem.*, vol. 62, no. 5, pp. 1376–1387, 1997.

[39] L. Grill, M. Dyer, L. Lafferentz, M. Person, M. V. Peters, and S. Hecht, "Nano-architectures by covalent assembly of molecular building blocks," *Nat. Nanotechnol.*, vol. 2, pp. 687–691, 2007.

[40] N. R. Champsee, "Building with molecules," *Nat. Nanotechnol.*, vol. 2, pp. 671–672, 2007.

[41] R. Otero, A. Vázquez de Parga, and J. Gallego, "Electronic, structural and chemical effects of charge-transfer at organic/inorganic interfaces," *Surf. Sci. Rep.*, vol. 72, no. 3, pp. 105–145, 2017.

[42] T. C. Tseng, C. Urban, Y. Wang, R. Otero, S. L. Tait, M. Alcamí, D. Écija, M. Trelka, J. M. Gallego, N. Lin, M. Konuma, U. Starke, A. Nefedov, A. Langner, C. Wöll, M. A. Herranz, F. Martín, N. Martín, K. Kern, and R. Miranda, "Charge-transfer-induced structural rearrangements at both sides of organic/metal interfaces," *Nat. Chem.*, vol. 2, pp. 374–379, 2010.

[43] L. Romaner, G. Heimel, J. L. Brédas, A. Gerlach, F. Schreiber, R. L. Johnson, J. Zegenhagen, S. Duhm, N. Koch, and E. Zojer, "Impact of bidirectional charge transfer and molecular distortions on the electronic structure of a metal-organic interface," *Phys. Rev. Lett.*, vol. 99, no. 25, p. 256801, 2007.

[44] X. Torrelles, V. Langlais, M. De Santis, H. C. N. Tolentino, and Y. Gauthier, "Nanoscale patterning by C_{60} ordering on Pt(110)," *J. Phys. Chem. C*, vol. 114, no. 37, pp. 15645–15652, 2010.

[45] X. Zhang, W. He, A. Zhao, H. Li, L. Chen, W. W. Pai, J. Hou, M. M. T. Loy, J. Yang, and X. Xiao, "Geometric and electronic structure of a C_{60} monolayer on Ag(100)," *Phys. Rev. B*, vol. 75, no. 23, p. 235444, 2007.

[46] S. Bedwani, D. Wegner, M. F. Crommie, and A. Rochefort, "Strongly reshaped organic-metal interfaces: Tetracyanoethylene on Cu(100)," *Phys. Rev. Lett.*, vol. 101, no. 21, p. 216105, 2008.

[47] D. Zhong, J. H. Franke, S. K. Podiyanachari, T. Blömker, H. Zhang, G. Kehr, G. Erker, H. Fuchs, and L. Chi, "Linear alkane polymerization on a gold surface," *Science*, vol. 334, no. 6053, pp. 213–216, 2011.

[48] M. In't Veld, P. Iavicoli, D. B. Haq, Sam Amabilino, and R. Raval, "Unique intermolecular reaction of simple porphyrins at a metal surface gives covalent nanostructures," *Chem. Commun.*, vol. 334, no. 13, pp. 1536–1538, 2008.

[49] R. Mas-Ballesté, C. Gómez-Navarro, J. Gómez-Herrero, and F. Zamora, "2D materials: to graphene and beyond," *Nanoscale*, vol. 3, pp. 20–30, 2011.

[50] K. S. Novoselov, D. Jiang, F. Schedin, T. J. Booth, V. V. Khotkevich, S. V. Morozov, and A. K. Geim, "Two-dimensional atomic crystals," *PNAS*, vol. 102, no. 30, p. 10451–10453, 2005.

[51] R. H. Baughman, H. Eckhardt, and M. Kertesz, "Structure-property predictions for new planar forms of carbon: Layered phases containing sp^2 and sp atoms," *J. Chem. Phys.*, vol. 87, no. 11, p. 6687, 1987.

[52] J. W. Colson and W. R. Dichtel, "Rationally synthesized two-dimensional polymers," *Nat. Chem.*, vol. 5, pp. 453–465, 2013.

[53] N. A. A. Zwaneveld, R. Pawlak, M. Abel, D. Catalin, D. Gigmes, D. Bertin, and L. Porte, "Organized formation of 2d extended covalent organic frameworks at surfaces," *J. Am. Chem. Soc.*, vol. 130, no. 21, pp. 6678–6679, 2008.

[54] O. Ourdjini, R. Pawlak, M. Abel, S. Clair, L. Chen, N. Bergeon, M. Sassi, V. Oison, J. M. Debierre, R. Coratger, and L. Porte, "Substrate-mediated ordering and defect analysis of a surface covalent organic framework," *Phys. Rev. B*, vol. 84, no. 12, pp. 125421–125429, 2011.

[55] A. C. Marele, R. Mas-Ballesté, L. Terracciano, J. Rodríguez-Fernández, I. Berlanga, S. S. Alexandre, R. Otero, J. M. Gallego, F. Zamora, and J. M. Gómez-Rodríguez, "Formation of a surface covalent organic framework based on polyester condensation," *Chem. Commun.*, vol. 48, no. 12, pp. 6779–6781, 2012.

[56] T. Faury, S. Clair, M. Abel, F. Dumur, D. Gigmes, and L. Porte, "Sequential linking to control growth of a surface covalent organic framework," *J. Phys. Chem. C*, vol. 116, no. 7, pp. 4819–4823, 2012.

[57] R. Lindner and A. Kühnle, "On-surface synthesis," *Chem. Phys. Chem.*, vol. 16, no. 8, pp. 1582–1592, 2015.

[58] J. Méndez, M. F. López, and J. A. Martín-Gago, "On-surface synthesis of cyclic organic molecules," *Chem. Soc. Rev.*, vol. 40, no. 9, pp. 4578–4590, 2011.

[59] M. Bieri, M. T. Nguyen, O. Groening, J. Cai, M. S. Treier, K. Aït-Mansour, P. Ruffieux, C. A. Pignedoli, D. Passerone, M. Kastler, K. Müllen, and R. Fasel, "Two-dimensional polymer formation on surfaces: insight into the roles of precursor mobility and reactivity," *J. Am. Chem. Soc.*, vol. 132, no. 46, pp. 16669–16676, 2010.

[60] G. Ertl, ed., *Reactions at solid surfaces*. New York: John Wiley & Sons, 2009.

[61] J. K. Norskov, "Chemisorption on metal surfaces," *Rep. Prog. Phys.*, vol. 53, pp. 1253–1295, 1990.

[62] M. Cinchetti, V. A. Dediu, and L. E. Hueso, "Activating the molecular spinterface," *Nat. Matter.*, vol. 17, pp. 507–515, 2017.

[63] F. Tautz, "Structure and bonding of large aromatic molecules on noble metal surfaces: The example of PTCDA," *Prog. Surf. Sci.*, vol. 82, no. 9, pp. 479–520, 2007.

[64] J. P. Muscat and D. M. Newns, "Chemisorption on metals," *Prog. Surf. Sci.)*, vol. 9, no. 1, pp. 1–43, 1978.

[65] R. Gutzler, H. Walch, G. Eder, S. Kloft, W. M. Hecklab, and M. Lackinger, "Surface mediated synthesis of 2d covalent organic frameworks: 1,3,5-tris(4-bromophenyl)benzene on graphite(001), Cu(111), and Ag(110)," *Chem. Commun.*, vol. 40, no. 29, pp. 4456–4458, 2009.

[66] H. Y. Gao, J. H. Franke, H. Wagner, D. Zhong, P. A. Held, A. Studer, and H. Fuchs, "Effect of metal surfaces in on-surface glaser coupling," *J. Phys. Chem. C*, vol. 117, no. 36, pp. 18595–18602, 2013.

[67] A. Saywell, J. Schwarz, S. Hecht, and L. Grill, "Polymerization on stepped surfaces: alignment of polymers and identification of catalytic sites," *Angew. Chem.*, vol. 124, no. 21, pp. 5186–5190, 2012.

[68] S. H. Kim, J. Méndez, J. Wintterlin, and G. Ertl, "Enhanced reactivity of adsorbed oxygen on Pd(111) induced by compression of the oxygen layer," *Phys. Rev. B*, vol. 72, no. 15, p. 155414, 2005.

[69] E. L. Spitler and W. R. Ditchel, "Lewis acid-catalysed formation of two-dimensional phtalocyanine covalent organic framework," *Nat. Chem.*, vol. 2, pp. 672–677, 2010.

[70] K. Fujita, T. Ishikawa, and T. Tsutsui, "Novel method for polymer thin film preparation: spray deposition of highly diluted polymer solutions," *Jpn. J. Appl. Phys.*, vol. 41, pp. L70–L72, 2002.

[71] J. Barth, J. Weckesser, N. Lin, A. Dmitriev, and K. Kern, "Electronic structure of few-layer epitaxial graphene on Ru(0001)," *Appl. Phys. A*, vol. 76, no. 5, pp. 645–652, 2003.

[72] N. Lin, A. Dmitriev, J. Weckesser, J. V. Barth, and K. Kern, "Real-time single-molecule imaging of the formation and dynamics of coordination compounds," *Angew. Chem. Int. Ed.*, vol. 41, no. 24, pp. 4779–4784, 2002.

[73] A. Hauschild, K. Karki, B. C. C. Cowie, M. Rohlfing, F. S. Tautz, and M. Sokolowski, "Molecular distortions and chemical bonding of a large π–conjugated molecule on a metal surface," *Phys. Rev. Lett.*, vol. 94, no. 3, p. 036106, 2005.

[74] F. Ullmann, "Ueber symmestrische biphenylderivate," *Liebigs Annalen*, vol. 332, pp. 38–81, 1904.

[75] R. Gutzler, L. Cardenas, J. Lipton-Duffin, M. E. Garah, L. E. Dinca, C. E. Szakacs, C. Fu, M. Gallagher, M. Vondráček, M. Rybachuk, D. F. F.Perepichka, and F. Rosei, "Ullmann-type coupling of brominated tetrathienoanthracene on copper and silver," *Nanoscale*, vol. 6, no. 5, pp. 2660–2668, 2014.

[76] X. H. Liu, W. L. Hu, W. J. Jiang, Y. W. Yang, S. Niu, B. Sun, J. Wu, and J. S. Hu, "Well-defined metal–O6 in metal–catecholates as a novel active site for oxygen electroreduction," *ACS Appl. Mater. Interfaces*, vol. 9, no. 34, pp. 28473–28477, 2017.

[77] J. Eichhorn, T. Strunskus, A. Rastgoo-Lahrood, D. Samanta, M. Schmittel, and M. Lackinger, "On-surface Ullmann polymerization via intermediate organometallic networks on Ag(111," *Chem. Commun.*, vol. 50, no. 57, p. 7680, 2014.

[78] C. Moreno, M. Vilas-Varela, B. Kretz, A. Garcia-Lekue, M. V. Costache, M. Paradinas, M. Panighel, G. Ceballos, S. O. Valenzuela, D. Peña, and A. Mugarzal, "Bottom-up synthesis of multifunctional nanoporous graphene," *Science*, vol. 360, pp. 199–203, 2018.

[79] C. Moreno, M. Paradinas, M. Vilas-Varela, M. Panighel, G. Ceballos, D. Peña, and A. Mugarzal, "On-surface synthesis of superlattice arrays of ultralong graphene nanoribbons," *Chem. Commun.*, vol. 54, no. 68, pp. 9402–9405, 2018.

[80] L. Lafferentz, V. Eberhardt, C. Dri, C. Africh, G. Comelli, F. Esch, S. Hecht, and L. Grill, "Controlling on-surface polymerization by hierarchical and substrate-directed growth," *Nat. Chem.*, vol. 4, pp. 215–220, 2012.

[81] C. Steiner, J. Gebhardt, M. Ammon, Z. Yang, A. Heidenreich, N. Hammer, A. Görling, M. Kivala, and S. Maier, "Hierarchical on-surface synthesis and electronic structure of carbonyl-functionalized one- and two-dimensional covalent nanoarchitectures," *Nat. Commun.*, vol. 8, p. 14765, 2017.

[82] V. K. Kanuru, G. Kyriakou, S. K. Beaumont, A. C. Papageorgiou, D. J. Watson, and R. M. Lambert, "Sonogashira coupling on an extended gold surface in vacuo: reaction of phenylacetylene with iodobenzene on Au(111)," *J. Am. Chem. Soc.*, vol. 132, no. 23, pp. 8081–8086, 2010.

[83] K. J. Shi, C. H. Shu, C. X. Wang, X. Y. Wu, H. Tian, and P. N. Liu, "On-surface Heck reaction of aryl bromides with alkene on Au(111) with palladium as catalyst," *Org. Lett.*, vol. 19, no. 11, pp. 2801–2804, 2017.

[84] S. L. Tait, Y. Wang, G. Costantini, N. Lin, A. Baraldi, F. Esch, L. Petaccia, S. Lizzit, and K. Kern, "Metal-organic coordination interactions in Fe-terephthalic acid networks on Cu(100)," *J. Am. Chem. Soc.*, vol. 130, no. 6, pp. 2108–2113, 2008.

[85] J. Cai, P. Ruffieux, R. Jaafar, M. Bieri, T. Braun, S. Blankenburg, M. Muoth, A. P. Seitsonen, M. Saleh, X. Feng, K. Müllen, and R. Fasel, "Atomically precise bottom-up fabrication of graphene nanoribbons," *Nature*, vol. 466, pp. 470–473, 2010.

[86] S. Weigelt, C. Busse, C. Bombis, M. M. Knudsen, K. V. Gothelf, T. Strunskus, C. Wöll, M. Dahlbom, B. Hammer, E. Lægsgaard, F. Besenbacher, and T. R. Linderoth, "Covalent interlinking of an aldehyde and an amine on a Au(111) surface in ultrahigh vacuum," *Angew. Chem. Int. Ed.*, vol. 46, no. 48, pp. 9227–9230, 2007.

[87] S. Weigelt, C. Busse, C. Bombis, M. M. Knudsen, K. V. Gothelf, E. Lægsgaard, F. Besenbacher, and T. R. Linderoth, "Surface synthesis of 2d branched polymer nanostructures," *Angew. Chem. Int. Ed.*, vol. 47, no. 23, pp. 4406–4410, 2008.

[88] C. H. Schmitz, J. Ikonomov, and M. Sokolowski, "Two-dimensional ordering of poly(p-phenylene-terephthalamide) on the Ag(111) surface investigated by scanning tunneling microscopy," *J. Phys. Chem. C*, vol. 133, no. 28, pp. 11984–11987, 2009.

[89] M. Treier, R. Fasel, N. R. Champness, S. Argent, and N. V. Richardson, "Molecular imaging of polyimide formation," *Phys. Chem. Chem. Phys.*, vol. 111, pp. 1209–1214, 2009.

[90] R. Coratger, B. Calmettes, M. Abel, and L. Porte, "Stm observations of the first polymerization steps between hexahydroxy-tri-phenylene and benzene-di-boronic acid molecules," *Surf. Sci.*, vol. 605, no. 7-8, pp. 831–837, 2011.

[91] M. Lischka, R. Dong, M. Wang, N. Martsinovich, M. Fritton, L. Grossmann, W. M. Heckl, X. Feng, and M. Lackinger, "Competitive metal-coordination of hexaaminotriphenylene on Cu(111) by intrinsic copper versus extrinsic nickel adatoms," *Chem. Eur. J.*, vol. 25, no. 8, pp. 1975–1983, 2019.

[92] M. Matena, M. Stöhr, T. Riehm, J. Björk, S. Martens, M. S. Dyer, M. Persson, J. Lobo-Checa, K. Müller, M. Enache, H. Wadepohl, J. Zegenhagen, T. A. Jung, and L. H. Gade, "Aggregation and contingent metal/surface reactivity of 1,3,8,10-tetraazaperopyrene (TAPP) on Cu(111)," *Chem. Eur. J.*, vol. 16, no. 7, pp. 2079–2091, 2010.

[93] D. D. Medina, J. M. Rotter, Y. Hu, D. Mirjam, V. Werner, F. Auras, J. T. Markiewicz, P. Knochel, and T. Bein, "Room temperature synthesis of covalent-organic framework films through vapor-assisted conversion," *J. Am. Chem. Soc.*, vol. 137, no. 3, pp. 1016–1019, 2015.

[94] U. Schlickum, R. Decker, F. Klappenberger, G. Zoppellaro, S. Klyatskaya, M. Ruben, I. Silanes, A. Arnau, K. Kern, H. Brune, and J. V. Barth, "Metal-organic honeycomb nanomeshes with tunable cavity size," *Nano. Lett.*, vol. 7, no. 12, pp. 3813–3817, 2017.

[95] Y. Q. Zhang, N. Kepčija, M. Kleinschrodt, K. Diller, S. Fischer, A. C. Papageorgiou, F. Allegretti, J. Björk, S. Klyatskaya, F. Klappenberger, M. Ruben, and J. V. Barth, "Homo-coupling of terminal alkynes on a noble metal surface," *Nat. Commun.*, vol. 3, p. 1286, 2012.

[96] C. Dinca, Laurentiu E.and Fu, J. M. MacLeod, J. Lipton-Duffin, J. L. Brusso, C. E. Szakacs, D. Ma, D. F. Perepichka, and F. Rosei, "Unprecedented transformation of tetrathienoanthracene into pentacene on Ni(111)," *ACS Nano*, vol. 7, no. 2, pp. 1652–1657, 2013.

[97] M. Matena, T. Riehm, M. Stöhr, T. A. Jung, and L. H. Gade, "Transforming surface coordination polymers into covalent surface polymers: linked polycondensed aromatics through oligomerization of N-heterocyclic carbene intermediates," *Angew. Chem. Int. Ed.*, vol. 47, no. 13, pp. 2414–2417, 2008.

[98] V. Rubio-Giménez, M. Galbiati, J. Castells-Gil, N. Almora-Barrios, J. Navarro-Sánchez, G. Escorcia-Ariza, M. Mattera, T. Arnold, J. Rawle, S. Tatay, E. Coronado, and C. Martí-Gastaldo, "Bottom-up fabrication of semiconductive metal–organic framework ultrathin films," *Adv. Mater.*, vol. 30, no. 10, p. 1704291, 2018.

[99] T. Bauer, Z. Zheng, A. Renn, R. Enning, A. Stemmer, J. Sakamoto, and A. D. Schlüter, "Synthesis of free-standing, monolayered organometallic sheets at the air/water interface," *Angew. Chem. Int. Ed.*, vol. 50, no. 34, pp. 7879–7884, 2011.

[100] P. Payamyar, K. Kaja, C. Ruiz-Vargas, A. Stemmer, D. J. Murray, C. J. Johnson, B. T. King, F. Schiffmann, J. VandeVondele, A. Renn, S. Götzinger, P. Ceroni, A. Schütz, L. T. Lee, Z. Zheng, J. Sakamoto, and A. D. Schlüter, "Synthesis of a covalent monolayer sheet by photochemical anthracene dimerization at the air/water interface and its mechanical characterization by afm indentation," *Adv. Mater.*, vol. 26, no. 13, pp. 2052–2058, 2014.

[101] L. Dai, ed., *Chapter 2. Conductive polymers in: Intelligent macromolecules for smart devices*, vol. 180. Elservier, 2004.

[102] S. Banerjee and A. Tyagi, eds., *Chapter 2. Conducting polymer sensors, actuators and field-effect transistors in functional materials: preparation, processing and applications.* Elservier, 2012.

[103] T. Kambe, R. Sakamoto, K. Hoshiko, K. Takada, M. Miyachi, J. H. Ryu, S. Sasaki, J. Kim, K. Nakazato, M. Takata, and H. Nishihara, "π–conjugated nickel bis(dithiolene) complex nanosheet," *J. Am. Chem. Soc.*, vol. 135, no. 7, pp. 2462–2465, 2013.

[104] T. Kambe, R. Sakamoto, T. Kusamoto, T. Pal, N. Fukui, K. Hoshiko, T. Shimojima, Z. Wang, T. Hirahara, K. Ishizaka, S. Hasegawa, F. Liu, and H. Nishihara, "Redox control and high conductivity of nickel bis(dithiolene) complex π–nanosheet: A potential organic two-dimensional topological insulator," *J. Am. Chem. Soc.*, vol. 136, no. 41, pp. 14357–14360, 2014.

[105] R. Matsuoka, R. Sakamoto, T. Kambe, K. Takada, T. Kusamoto, and H. Nishihara, "Ordered alignment of a one-dimensional π–conjugated nickel bis(dithiolene) complex polymer produced via interfacial reactions," *Chem. Commun*, vol. 50, no. 60, p. 8137, 2014.

[106] X. Huang, P. Sheng, Z. Tu, F. Zhang, J. Wang, H. Geng, Y. Zou, C.-a. Di, Y. Yi, Y. Sun, W. Xu, and D. Zhu, "A two-dimensional π–d conjugated coordination polymer with extremely high electrical conductivity and ambipolar transport behaviour," *Nat. Commun.*, vol. 6, p. 7408, 2015.

[107] R. Matsuoka, R. Sakamoto, K. Hoshiko, S. Sasaki, H. Masunaga, K. Nagashio, and H. Nishihara, "Crystalline graphdiyne nanosheets produced at a gas/liquid or liquid/liquid interface," *J. Am. Chem. Soc.*, vol. 139, no. 8, pp. 3145–3152, 2017.

[108] S. J. Rowan, S. J. Cantrill, G. R. L. Cousins, J. K. M. Sanders, and J. F. Stoddart, "Dynamic covalent chemistry," *Angew. Chem. Int. Ed.*, vol. 41, no. 6, pp. 898–952, 2002.

[109] C. D. Meyer, C. S. Joiner, and J. F. Stoddart, "Template-directed synthesis employing reversible imine bond formation," *Chem. Soc. Rev.*, vol. 36, pp. 1705–1723, 2007.

[110] M. E. Belowich and S. J. Fraser, "Dynamic imine chemistry," *Chem. Soc. Rev.*, vol. 41, pp. 2003–2024, 2012.

[111] W. Dai, F. Shao, J. Szczerbiński, R. McCaffrey, R. Zenobi, Y. Jin, A. D. Schlîter, and W. Zhang, "Synthesis of a two-dimensional covalent organic monolayer through dynamic imine chemistry at the air/water interface," *Angew. Chem. Int. Ed.*, vol. 55, no. 1, pp. 213–217, 2016.

[112] H. Sahabudeen, H. Qi, B. A. Glatz, D. Tranca, R. Dong, Y. Hou, T. Zhang, C. Kuttner, T. Lehnert, G. Seifert, U. Kaiser, A. F. Zhikun-Zheng, and X. Feng, "Wafer-sized multifunctional polyimine-based two-dimensional conjugated polymers with high mechanical stiffness," *Nat. Commun.*, vol. 7, p. 13461, 2016.

[113] K. Takada, R. Sakamoto, S. T. Yi, S. Katagiri, T. Kambe, and H. Nishihara, "An electrochromic bis(terpyridine)metal complex nanosheet," *J. Am. Chem. Soc.*, vol. 137, no. 14, pp. 4681–4689, 2015.

[114] A. Mähringer, A. C. Jakowetz, J. M. Rotter, B. J. Bohn, J. K. Stolarczyk, J. Feldmann, T. Bein, and D. D. Medina, "Oriented thin films of electroactive triphenylene catecholate-based two-dimensional metalorganic frameworks," *ACS Nano*, vol. 13, no. 6, pp. 6711–6719, 2019.

[115] D. D. Medina, T. Sick, and T. Bein, "Photoactive and conducting covalent organic frameworks," *Adv. Energy Mater.*, vol. 7, p. 1700387, 2017.

[116] J. Park, A. C. Hinckley, Z. Huang, D. Feng, A. A. Yakovenko, M. Lee, S. Chen, X. Zou, and Z. Bao, "Synthetic routes for a 2D semiconductive copper hexahydroxybenzene metalorganic framework," *J. Am. Chem. Soc.*, vol. 140, pp. 14533–14537, 2018.

[117] L. Sun, M. G. Campbell, and M. Dincă, "Electrically conductive porous metal–organic frameworks," *Angew. Chem. Int. Ed.*, vol. 55, pp. 3566–3579, 2016.

[118] D. Sheberla, L. Sun, M. A. Blood-Forsythe, S. Er, C. R. Wade, C. K. Brozek, A. Aspuru-Guzik, and M. Dincaă, "High electrical conductivity in Ni_3(2,3,6,7,10,11-hexaiminotriphenylene)$_2$, a semiconducting metal–organic graphene analogue," *J. Am. Chem. Soc.*, vol. 133, no. 20, pp. 7909–7915, 2011.

[119] R. Gutzler and D. F. Perepichka, "π-electron conjugation in two-dimensions," *J. Am. Chem. Soc.*, vol. 135, no. 4, pp. 16585–16594, 2013.

[120] M. Hmadeh, Z. Lu, Z. Liu, F. Gaándara, H. Furukawa, S. Wan, V. Augustyn, R. Chang, L. Liao, F. Zhou, E. Perre, V. Ozolins, K. Suenaga, X. Duan, B. Dunn, Y. Yamamto, O. Terasaki, and O. M. Yaghi, "New porous crystals of extended metal-catecholates," *Chem. Mater.*, vol. 24, no. 18, pp. 3511–3513, 2012.

[121] M. Yao, X. Lv, W. Fu, Z.H.and Li, W. Deng, G. Wu, and G. Xu, "Layer-by-layer assembled conductive metal-organic framework nanofilms for room-temperature chemiresistive sensing.," *Angew. Chem. Int. Ed.*, vol. 56, no. 52, pp. 16510–16514, 2017.

[122] A. Karmakar, P. Samanta, A. V. Desai, and S. K. Ghosh, "Guest-responsive metal-organic frameworks as scaffolds for separation and sensing applications," *Acc. Chem. Res.*, vol. 50, no. 10, pp. 2457–2469, 2017.

[123] S. S. Nagarkar, B. Joarder, A. K. Chaudhari, S. Mukherjee, and S. K. Ghosh, "Highly selective detection of nitro explosives by a luminescent metal–organic framework," *Angew. Chem. Int. Ed.*, vol. 52, no. 10, pp. 2881–2885, 2013.

[124] A. J. Clough, J. W. Yoo, M. H. Mecklenburg, and S. C. Marinescu, "2D metal-organic surfaces for efficient hydrogen evolution from water," *J. Am. Chem. Soc.*, vol. 137, no. 1, pp. 118–121, 2015.

[125] L. Zhu, X.-Q. Liu, H. L. Jiang, and L. B. Sun, "Metal–organic frameworks for heterogeneous basic catalysis," *Chem. Rev.*, vol. 117, no. 12, pp. 8129–8176, 2017.

[126] D. B. Shinde, S. Kandambeth, P. Pachfule, R. R. Kumara, and R. Banerjee, "Bifunctional covalent organic frameworks with two dimensional organocatalytic micropores," *Chem. Commun.*, vol. 50, no. 2, pp. 310–313, 2015.

[127] L. Wang, Y. Han, X. Feng, J. Zhou, P. Qi, and B. Wang, "Metal–organic frameworks for energy storage: Batteries and supercapacitors.," *Coord. Chem. Rev.*, vol. 307, no. 52, pp. 361–381, 2016.

[128] W. Li, K. Ding, H. Tian, M. Yao, B. Nath, W. Deng, Y. Wang, and G. Xu, "Conductive metal–organic framework nanowire array electrodes for high-performance solid-state supercapacitors," *Adv. Funct. Mater.*, vol. 27, no. 27, p. 1702067, 2017.

[129] L. Stegbauer, K. Schwinghammer, and B. V. Lotsch, "A hydrazone-based covalent organic framework for photocatalytic hydrogen production," *Chem. Sci.*, vol. 5, pp. 2789–2793, 2014.

[130] D. A. Vazquez-Molina, G. S. Mohammad-Pour, C. Lee, M. W. Logan, X. Duan, J. K. Harper, and F. J. Uribe-Romo, "Mechanically shaped two-dimensional covalent organic frameworks reveal crystallographic alignment and fast Li-ion conductivity," *J. Am. Chem. Soc.*, vol. 138, no. 31, pp. 9767–9770, 2016.

[131] K. Saravanan, M. Nagarathinam, P. Balaya, and J. J. Vittal, "Lithium storage in a metal organic framework with diamondoid topology: a case study on metal formates," *J. Mater. Chem.*, vol. 20, no. 38, pp. 8329–8335, 2010.

[132] G. Binnig and H. Röhrer, "Scanning tunneling microscopy," *Helv. phys. acta*, vol. 55, pp. 726–735, 1982.

[133] G. Binnig, H. Röhrer, C. Gerber, and E. Weibel, "Surface studies by scanning tunneling microscopy," *Phys. Rev. Lett.*, vol. 49, no. 1, pp. 57–61, 1982.

[134] R. Wiesendanger, ed., *Scanning probe microscopy and spectroscopy: Methods and applications*. Trumpington Street, Cambridge CB2 1RP, United Kingdom: Cambridge University press, 1994.

[135] O. Fischer, M. Kugler, I. Maggio-Aprile, C. Berthod, and C. Renner, "Tunneling from a many-particle point of view," *Rev. Mod. Phys.*, vol. 79, p. 353, 2007.

[136] J. Bardeen, "Tunneling from a many-particle point of view," *Phys. Rev. Lett.*, vol. 6, no. 2, pp. 57–59, 1961.

[137] A. Artaud, ed., *Thesis amnuscript: Quasi-long-range order and topological defects in graphene on rhenium studied by scanning tunneling microscopy*. Grenoble, France: Université Grenoble-Alpes, 2017.

[138] C. R. Brundle and A. D. Baker, eds., *Electron Spectroscopy: Theory, techniques and applications*, vol. 2. Academic press, 1978.

[139] D. Briggs and M. P. Seah, eds., *Practical surface analysis: Auger and X-ray photoelectron spectroscopy*, vol. 1. New York: John Wiley, second ed., 1990.

[140] C. Sánchez-Sánchez, ed., *Tesis amnuscript: Structure and Electronic Properties of Different Adsorbates on the rutile TiO_2 (110) surfaces.* Madrid, Spain: Universidad Autónoma de Madrid, 2011.

[141] L. Floreano, G. Naletto, D. Cvetko, R. Gotter, M. Malvezzi, L. Marassi, A. Morgante, A. Santaniello, A. Verdini, F. Tommasini, and G. Tondello, "Performance of the grating-crystal monochromator of the ALOISA beamline at the Elettra synchrotron," *Rev. Sci. Instrum.*, vol. 70, pp. 70, 3855, 1999.

[142] J. Stöhr, ed., *NEXAFS spectroscopy*, vol. 25. New York: Springer series Surface Science, first ed., 1992.

[143] G. Hähner, "Near edge X-ray absorption fine structure spectroscopy as a tool to probe electronic and structural properties of thin organic films and liquids," *Chem. Soc. Rev.*, vol. 35, no. 12, pp. 1244–1255, 2006.

[144] SSRL, "https://www-ssrl.slac.stanford.edu/nexafs.html - stanford synchrotron radiation lightsource," 2019.

[145] N. M. Harrison, "An introduction to density functional theory."

[146] M. J. Frisch, G. W. Trucks, H. B. Schlegel, G. E. Scuseria, M. A. Robb, J. R. Cheeseman, G. Scalmani, V. Barone, B. Mennucci, G. A. Petersson, H. Nakatsuji, M. Caricato, X. Li, H. P. Hratchian, A. F. Izmaylov, J. Bloino, G. Zheng, J. L. Sonnenberg, M. Hada, M. Ehara, K. Toyota, R. Fukuda, J. Hasegawa, M. Ishida, T. Nakajima, Y. Honda, O. Kitao, H. Nakai, T. Vreven, J. A. Montgomery, Jr., J. E. Peralta, F. Ogliaro, M. Bearpark, J. J. Heyd, E. Brothers, K. N. Kudin, V. N. Staroverov, R. Kobayashi, J. Normand, K. Raghavachari, A. Rendell, J. C. Burant, S. S. Iyengar, J. Tomasi, M. Cossi, N. Rega, J. M. Millam, M. Klene, J. E. Knox, J. B. Cross, V. Bakken, C. Adamo, J. Jaramillo, R. Gomperts, R. E. Stratmann, O. Yazyev, A. J. Austin, R. Cammi, C. Pomelli, J. W. Ochterski, R. L. Martin, K. Morokuma, V. G. Zakrzewski, G. A. Voth, P. Salvador, J. J. Dannenberg, S. Dapprich, A. D. Daniels, . Farkas, J. B. Foresman, J. V. Ortiz, J. Cioslowski, and D. J. Fox, "Gaussian09 Revision E.01." Gaussian Inc. Wallingford CT 2009.

[147] A. D. Becke, "Density functional thermochemistry III. the role of exact exchange," *J. Chem. Phys.*, vol. 98, no. 7, pp. 5648–5652, 1993.

[148] P. J. Stephens, F. J. Devlin, C. F. Chabalowski, and M. J. Frisch, "Ab initio calculation of vibrational absorption and circular dichroism spectra using density functional force fields," *J. Phys. Chem.*, vol. 98, no. 45, pp. 11623–11627, 1994.

[149] T. H. Dunning Jr., "Gaussian basis sets for use in correlated molecular calculations I. the atoms boron through neon and hydrogen," *J. Phys. Phys.*, vol. 90, no. 2, p. 1007, 1989.

[150] P. Giannozzi, S. Baroni, N. Bonini, M. Calandra, R. Car, C. Cavazzoni, D. Ceresoli, G. L. Chiarotti, M. Cococcioni, I. Dabo, A. Dal-Corso, S. de Gironcoli, S. Fabris, G. Fratesi, R. Gebauer, U. Gerstmann, G. C., A. Kokalj, M. Lazzeri, L. Martin-Samos, M. N., F. Mauri, R. Mazzarello, S. Paolini, A. Pasquarello, L. Paulatto, C. Sbraccia, S. Scandolo, G. Sclauzero, A. P. Seitsonen, A. Smogunov, P. Umari, and R. M. Wentzcovitch, "QUANTUM ESPRESSO: a modular and open-source software project for quantum simulations of materials.," *J. Phys. Condens. Matter.*, vol. 21, no. 39, p. 395502, 2009.

[151] S. Grimme, "Semiempirical GGA-type density functional constructed with a long-range dispersion correction," *J. Comp. Chem.*, vol. 27, no. 15, pp. 1787–1799, 2006.

[152] J. P. Perdew, K. Burke, and M. Ernzerhof, "Generalized gradient approximation made simple," *Phys. Rev. Lett.*, vol. 77, no. 18, p. 3865, 1996.

[153] A. M. Rappe, K. M. Rabe, E. Kaxiras, and J. D. Joannopoulos, "Optimized pseudopotentials," *Phys. Rev. B*, vol. 41, no. 2, p. 1227, 1990.

[154] N. Mounet and N. Marzari, "First-principles determination of the structural, vibrational and thermodynamic properties of diamond, graphite, and derivatives," *Phys. Rev. B*, vol. 71, no. 20, p. 205214, 2005.

[155] J. D. Pack and H. J. Monkhorst, "Special points for brillouin-zone integrations—a reply," *Phys. Rev. B*, vol. 16, no. 4, p. 1748, 1977.

[156] M. Parrinello and A. Rahman, "Crystal structure and pair potentials: A molecular-dynamics study," *Phys. Rev. Lett.*, vol. 45, no. 14, p. 1196, 1980.

[157] M. Parrinello and A. Rahman, "Cpolymorphic transitions in single crystals: A new molecular dynamics method," *J. App. Phys.*, vol. 52, no. 12, p. 7182, 1981.

[158] R. M. Wentzcovitch, "Invariant molecular-dynamics approach to structural phase transitions," *Phys. Rev. B*, vol. 44, no. 5, p. 2358, 1991.

[159] G. Froehlicher, ed., *Etude par spectroscopie Raman de monocouches de graphéne intégrées dans des transistors à effet de champ.* Ecole Normale Supérieure de Cachan, Master report, 2013.

[160] D. Lin-Vien, N. Colthup, W. Fateley, and J. Grasselli, *The handbook of infrared and Raman characteristic frequencies of organic molecules.* Elsevier, 1991.

[161] B. SchraderF, *Infrared and Raman Spectroscopy: Methods and Applications.* VCH Verlagsgesellschaft mbH, 1995.

[162] R. F. Egerton, ed., *Physical Principles of Electron Microscopy.* Springer, 2005.

[163] C. Mannich, "Uber die kondensntion des cyclohexanons," *Bev.*, vol. 40, p. 153, 1907.

[164] L. F. Fieser and L. M. Joshel, "Methyl homologs of triphenylene," *J. Am. Chem. Soc.*, vol. 61, no. 10, pp. 2958–2961, 1939.

[165] W. E. Bachmann and W. S. Struve, "Reactions of tetrahydrophenanthrene. synthesis of thiphenylene and methyltriphenylene," *J. Org. Chem.*, vol. 4, no. 4, pp. 472–479, 1939.

[166] W. S. Rapson, "1-methoxy- and 2-methoxy-triphenylene," *J. Chem. Soc.*, no. 0, pp. 15–18, 1941.

[167] K. D. Bartle and D. W. Jones, "Proton chemical shifts in triphenylene and methyl triphenylenes," *Trans. Faraday Soc.*, no. 63, pp. 2868–2873, 1967.

[168] J. Yerkess, D. W. Jones, and W. Denne, "Preliminary crystallographic data for methyl-substituted triphenylenes," *Acta Cryst.*, vol. B52, p. 2649, 1969.

[169] F. Thébault, L. Öhrströma, and M. Haukkab, "2,3,6,7,10,11-hexahydroxytriphenylene tetrahydrate: a new form of an important starting material for supramolecular chemistry and covalent organic frameworks," *Acta Cryst.*, vol. C67, pp. o143–0145, 2011.

[170] J. P. Rabe, S. Buchholz, and L. Askadskaya, "Scanning tunneling microscopy of chain-molecules at solid-fluid-interfaces," *Phys. Scr.*, vol. T49, pp. 260–263, 1993.

[171] A. M. Barthram, R. L. Cleary, R. Kowallick, and M. D. Ward, "A new redox-tunable near-IR dye based on a trinuclear ruthenium(II) complex of hexahydroxytriphenylene," *Chem. Commun.*, no. 24, pp. 2695–2696, 1998.

[172] N. T. T. Nguyen, H. Furukawa, F. Gaándara, C. A. Trickett, H. M. Jeong, K. E. Cordova, and O. M. Yaghi, "Three-dimensional metal-catecholate frameworks and their ultrahigh proton conductivity," *J. Am. Chem. Soc.*, vol. 137, no. 49, pp. 15394–15397, 2015.

[173] S. Slade, S. A. Campbell, T. R. Ralph, and F. C. Walsh, "Ionic conductivity of an extruded Nafion 1100 ew series of membranes," *J. Electrochem. Soc*, vol. 149, no. 21, pp. A1556–A1564, 2002.

[174] B. Hoppe, K. D. J. Hindricks, D. P. Warwas, H. A. Schulze, A. Mohmeyer, T. J. Pinkvos, S. Zailskas, M. R. Krey, C. Belke, S. König, M. Fröba, R. J. Haug, and P. Behrens, "Graphene-like metal–organic frameworks: morphology control, optimization of thin film electrical conductivity and fast sensing applications," *Cryst. Eng. Comm.*, vol. 20, pp. 6458–6471, 2018.

[175] Y. L. Li, J. J. Zhou, M.-K. Wu, C. Chen, K. Tao, F. Y. Yi, and L. Han, "Hierarchical two-dimensional conductive metal–organic framework/layered double hydroxide nanoarray for a high-performance supercapacitor," *Inorg. Chem.*, vol. 57, no. 11, pp. 6202–6205, 2018.

[176] R. Pawlak, S. Clair, V. Oison, M. Abel, O. Ourdjini, N. A. A. Zwaneveld, D. Gigmes, D. Bertin, L. Nony, and L. Porte, "Robust supramolecular network on Ag(111): Hydrogen-bond enhancement through partial alcohol dehydrogenation," *Chem. Phys. Chem.*, vol. 10, pp. 1032–1035, 2009.

[177] S. Clair, M. Abel, and L. Porte, "Mesoscopic arrays from supramolecular self-assembly," *Angew. Chem. Int. Ed.*, vol. 49, no. 44, pp. 8237–8239, 2010.

[178] S. Fischer, A. C. Papageorgiou, J. A. Lloyd, S. C. Oh, K. Diller, F. Allegretti, F. Klappenberger, A. P. Seitsonen, J. Reichert, and J. V. Barth, "Self–assembly and chemical modifications of bisphenol A on Cu(111): interplay between ordering and thermally activated stepwise deprotonation," *ACS Nano*, vol. 8, no. 1, pp. 207–215, 2014.

[179] L. Giovanelli, O. Ourdjini, M. Abel, R. Pawlak, J. Fujii, L. Porte, J. M. Themlin, and S. Clair, "Combined photoemission spectroscopy and scanning tunneling microscopy study of the sequential dehydrogenation of hexahydroxytriphenylene on Ag(111)," *J. Phys. Chem. C*, vol. 118, no. 27, pp. 14899–14904, 2014.

[180] A. C. Marele, I. Corral, P. Sanz, R. Mas-Ballesté, F. Zamora, M. Yáñez, and J. M. Gómez-Rodríguez, "Some pictures of alcoholic dancing: From simple to complex hydrogen-bonded networks based on polyalcohols," *J. Phys. Chem. C*, vol. 117, no. 9, pp. 4680–4690, 2013.

[181] F. Bebensee, K. Svane, C. Bombis, F. Masini, S. Klyatskaya, F. Besenbacher, M. Ruben, B. Hammera, and T. Linderoth, "Adsorption and dehydrogenation of tetrahydroxybenzene on Cu(111)," *Chem. Commun.*, vol. 49, no. 81, p. 9308, 2013.

[182] B. Lesiak, L. Kövér, J. Tóth, J. Zemek, P. Jiricek, A. Kromka, and N. Rangam, "C-sp^2/sp^3 hybridisations in carbon nanomaterials: XPS and XAES study," *Appl. Surf. Sci.*, vol. 452, pp. 223–231, 2018.

[183] X. Zhou and J. M. White, "Photon and electroninduced chemistry of chlorobenzene on Ag(111)," *J. Chem. Phys.*, vol. 92, no. 9, pp. 5612–5621, 1990.

[184] G. Olivieri, A. Cossaro, E. Capria, L. Benevoli, M. Coreno, M. De Simone, K. C. Prince, G. Kladnik, D. Cvetko, B. Fraboni, A. Morgante, L. Floreano, and A. Fraleoni-Morgera, "Intermolecular hydrogen bonding and molecular orbital distortion in 4-hydroxycyanobenzene investigated by X-ray spectroscopy," *J. Phys. Chem. C*, vol. 119, no. 1, pp. 121–129, 2015.

[185] F. Bebensee, K. Svane, C. Bombis, F. Masini, S. Klyatskaya, F. Besenbacher, R. Mario, B. Hammer, and T. R. Linderoth, "A surface coordination network based on copper adatom trimers," *Angew. Chem. Int. Ed.*, vol. 53, no. 17, pp. 12955–12959, 2014.

[186] J. Francis and A. Hitchcock, "Inner-shell spectroscopy of p -benzoquinone, hydroquinone, and phenol: Distinguising quinoid and benzenoid structures," *J. Phys. Chem.*, vol. 96, pp. 6598–6610, 1992.

[187] J. Solomon and R. Madix, "Orientation and absolute coverage of benzene, aniline, and phenol on Ag(110) determined by NEXAFS and XPS," *Surf. Sci.*, vol. 255, no. 1-2, pp. 12–30, 1991.

[188] D. Solomon, J. Lehmann, J. Kinyangi, B. Liang, K. Heymann, L. Dathe, and K. Hanley, "Carbon (1s) NEXAFS spectroscopy of biogeochemically relevant reference organic compounds," *SSSAJ*, vol. 73, no. 6, pp. 1817–1830, 2009.

[189] D. Käfer and G. Witte, "Evolution of pentacene films on Ag(111): Growth beyond the first monolayer," *Chem. Phys. Lett.*, vol. 442, no. 3, pp. 376–383, 2007.

[190] J. Stöhr and D. Outka, "Determination of molecular orientations on surfaces from the angular dependence of near-edge X-ray-absorption fine-structure spectra," *Phys. Rev. B*, vol. 36, no. 15, pp. 7891–7830, 1987.

[191] T. L. Andresen, F. C. Krebs, N. Thorup, and K. Bechgaard, "Robust supramolecular network on Ag(111): Hydrogen-bond enhancement through partial alcohol dehydrogenation," *Chem. Mater.*, vol. 12, no. 8, pp. 2428–2433, 2000.

[192] G. Pawin, K. L. Wong, K. Y. Kwon, and L. Bartels, "A homomolecular porous network at a Cu(111) surface," *Science*, vol. 313, no. 215789, pp. 961–962, 2006.

[193] M. Giesen, "Scaling transition of the time dependence of step fluctuations on Cu(111)," *J. Organomet. Chem.*, vol. 442, pp. 543–549, 1999.

[194] K. L. Svane, T. R. Linderoth, and B. Hammer, "Structure and role of metal clusters in a metal-organic coordination network determined by density functional theory," *J. Chem. Phys.*, vol. 144, no. 8, p. 084708, 2016.

[195] G. Pawin, K. L. Wong, D. Kim, D. Sun, L. Bartels, S. Hong, T. S. Rahman, R. Carp, and M. Marsella, "A surface coordination network based on substrate-derived metal adatoms with local charge excess," *Angew. Chem. Int. Ed.*, vol. 47, no. 44, pp. 8442–8445, 2008.

[196] H. Walch, J. Dienstmaier, G. Eder, R. Gutzler, S. Schlögl, T. Sirtl, K. Das, M. Schmittel, and M. Lackinger, "Labyrinthine island growth during Pd/Ru(0001) heteroepitaxy," *J. Am. Chem. Soc.*, vol. 133, no. 20, pp. 7909–7915, 2011.

[197] R. Muñoz and C. Gómez-Aleixandre, "Review of CVD synthesis of graphene," *Chem. Vap. Deposition*, vol. 19, no. 11, pp. 297–322, 2013.

[198] W. Yang, G. Chen, Z. Shi, C. Liu, L. Zhang, G. Xie, M. Cheng, D. Wang, R. Yang, D. Shi, K. Watanabe, T. Taniguchi, Y. Yao, Y. Zhang, and G. Zhang, "Epitaxial growth of single–domain graphene on hexagonal boron nitride," *Nat. Mater.*, vol. 13, pp. 792–797, 2013.

[199] Z. Wang, Z. Liu, and F. Liu, "Organic topological insulators in organometallic lattices," *Nat. Commun.*, vol. 64, p. 1471, 2013.

[200] L. Z. Zhang, Z. F. Wang, B. Huang, B. Cui, Z. Wang, S. X. Du, H. J. Gao, and F. Liu, "Intrinsic two-dimensional organic topological insulators in metaldicyanoanthracene lattices," *Nano Lett.*, vol. 16, no. 3, pp. 2072–2075, 2016.

[201] Y. Chen and Q. Sun, "Magnetic two-dimensional organic topological insulator: Au–1,3,5-triethynylbenzene framework," *J. Chem. Phys.*, vol. 137, no. 10, p. 104704, 2017.

[202] Z. Wang, N. Su, and F. Liu, "Prediction of a two–dimensional organic topological insulator," *Nano Lett.*, vol. 13, no. 6, pp. 2842–2845, 2013.

[203] A. Kumar, K. Banerjee, A. S. Foster, and P. Liljeroth, "Two-dimensional band structure in honeycomb metalorganic frameworks," *Nano Lett.*, vol. 18, no. 9, pp. 5596–5602, 2018.

[204] D. J. Murray, D. D. Patterson, P. Payamyar, R. Bhola, W. Song, M. Lackinger, A. D. Schlüter, and B. T. King, "Large area synthesis of a nanoporous two-dimensional polymer at the air/water interface," *J. Am. Chem. Soc.*, vol. 137, no. 10, pp. 3450–3453, 2015.

[205] J. Coraux, W. Hourani, V. L. Müller, S. Lamare, D. A. Kamaruddin, L. Magaud, N. Bendiab, M. D. Hertog, O. Leynaud, F. Palmino, R. Salut, and F. Chérioux, "Soluble two-dimensional covalent organometallic polymers by (arene)Ruthenium-sulfur chemistry," *Chem. Eur. J.*, vol. 23, no. 46, pp. 10969–109737, 2017.

[206] R. Zelonka and M. Baird, "Benzene complexes of Ruthenium(II)," *Can. J. Chem.*, vol. 50, no. 18, pp. 3063–3072, 1972.

[207] J. Wang, K. Moseley, and P. Maitlis, "Pentamethylcyclopentadienylrhodium and -iridium halides. I. Synthesis and properties," *J. Am. Chem. Soc.*, vol. 91, no. 22, pp. 970–977, 1969.

[208] M. Bennett and A. Smith, "Arene Ruthenium(II) complexes formed by dehydrogenation of cyclohexadienes with Ruthenium(III) trichloride," *J. Chem. Soc., Dalton Trans.*, no. 2, pp. 233–241, 1974.

[209] F. Chérioux, B. Therrien, and G. Süss-Fink, "First star-like oligophenylene molecules containing a dinuclear organometallic core," *Eur. J. Inorg. Chem.*, no. 6, pp. 1043–1047, 2003.

[210] F. Chérioux, B. Therrien, and G. Süss-Fink, "Synthesis and structural characterisation of new cationic dinuclear ruthenium(II) thiolato complexes of the type $[Ru_2(\eta^6\text{-arene})_2(\mu\text{-}p\text{-s–}C_6H_4\text{–Br})_3]^+$," *Inorg. Chim. Acta*, vol. 357, no. 3, pp. 834–838, 2004.

[211] F. Chérioux, B. Therrien, S. Sadki, C. Comminges, and G. Süss-Fink, "Synthesis, molecular structure and electrochemical properties of the star-shaped dinuclear complexes $[Ru_2(\eta^6 - p - \mathrm{Me} - C_6H_4 - {}^i Pr)_2(\mu_2 - S - p - C_6H_4 - C_4H_3S)_3]^+$ *and* $[Rh_2(\eta^5\text{–}C_5Me_5)_2(\mu_2\text{–S–}p\text{–}C_6H_4\text{–}C_4H_3S)_3]^+$," *J. Organomet. Chem.*, vol. 690, no. 9, pp. 2365–2371, 2005.

[212] H. M. Badawi, W. Förner, and A. S. A., "A comparative study of the infrared and Raman spectra of aniline and o-, m-, p-phenylenediamine isomers," *Spectrochim. Acta A*, vol. 112, pp. 388–396, 2013.

[213] K. Liu, H. Qi, R. Dong, R. Shivhare, M. Addicoat, T. Zhang, H. Sahabudeen, T. Heinea, S. Mannsfeld, U. Kaiser, Z. Zheng, and X. Feng, "On-water surface synthesis of crystalline, few-layer two-dimensional polymers assisted by surfactant monolayers," *Nat. Chem.*, vol. 11, pp. 994–1000, 2019.

Ana Cristina Gomez-Herrero

Doctor in physical-chemistry of materials

83, Cours Jean Jaurès
38000 Grenoble
07 67 59 60 67
ana.gomezherrero@gmail.com

Academic formation

09/2016 – 12/2019 **Ph.D in Physics**, *Université Grenoble Alpes, CNRS - Institut Néel*, Grenoble.
Towards two-dimensional organo-metallic molecular architecture via interface chemistry

02/2016 – 09/2016 **Master's degree Advanced Materials (Specialty in Nanotechnology)**, *Autónoma University*, Madrid.
Focused on thin films and nanomaterials growth (CVD, MBE, PLD, Sputtering, chemical synthesis) and characterization techniques (XRD, LEED, AFM, STM, XPS, FT-IRRAS).

09/2007 – 06/2013 **Grade in fundamental Chemistry**, *Complutense University*, Madrid.
Five years degree with specialty in inorganic chemistry.

Work experience

10/2016–Now **PhD work**, *CNRS/Institut Néel*, Grenoble.
Towards two-dimensional organo-metallic molecular architecture via interface chemistry

12/2018 and 02/2019 **STM measurements campaigns**, *ICMM/CSIC*, Madrid, Group of Prof. J.A. Martín-Gago.
Hexaxydroxyl-triphenylene deposition on Cu(111) monitored by low-temperature STM and LEED.

2015–2016 **Final Project of Master's degree**, *ICMM/CSIC*, Madrid, Group of Prof. J.A. Martín-Gago.
Growth and characterization of 2D structures obtained by on-surface chemistry. Under supervision of Dr. Carlos Sánchez Sánchez and Prof. J.A. Martín-Gago.

Languages

Spanish	Native
English	Advanced
French	Advanced

Profesional Skills

Langages	Igor,Python
Softwares	Gwyddion and InkScape
PAO	Latex

List of publications

to be submitted "Synthesis of polymeric arene(ruthenium) nano-sheets via imine chemistry at a liquid/liquid interface". **A. C. Gómez Herrero**, M. Feron, N. Bendiab, M. Der-Hertog, V. Reita, J. Coraux, F. Chérioux

to be submitted "Stepwise oxidation, reorganisation, and bonding strength of a hexahydroxyl-triphenylene on a copper surface". **A. C. Goméz Herrero**, C. Sanchéz-Sanchéz, F. Chérioux, J. I. Martínez, J. Abad, L. Floreano, A. Verdini, A. Cossaro, E. Mazaleyrat, V. Guisset, P. David, S. Lisi, J. A. Martín-Gago and J. Coraux.

submitted "Decoupling molybdenum disulfide from its substrate by cesium intercalation". R. Sant, S. Lisi, V. D. Nguyen, E. Mazaleyrat, **A. C. Goméz Herrero**, O. Geaymond, V. Guisset, P. David, A. Marty, M. Jamet, C. Chapelier, L. Magaud, Y. J. Dappe, M. Bianchi, P. Hofman, G. Renaud and J. Coraux.

to be submitted "Structure of graphene and a surface carbide grown on the (0001) surface of rhenium". E. Mazaleyrat, A. Artaud, L. Magaud, **A. C. Goméz Herrero**, S. Lisi, V. Guisset, P. David, C. Chapelier and J. Coraux.

to be submitted — "Defective, hole-doped and superconducting quasi free-standing graphene on Re(0001) obtained by gold intercalation". E. Mazaleyrat, S. Vlaic, A. Artaud, L. Magaud, **A. C. Goméz Herrero**, S. Lisi, P. Singh, N. Bendiab, V. Guisset, P. David, S. Pons, D. Roditchev, C. Chapelier and J. Coraux.

to be submitted — "Clockwise and anti-clockwise rotational epitaxy confined under a graphene layer". S. Lisi, E. Mazaleyrat, **A. C. Goméz Herrero**, V. D. Nguyen, V. Guisset, P. David and J. Coraux.

to be submitted — "On-Surface driven formal Michael reaction produces *m*-polyaniline oligomers on Pt(111)". Nerea Ruiz del Árbol, Carlos Sánchez-Sánchez, Gonzalo Otero-Irurueta, Jose I. Martínez, Pedro L. de Andrés, **A. C. Goméz Herrero**, Pablo Merino, Martin Piantek, David Serrate, Paolo Lacovig, Silvano Lizzit, Jose Alemán, Gary J. Ellis, María F. López, José A. Martín-Gago.

Conferences

June 2019 - Oral presentation — **XI Iberian Vacuum Conference-RIVA in Sevilla - Spain**- "Metal-Coordination Cross-linking via On-Surface Formed Radical Structures"

January 2019 - Poster contribution — **Journées Surfaces & Interfaces in Nancy - France**- "Towards two-dimensional molecular crystals"

August 2018 - Poster contribution — **Journées de la matiére condensée in Grenoble - France**- "Towards two-dimensional molecular crystals"

May 2018 - Poster contribution — **European workshop on epitaxial graphene and two-dimensional materials in Salamanca - Spain**- "Towards two-dimensional molecular crystals"